OPTIMAL DESIGNS OF SUBMERGED DOMES

VO KHOI KHOA

NATIONAL UNIVERSITY OF SINGAPORE

2007

OPTIMAL DESIGNS OF SUBMERGED DOMES

VO KHOI KHOA

(B. Eng, University of Technology, Vietnam)

A THESIS SUBMITTED

FOR THE DEGREE OF DOCTOR OF PHILOSOPHY

DEPARTMENT OF CIVIL ENGINEERING

NATIONAL UNIVERSITY OF SINGAPORE

2007

ACKNOWLEDGMENTS

First and foremost I wish to express my sincere gratitude to my supervisor, Professor Wang Chien Ming (Engineering Science Programme and Department of Civil Engineering, National University of Singapore) for his highly valuable supervision throughout my course of study. His constant inspiration, kind encouragement, extensive knowledge, serious research attitude and enthusiasm have extremely assisted me in completion of this thesis. Also special thanks go to Professor Rob Y.H. Chai (Department of Civil and Environmental Engineering, University of California, Davis) for his valuable suggestions, discussions and help in the research work.

I want to express my gratitude to the National University of Singapore for providing the Research Scholarship during this doctoral study in the Department of Civil Engineering.

My parents and sisters have been extraordinary sacrificial for providing me with whatever requirements for my education opportunity. For this, I am thankful. Finally, I am also grateful to my girlfriend, Ms Le Nguyen Anh Minh, and to my friends Mr. Dang The Cuong, Mr. Nguyen Dinh Tam and Mr. Tun Myint Aung for their kind help and encouragement.

TABLE OF CONTENTS

SUMMARY

So far, little research has been done on submerged large dome structures. This prompted the present study on the optimal design of submerged domes for minimum weight as well as for maximum buckling capacity.

The first part of the thesis presents the membrane analysis and minimum weight design of submerged spherical domes. By adopting a uniform strength design as governed by the Tresca yield condition, an analytical expression in the form of a power series for the thickness variation of a submerged spherical dome was derived. Further, based on a family of uniform strength designs associated with a given depth of water and base radius of the dome, the optimal subtended angle 2α and the optimal dome height for the minimum weight design of submerged spherical domes were determined.

Extending the research on spherical domes, membrane analysis and optimal design of submerged general shaped domes were treated. By adopting a constant strength design, equations governing the meridional curve and thickness variation of submerged domes were derived with allowance for hydrostatic pressure, selfweight and skin cover load. The set of nonlinear differential equations, which correspond to a two-point boundary problem, was solved by the shooting-optimization method. A notable advantage of the equations derived in this part is the parameterization of the

equations using the arc length s as measured from the apex of the dome. Such parameterization allows the entire shape of the submerged dome to be determined in a single integration process whereas previous methods that made used of the Cartesian coordinates gave problems when vertical or infinite slope was encountered in the meridian curve. For the special case of a weightless dome without skin cover load, the thickness of the dome was found to be constant when subjected to hydrostatic pressure only. The shape of the dome was also found to agree well with the shape currently reported in the literature. Further, parametric studies of dome shapes under different water depths and selfweight also led to a better understanding of the optimal shape of submerged domes. Numerical examples indicated that the airspace enclosed by the optimal dome reduces in the presence of large hydrostatic pressure. The reduced airspace is accompanied by a significant increase in the dome thickness, which in turn results in an increased overall weight of the dome.

In the second part of the thesis, the optimal design of domes against buckling is focused. Although buckling of shells under compressive loading is of practical significance in the design of these structures, most of the studies thus far have focused on spherical domes using a thin shell theory. This study presents the formulation and solution technique to predict the critical buckling pressure of moderately thick rotational shells generated by any meridional shape under external pressure. The effect of transverse shear deformation is included by using Mindlin shell theory so that the critical buckling pressure will not be excessively overestimated when the shell is relatively thick.

The critical buckling pressure of moderately thick shells under uniform pressure, formulated as an eigenvalue problem, is derived using the well accepted Ritz method.

One feature of the proposed method is the high accuracy of the solutions by using an adequate number of terms in the Ritz functions. The formulation is also capable of handling different support conditions. This is made possible by raising the boundary equations to the appropriate power so that the geometric boundary conditions are satisfied *a priori*. The validity of the developed Ritz method as well as the convergence and accuracy of the buckling solutions are demonstrated using examples of spherical domes (a special case of generic dome structures) where closed-form solutions exist. Based on comparison and convergence studies, the Ritz method is found to be an efficient and accurate numerical method for the buckling of dome structures. New solutions for the buckling pressure of moderately thick spherical and parabolic shells of various dimensions and boundary conditions are presented and, although these results are limited by the material properties assumed, they are nonetheless useful for the preliminary design of shell structures.

Upon establishment of the validity of method and its ability to furnish accurate results for the buckling of dome structures under uniform pressure, the research was extended to submerged domes. In addition to hydrostatic pressure, loads acting on the dome include the selfweight. New solutions for the buckling pressure of moderately thick spherical and parabolic shells of various dimensions and boundary conditions are presented. Further, based on a family of spherical and parabolic domes associated with a given dome height submerged under a given water depth, we determine the Pareto optimal design for maximum enclosed airspace and minimum weight dome design.

This thesis should serve as a useful reference source for vast optimal dome design data for researchers and engineers who are working on analysis and design of shell structures.

NOMENCLATURE

D	water depth
E_s, E_θ,	Young's moduli in the direction of the meridian and parallel circle, respectively
$G_{s\zeta}$	shear modulus in the $s-\zeta$ plane
H	dome height
h	dome thickness
κ^2	Mindlin's shear correction factor
L	dome base radius
l	curve length of one-half of the meridian
N_{rs}, N_{zs}	horizontal and vertical components of the meridian forces N_s
N_s, N_ϕ	membrane force in the meridian direction
N_θ	membrane force in the circumference direction
p_h, p_c, p_a	hydrostatic pressure, skin cover load and self-weight
p_s, p_n	loads normal and tangential to the middle surface
R	radius of spherical domes
r_0	the distance of one point on the shell to the axis of rotation
r_1, r_2	principal radii of curvature of the dome

s	arc length along the meridian as measured from the apex of the dome
U	elastic strain energy functional
W	work done functional
W_0	dome weight
u , w	middle-surface displacement along the meridional and normal directions, respectively
z	vertical coordinate
α	subtended angle
γ_a	specific weight of dome material
$\gamma_{s\zeta}$	transverse shear strain associated with rotation of the shell in the meridian direction
γ_w	specific weight of water
ε_s , ε_θ	normal strain in the direction of the meridional and circumference direction, respectively
λ	buckling pressure parameter
ν_s , ν_θ	Poisson's ratios
ξ	normalized thickness
Π	total potential energy functional
σ_0	the allowable compressive stress
σ_ϕ , σ_θ	the meridian and circumferential stress
ϕ	meridian angle
ψ	rotation of the middle-surface in the meridional direction

LIST OF FIGURES

LIST OF TABLES

CHAPTER 1

INTRODUCTION

Shell structures have been widely used since ancient times as one of the most common types of structural form. One of the earliest applications of the shell as a structural form is represented by beautiful domes that have been constructed as roofs for temples, mosques, monuments and other buildings. A small dome was even discovered inside the Bent Pyramid which was built during the Fourth Egyptian Dynasty in about 2900 B.C. (Cowan, 1977). However, domes were not widely used until the Roman Empire. A good example of the dome construction during the Roman Empire is the Pantheon dome, which had the longest span (43 m) prior to the 19th century and is still in use today as a church. The Hagia Sophia of Constantinople (now Istanbul) was built approximately 1500 years ago, St Peter's Cathedral in Rome was designed by Michelangelo in about 1590. In the modern shell applications, many domes were constructed all over the world for different purposes such as the Millennium Dome (in England) for exhibition purposes and the Georgia Dome (in USA) for sporting events.

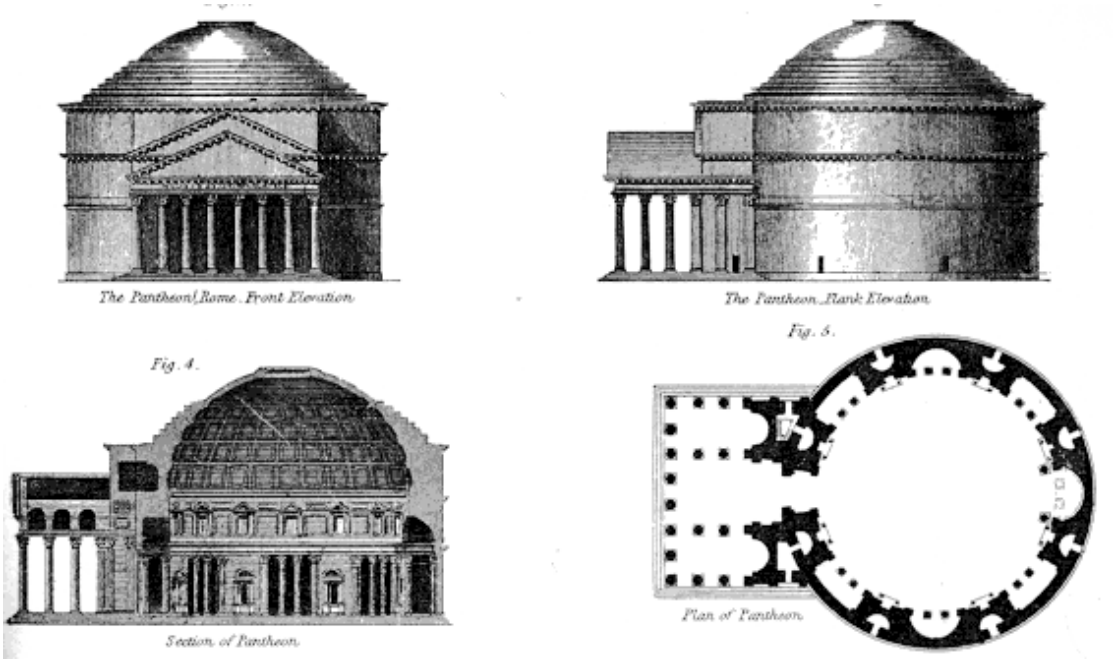

Fig 1.1 Pantheon domes

(Source: 1897 *Encyclopaedia Britannica)*

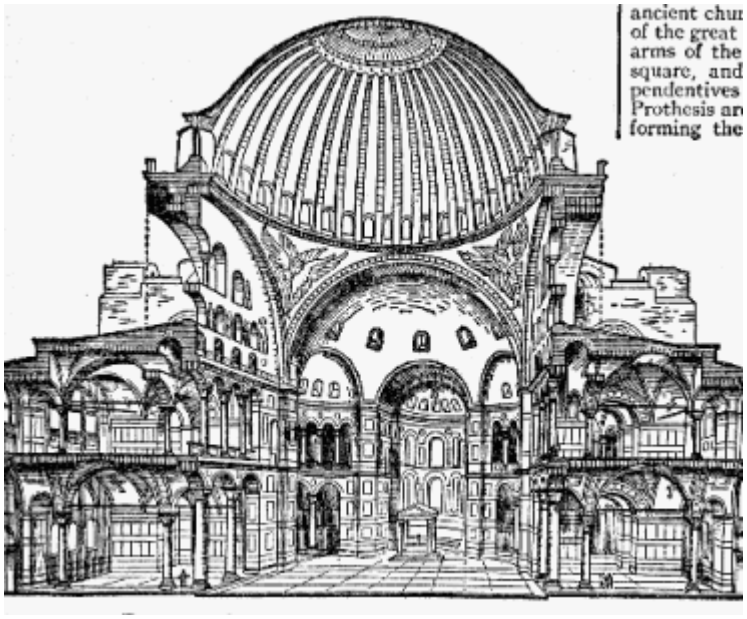

Fig 1.2 Hagia Sophia of Constantinople

(Source: 1911 *Encyclopaedia Britannica)*

1.1 Submerged dome ideas

As the population and urban development expand in coastal cities, city planners and engineers resort to land reclamation and construction on and under the sea to create additional space so as to ease the pressure on existing land use. In recent times, we have seen very large floating structures being constructed on the coast of densely populated cities. For example, Japanese engineers have constructed a floating steel arch bridge that spans 410m across the Yumemai channel in Osaka (Watanabe and Utsunomiya, 2003), floating oil storage facilities at Shirashima and Kamigoto, a floating amusement facility at Onomichi and floating emergency rescue bases in Osaka Bay, Ise Bay and Tokyo Bay. Based on the knowledge gained from the Mega-Float which measures 1000m x 60m x 3m test model for a floating runway (Yoshida, 2003), the Japanese are considering the construction of a floating runway of 3.6km x 500m x 20m in the expansion programme for the Haneda International Airport. Other countries having floating structures include Norway with its famous floating Bergsøysund bridge and Nordhordland bridge (Watanabe and Utsunomiya, 2003), Hong Kong with its floating restaurant <http://www.jumbo.com.hk/eng/main.php>, Saudi Arabia with its floating desalination plant (Abdul Azis *et al*., 2002), North Korea with its floating hotel, Canada with its floating heliport and piers, Brazil with its floating pulp plant and Singapore with its floating performance platform.

Many submerged tunnels have been constructed to join two parts of cities across a river or to connect two countries over a channel (for example the Channel Tunnel Crossing between France and England and the Oresund Link between Sweden and Denmark). These tunnels enhance greater connectivity, and help to redistribute the population concentrations and generate more economic activities. Research studies on

seeking optimal shapes of these submerged tunnels in the form of funicular arches have been carried out by Gavin and Reilly (2000), Wang and Wang (2002), Fung (2003), Wang and Ler (2003) and Chai and Kunnath (2003).

Offshore activities are also increasing as mankind seeks to tap the riches of the seas and oceans. In addition to drilling for oil and natural gas in deep water, there has been recent interest among engineers to mine methane hydrate (Komai 2003; Ichikawa and Yonezawa 2003) scattered over the seabed for a cleaner source of fuel. This 21st century will also likely see the construction of floating and underwater cities, for example, the Hydropolis project which is an underwater complex featuring a luxurious hotel with 220 underwater suites in Dubai, the United Arab Emirates <http://www.hydropolis.com/project/>. For submerged cities, a dome complex may be used to create the living environment suitable for sustaining human activities for a long time (see Fig. 1.6). This vision prompted the author to study the optimal design of submerged domes. Before tackling the aforementioned problem herein, a literature survey on design of rotational shells is presented.

Fig. 1.3 Yumemai floating bridge

(Source: *http://www.tokyo-wankou.com/)*

Fig. 1.4 Mega-Float in Tokyo Bay

(Photo courtesy of Prof E. Watanabe - Kyoto University)

Fig. 1.5 Floating oil storage facility

(Photo courtesy of Dr Namba - Shipbuilding Research Centre of Japan)

Fig. 1.6 Author's impression of a submerged dome complex

1.2 Rotational shells

In thin shell structures used in engineering practice, rotational shells or domes have the widest application because of their elegance and strength. Large span vaults of revolution, chiefly as the roofs of sacred buildings, were built in ancient times without any strength calculations being used. Of course, the domes of stone or brick constructed those days were many times thicker than the thin shells of buildings, aircraft and naval structures built over the past forty years based on suitable analytic methods.

The classical thin shell theory was firstly developed by Aron (1874). However, in 1888, Love (1888) noticed Aron's inaccuracies and proposed a shell theory that is analogous to the plate theory proposed by Kirchhoff (1876). Galerkin (1942) also played an important part in the development of the theory of thin shell by his work. Goldenweizer (1946) and Mushtari (1949) gave the basis for a general principle for simplification of the equations of theory of shells.

The above general thin shell theory of shells was preceded by the momentless or membrane theory. Membrane theory was firstly used in 1833 by Lame and Claperon (1833). In this work, Lamé and Claperon (1833) considered the symmetrical loading of shells of revolution. Beltrami (1881) and Lecornu (1938) established the general form of the equations of membrane theory. Sokolovskii (1938) made a significant contribution by reducing the equations of the problem to canonical sform and revealed a number of their characteristic properties. Moreover, Vlasov (1939) Sokolovskii (1938) investigated the shell of revolution under arbitrary loads. So far, a brief mention of thin shell theory and membrane theory for thin shell structures is given. In this next part, a literature review on buckling analysis of the rotational shells will be presented.

1.3 Buckling of rotational shells

Shell structures are efficient three-dimensional entities that are capable of resisting high compressive stresses with essentially little or no bending deformation. Their inherent efficiency, coupled with elegant shapes and geometry, often results in thicknesses that are small compared to their span length. Owing to their relatively small thickness when compared to the length dimensions, the design strength of these structures is commonly governed by their buckling capacities. Buckling is a phenomenon in which a structure undergoes visibly large transverse deflection in one of the possible instability modes. Buckling of a structural component may affect the strength or stiffness of the whole structure and even triggers unexpected global failure of the structure. Therefore, it is important to know the buckling capacities of structures in order to avoid premature failure.

The first notable buckling analysis of shell structures was carried out by Zoelly in 1915 for spherical caps under uniform external pressure. While earlier investigations mainly centered on the provision of analytical solutions, later approaches relied more on numerical techniques as facilitated by the advent of modern computers. Bushnell (1976, 1984) developed a general-purpose computer program for the analysis of shells of revolution based on the finite-difference method. At about the same time, Cohen (1981) developed a computer code FASOR, based on a numerical integration method called the field method, for the analysis of stiffened, laminated axisymmetric shells.

By using the Kalnins and Lestingi (1967) method of multi-segment integration, Uddin (1987) solved the governing differential equations for axisymmetric buckling of spherical shells. In Uddin's (1987) paper, numerical results were presented for spherical shells with various subtended angles and these results were in good agreement with those obtained by Huang (1964), Budiansky (1959), Thurston (1961)

and Dumir (1984). Chao *et al.* (1988) presented a semi-analytical solution for axisymmetric buckling of thick, orthotropic, complete spherical shells and hemispherical shells with various boundary conditions. Their solutions were derived from the Ritz method with the displacement functions approximated by Legendre polynomials. Muc (1992) presented the buckling analysis of axisymmetric composite shells of revolution such as spherical caps, torispheres and hemispheres. Its first part is devoted to linear buckling analysis in order to determine the appropriate divisors for buckling pressures. Uddin and Haque (1994) also investigated the buckling behavior of semi-ellipsoidal shells, where the critical buckling pressure was found to increase with increasing ratio of minor axis to major axis lengths of the ellipsoidal shell, and the critical pressure was found to increase with increasing thickness-to-radius ratios.

Other notable contributions on this subject were made by Ross and his colleagues. In 1981, Ross and Mackney (1983) presented a constant meridional curvature element for the buckling of hemi-ellipsoidal domes under uniform external pressure. In this study, only linear variations were assumed for the meridional and circumferential displacements along the meridian of these elements. Ross (1990) presented a varying meridional curvature element to extend this study. Furthermore, Ross (1996) extended this work to a cubic and a quadratic variation being assumed for the meridional and the circumferential displacements along the meridian of these elements. In this study, comparisons were made between experiment and theory for both buckling and vibration of hemi-ellipsoidal shell domes, which varied from very flat oblate vessels to very long prolate vessels. In general, agreement between experiment and theory was good for the hemi-spherical dome and the prolate vessels, but not very good for the flat oblate vessels. Ross *et al.* (2001) conducted many experiments on buckling, post-buckling and plastic collapse of spherical shells subjected to external pressure. Ross *et*

al. (2003) reported on a theoretical and an experimental investigation into six GRP hemi-ellipsoidal dome shells, which were tested to destruction under external hydrostatic pressure.

As another attempt, Redekop (2005) developed a new method to predict the buckling characteristics of an orthotropic shell of revolution with an arbitrary meridian subjected to a normal pressure. The solution was given within the context of the linearized Sanders–Budiansky shell buckling theory and makes use of the differential quadrature method. Dumir *et al.* (2005) investigated the axisymmetric buckling analysis of moderately thick laminated shallow annular spherical cap under transverse load. Buckling under central ring load and uniformly distributed transverse load, applied statically or as a step function load, was presented.

Recently, applying the boundary element formulation, Baiz and Aliabadi (2007) presented the buckling analysis of shear deformable shallow shells. The boundary element formulation is presented as an eigenvalue problem, to provide direct evaluation of critical load factors and buckling modes.

However, their studies were confined to the treatment of spherical shells, and their formulations were based on either classical thin shell theory or shallow shell theory. A literature survey conducted as part of this study indicated that previous treatments of moderately thick rotational shells had all assumed the specific shape of spherical shells, limiting their general applications. The methodology developed herein for buckling analysis is applicable to rotational shells of any meridional shape.

1.4 Optimal design of domes against buckling

Over the past four decades, structural optimization has widened considerably, but optimization to enhance the elastic buckling resistance of structures remains an active area of research. Structural optimization for problems with buckling constraints is complicated because calculation of buckling loads is generally an involved process that requires the solution of two boundary value problems (static analysis and eigenvalue solution) at each optimization step. While earlier investigations mainly centered on the provision of analytical solutions, later approaches have relied more on numerical techniques as facilitated by the advent of modern computers. Buckling of general rotational shells depends on many variables, such as the geometric properties of the shell, the material properties and the type of the applied loads. The various parameters change the buckling behavior of shells, making it difficult to achieve a general optimal design. Many techniques have been used for optimal design of shells under stability constraints. A detailed survey of these problems was given by Krużelecki and Życzkowski (1985) and Życzkowski (1992). The monograph by Gajewski and Życzkowski (1988) was devoted to structural optimization under stability constraints.

The largest number of papers is concerned with optimization of cylindrical shells. A lateral pressured cylindrical shell was considered by Hyman (1971), Sun and Hansen (1988), Sun (1989), Levy and Spillers (1989) and Gajewski (1990). More complex optimization problems are presented in shells with a double curvature. In this case, a single loading already causes a combined state of stress. Parametrical optimization of barrel shaped shells under stability constraints was presented by Blachut (1987), Krużelecki and Trzeciak (2000). As another attempt, the monograph by Hinton *et al.* (2003) was devoted to the buckling analysis and optimization of plates and shells.

Research on optimization of shell structures has been extended to multi-objective optimization. Multi-objective optimizations of cylindrical shells under torsional, axial, external and internal pressure have been carried out by Sun and Hansen (1988) and Tennyson and Hanse (1983). Walker *et al.* (1995) studied the Pareto optimal design of a symmetrically laminated shell with the objectives defined as the maximization of the axial and torsional buckling loads.

So far, little work has been done on the multi-objective optimization of submerged domes against buckling. Prompted by this fact, we focus our study on the Pareto optimal designs of submerged domes with allowance for selfweight.

1.5 Objectives and scope of study

This thesis investigates the optimal designs of submerged dome structures. First we consider the least weight design of rotationally symmetric shells. In particular, we consider

- *Submerged spherical domes of uniform strength design governed by the Tresca yield condition* - Based on a family of uniform strength designs associated with a given depth of water and the dome's base radius, the optimal subtended angle, the optimal dome height and optimal thickness variation for the minimum weight design of submerged spherical domes are determined.

- *Submerged general domes adopting constant strength design* - Based on a family of constant strength designs associated with a given water depth and dome height, the optimal dome shape and the optimal thickness variation for minimum weight are determined.

In the second part of the thesis, we focus our attention on the optimal design of rotational shells against buckling. For this research study, we first formulate the buckling problem and derive the governing eigenvalue equation using the Ritz method. The Ritz computer code for the buckling analysis is developed which can readily handle any support edge condition. The buckling analysis and problems considered are given below.

- *Buckling analysis of moderately thick domes under uniform pressure using the Ritz method* - The Ritz method was applied to determine the critical uniform buckling pressures of moderately thick, rotational orthotropic shells that include spherical, parabolic shells.

- *Buckling analysis of moderately thick submerged domes using the Ritz method* - The Ritz method was applied to determine buckling load of submerged domes or the maximum water depth that a rotational shell can sustain before buckling occurs. Next we solve the optimal design problem of submerged domes against buckling as well as for minimum weight and maximum enclosed airspace.

- *Optimal design of submerged domes* – The Pareto optimal design of submerged domes for minimum weight as well as maximum enclosed airspace whereby the dome will not buckle under the hydrostatic pressure and its own weight is investigated.

Results of the present study are useful in providing a basic knowledge for constructing a submerged dome that will be used to create a living environment under the sea. Moreover, the study may contribute to a better understanding of the buckling behaviour of shell structures under rotationally axisymmetric loads and hydrostatic pressure.

The thesis focuses on identifying the optimal design of submerged spherical and general dome structures. It is recognized that there are many criteria in designing a submerged dome structure such as strength, buckling, vibration, wave, current and blast effect. The current study only investigates the first two criteria, namely strength and buckling criteria. Moreover, during the analysis, since the bending stress in thin shell structures is negligibly small, we consider only domes under membrane stress conditions. Future studies may be carried out to investigate the other criteria for optimal design and also to investigate the bending of submerged domes under wave and current loads.

1.6 Layout of thesis

The background information on shell structures, literature review on buckling of shells of revolutions, the objectives and scope of study have been presented in this chapter.

In Chapter 2, the membrane analysis and minimum weight of the submerged spherical domes are investigated. In addition to the hydrostatic pressure, loads acting on the dome include the selfweight and a skin cover load. Based on a family of uniform strength designs associated with a given depth of water and the dome's base radius, we determine the optimal subtended angle 2α (and the optimal dome height) for the minimum weight design of submerged spherical domes.

In Chapter 3, membrane analysis and optimal design of submerged domes is considered. In addition to hydrostatic pressure, the domes are also subjected to selfweight and skin cover load, which are invariably present in this type of structure. Based on a family of constant strength designs associated with a given water depth and dome height, the optimal dome shape for minimum weight is determined.

By adopting Mindlin shell theory, the energy functionals and governing equations are derived in Chapter 4 for the elastic buckling analysis of moderately thick rotational shells under any rotational symmetric loading. Moreover, detailed formulations of the Ritz method for the buckling analysis are also presented.

Chapters 5 and 6 present buckling analyses of domes of various shapes (such as spherical and parabolic domes) and under different loading conditions. In Chapter 5, the buckling problem of rotational shells under uniform pressure is treated whilst Chapter 6 considers the buckling problem of submerged rotational shells. The validity, convergence and accuracy of the Ritz solutions are demonstrated using spherical shells (a special case of rotational shells), where closed-form solutions exist for some cases. A parametric study is conducted to study the buckling behaviour of spherical and parabolic domes with respect to the base-radius-to-height ratios, thickness-to-height ratios and different support conditions. The buckling solutions are presented for the first time for these shells.

In Chapter 7, the optimal design of the submerged rotational shells (such as spherical and parabolic domes) against buckling is investigated. Based on a family of spherical and parabolic domes associated with a given dome height, we investigated the Pareto optimal dome shape for minimum weight as well as maximum enclosed airspace whereby the dome will not buckle under the hydrostatic pressure and its own weight.

Chapter 8 summarizes the findings of this research study and presents some recommendations for future studies.

CHAPTER 2

UNIFORM STRENGTH DESIGNS OF SUBMERGED SPHERICAL DOMES

This chapter is concerned with the membrane analysis and minimum weight design of submerged spherical domes. In addition to hydrostatic pressure, loads acting on the dome include the selfweight and a skin cover load. By adopting a uniform strength design as governed by the Tresca yield condition, the variation of the shell thickness of spherical domes can be accurately defined by a power series. Based on a family of uniform strength designs associated with a given depth of water and the dome's base radius, we determine the optimal subtended angle 2α (and the optimal dome height) for the minimum weight design of submerged spherical domes.

2.1 Introduction

In 1958, Ziegler (1958) investigated the uniform strength design of spherical cupolas under their own weight. Using the Tresca yield hexagon, he found that if the stress point is restricted to the sides AB and AC of the Tresca hexagon (see Fig. 2.5), the cupola uses less material than when the stress point is confined only to the Tresca side AB. Issler (1964) considered membrane shell designs based on the Tresca hexagon as well as on the von Mises ellipse. He treated shells under constant vertical dead load per unit projected area. Schumann and Wuthrich (1972) and Sayir and Schumann (1972) studied membrane shells without rotational symmetry. Prager and Rozvany (1980) investigated the optimal design of spherical cupolas of a given base radius. The cupolas are assumed to be constructed from a material with negligible tensile strength. The combined action of the weights of the cupola proper and a cover of uniform thickness was considered and the minimum weight design was examined. Nakamura *et al.* (1981) extended Prager and Rozvany's (1980) work to include the weight of the roof cover, snow load, external and internal pressure. Moreover, Pesciullesi *et al.* (1997) obtained the shape of a uniform strength shell subjected to selfweight by solving the eigenvalue problem associated with the integral equilibrium equations. So far, the aforementioned studies on spherical domes do not include hydrostatic pressure. This prompted us to study the membrane and minimum weight design of spherical domes under hydrostatic pressure.

2.2 Membrane Theory

2.2.1 Basic assumptions of classical thin shell theory

In formulating the classical thin shell theory, the following assumptions are made (Love 1888)

- The shell thickness h is negligibly small in comparison with the smallest radius R of curvature of the middle surface. According to Novozhilov (1943), the thickness to radius ratio $h/R \le 1/20$ should be satisfied for the shell to qualify as a thin shell.

- Strains and displacements that arise within the shell are small. This implies that the products of deformation quantities occurring in the development of the theory may be neglected, ensuring that the system is described by a set of geometrically linear equations. This also makes it possible to formulate the equilibrium conditions of the deformed middle surface with reference to the original position of the middle surface prior to deformation.

- Straight line that are normal to the middle surface prior to deformation remain straight and normal to the middle surface during deformation, and experience no change in length. It implies that the direct strain in the direction normal to the middle surface, and the shearing strains in planes perpendicular to the middle surface and due to transverse shear forces, are all zero. This assumption is valid for thin shells. However, when the shell is thick, it is necessary to incorporate the effect of transverse shear deformation.

- The normal stresses σ_z transverse to the middle surface are small, and can be neglected.

2.2.2 Geometrical properties of rotational shells

Consider a surface of revolution generated by rotation of a plane curve about an axis in its plane as shown in Fig. 2.1. A point on the shell can be located by the θ-ϕ- r coordinate system where r_0 is the distance of one point on the shell to the axis of rotation, and

$$r_0 = r_2 \sin\phi \tag{2.1}$$

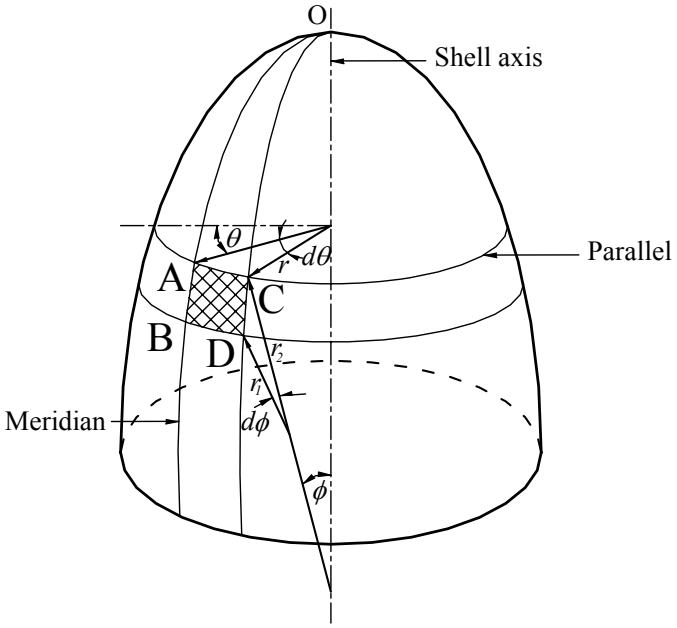

Fig. 2.1 Rotational shells (Domes)

Referring to Fig. 2.2, *s* is the arc length along the meridian as measured from the apex of the dome, r_1 is the radius of curvature of the meridian. The principal radius r_2 generates the middle surface of the dome in the direction perpendicular to the tangent on the meridian. Referring again to Fig. 2.2, for the line element *ds* of the meridian, we have

$$ds = r_1 d\phi \tag{2.2a}$$

$$dr_0 = ds\cos\phi \tag{2.2b}$$

$$dz = ds\sin\phi \tag{2.2c}$$

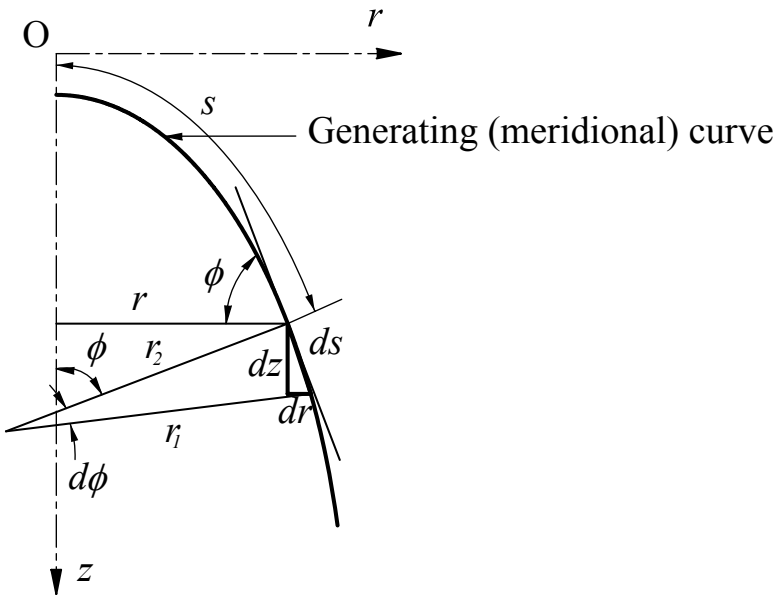

Fig. 2.2 Meridian of a dome

2.2.3 Membrane analysis

For membrane theory to be valid in the analysis, the following conditions must be satisfied:

- The middle surface of the shell is continuously curved and the curvatures are slowly varying.
- The thickness of the shell is small and constant or varies continuously.
- Surface loadings are distributed continuously.
- The boundary forces and reactions of the boundary constraints are oriented tangentially to the middle surface.

- The components of the state of displacement determined from the respective equation are finite.

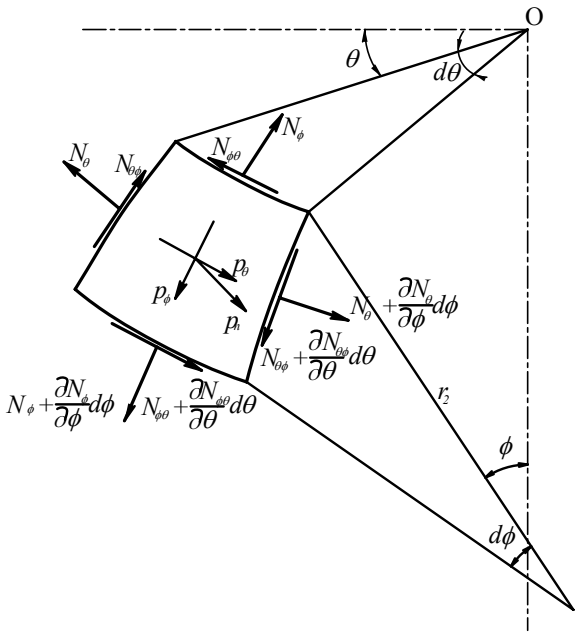

Fig. 2.3 Shell element

In general, the shell element is bounded by two meridional lines and two circumferential lines, each pair of aforementioned curves is close together as shown in Fig. 2.3. The conditions of its equilibrium will furnish three equations, which are necessary for solving the three unknown stress resultants, namely, the meridian force N_ϕ, the hoop force N_θ and the shear force $N_{\phi\theta}$. These three equilibrium equations are given by Kraus (1967)

$$\frac{\partial\left(rN_\phi\right)}{\partial\phi} + r_1 \frac{\partial N_{\theta\phi}}{\partial\theta} - r_1 N_\theta \cos\phi + p_\phi r r_1 = 0 \tag{2.3}$$

$$\frac{\partial\left(rN_{\phi\theta}\right)}{\partial\phi} + r_1 \frac{\partial N_\theta}{\partial\theta} + r_1 N_{\theta\phi} \cos\phi + p_\theta r r_1 = 0 \tag{2.4}$$

$$\frac{N_\phi}{r_1}+\frac{N_\theta}{r_2}=-p_n \tag{2.5}$$

By noting the relationship between s and ϕ, i..e. $ds=r_1 d\phi$, the equilibrium equations may also be expressed as

$$\frac{\partial(rN_s)}{\partial s}+\frac{\partial N_{\theta s}}{\partial \theta}-N_\theta\cos\phi+p_s r=0 \tag{2.6}$$

$$\frac{\partial(rN_{\theta s})}{\partial \phi}+\frac{\partial N_\theta}{\partial \theta}+N_{\theta s}\cos\phi+p_s r=0 \tag{2.7}$$

$$\frac{N_s}{r_1}+\frac{N_\theta}{r_2}=-p_n \tag{2.8}$$

In the case of axisymmetry loads, the stresses are independent of θ. Therefore, we have two equations to evaluate the two unknown stress-resultants N_ϕ and N_θ

$$\frac{\partial(rN_\phi)}{\partial \phi}-r_1 N_\theta\cos\phi+p_\phi r r_1=0 \tag{2.9a}$$

$$\frac{N_\phi}{r_1}+\frac{N_\theta}{r_2}=-p_n \tag{2.9b}$$

or

$$\frac{\partial(rN_s)}{\partial s}-N_\theta\cos\phi+p_s r=0 \tag{2.10a}$$

$$\frac{N_s}{r_1}+\frac{N_\theta}{r_2}=-p_n \tag{2.10b}$$

2.3 Problem definition and basic equations

2.3.1 Problem definition

Consider a submerged, spherical dome of radius *R*, subtended angle *2α* and specific weight γ_a as shown in Fig. 2.4.

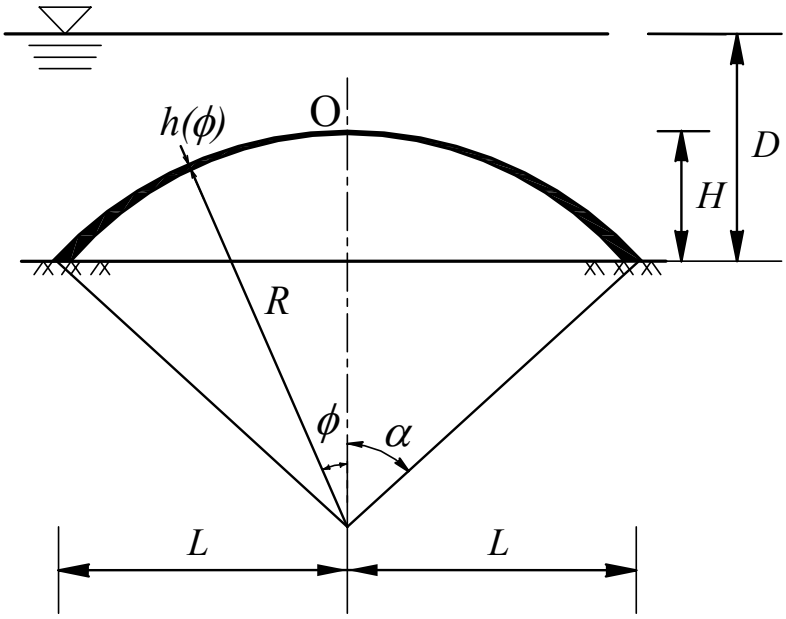

Fig. 2.4 Submerged spherical dome

From geometrical considerations, the base radius $L = R\sin\alpha$ and the dome height $H = R(1-\cos\alpha) = L(1-\cos\alpha)/\sin\alpha$. The dome is subjected to hydrostatic pressure, its own selfweight and skin cover load. The loads are assumed to be transmitted through the dome structure to the supporting ring foundation via membrane forces only. By adopting a uniform strength design governed by the Tresca yield condition (see Fig 2.5), the problem at hand is to seek the variation of the dome thickness *h*. From a family of such uniform strength designs associated with a

prescribed value of base radius L, we determine the optimal value of α (and hence the optimal shape) which gives the minimum weight of the submerged dome.

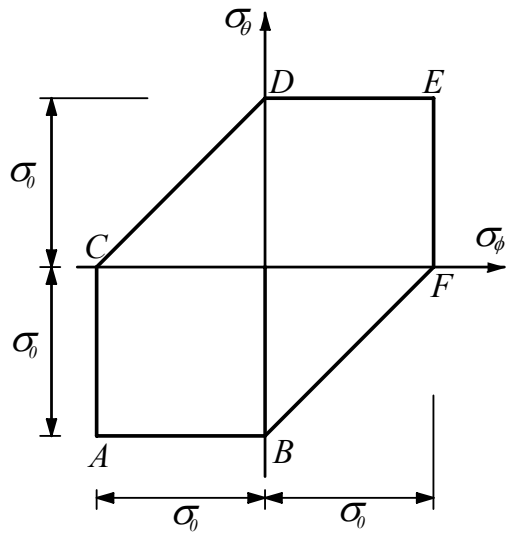

Fig. 2.5 Tresca yield condition

2.3.2 Basic equations

Consider a uniform strength design of a spherical shell under hydrostatic pressure, selfweight and skin cover load. Assuming the dome to carry the load to the foundation via membrane forces, we seek the variation of the shell thickness h with respect to the meridian angle.

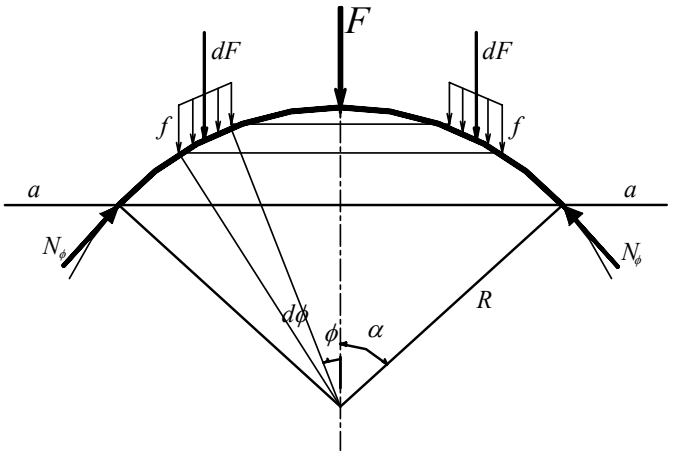

Fig. 2.6 Free body diagram of dome above horizontal plane a-a

Referring to Fig. 2.6, the vertical resultant force F on a free body of the spherical dome above the horizontal plane a-a (defined at angle ϕ) is given by

$$F = 2\pi N_\phi R \sin^2 \phi \tag{2.11}$$

where $N_\phi = -\sigma_\phi h$ is the meridian force per unit length and σ_ϕ the meridian stress.

The incremental vertical force dF corresponding to the incremental angle $d\phi$ is given by

$$dF = f\, 2\pi R^2 \sin\phi d\phi \tag{2.12}$$

where f is the vertical force acting on an elemental strip of the dome (see Fig. 2.6) and is given by

$$f = p_{hv} + p_c + p_a = \gamma_w (D + R\cos\alpha - R\cos\phi)\cos\phi + p_c + \gamma_a h \tag{2.13}$$

where p_{hv}, p_c, and p_a are the vertical components of the hydrostatic pressure, the skin cover load, and the selfweight, respectively, γ_a is the specific weight of the dome material, γ_w the specific weight of water and D the depth of water.

By taking total differential of Eq. (2.11) and noting that the meridian force is $N_\phi = -\sigma_\phi h$, Eq. (2.12) can be re-written as

$$-\left(\sigma_\phi h' \sin\phi + 2\sigma_\phi h \cos\phi\right) = fR \tag{2.14}$$

where the prime denotes differentiation with respect to ϕ. By substituting f given in Eq. (2.13) into Eq. (2.14), one obtains

$$-\left(\sigma_\phi h' \sin\phi + 2\sigma_\phi h \cos\phi\right) = \left[\gamma_a h + p_c + \gamma_w \cos\phi\left(D + R\cos\alpha - R\cos\phi\right)\right]R \quad (2.15)$$

Consider the fully stressed state of the dome material without tensile strength, i.e. the stress point lying on side AC of the Tresca hexagon. The meridian and circumferential stresses at this stress state are

$$\sigma_\phi = -\sigma_0 \,;\; 0 \geq \sigma_\theta \geq \sigma_\phi \quad (2.16)$$

where σ_0 is the allowable compressive stress and σ_θ the circumferential stress.

By applying Eq. (2.16) to Eq. (2.15) and dividing by $\left(\sigma_0 h_0\right)$, one obtains

$$\overline{h}' \sin\phi = \overline{h}\left(\overline{R} - 2\cos\phi\right) + \overline{p}_c \overline{R} + \overline{\gamma}_w \overline{R} \cos\phi\left(\overline{D} + \overline{R}\cos\alpha - \overline{R}\cos\phi\right) \quad (2.17)$$

where the non-dimensional terms with over-bars are given by

$$\overline{\sigma}_\phi = \frac{\sigma_\phi}{\sigma_0},\ \overline{\sigma}_\theta = \frac{\sigma_\theta}{\sigma_0} = \beta\overline{\sigma}_\phi, \quad (2.18a\text{-}b)$$

$$\overline{h} = \frac{h}{h_0},\ \overline{\gamma}_w = \frac{\gamma_w \sigma_0}{{\gamma_a}^2 h_0}, \quad (2.18c\text{-}d)$$

$$\overline{R} = \frac{R\gamma_a}{\sigma_0}, \quad (2.18e)$$

$$\overline{D} = \frac{D\gamma_a}{\sigma_0} \text{ and } \overline{p}_c = \frac{p_c}{\gamma_a h_0} \tag{2.18f-g}$$

Note that Eq. (2.17) contains the non-dimensional pressure $\overline{p}_c$ which can be eliminated as follows. The condition of equilibrium in the normal direction furnishes (Ugural, 1999)

$$N_\phi + N_\theta = -Rp_n \tag{2.19}$$

where p_n is the normal load component per unit area of the middle surface and is positive when acting inwards. The normal load consists of components from the hydrostatic pressure, dome selfweight and skin cover load and is given by

$$p_n = \left(\gamma_a h + p_c\right)\cos\phi + \gamma_w\left(D + R\cos\alpha - R\cos\phi\right) \tag{2.20}$$

From Eqs. (2.16), (2.18), (2.19) and (2.20), the ratio of the circumferential stress to the meridian stress is given by

$$\beta = \frac{\overline{\sigma}_\theta}{\overline{\sigma}_\phi} = \frac{\left(\overline{h} + \overline{p}_c\right)\overline{R}\cos\phi + \overline{\gamma}_w\overline{R}\left(\overline{D} + \overline{R}\cos\alpha - \overline{R}\cos\phi\right)}{\overline{h}} - 1 \tag{2.21}$$

where $0 \le \beta \le 1$ in order to ensure that the stress state condition (2.16) is satisfied.

In axisymmetric domes of revolution, the stresses σ_ϕ and σ_θ at the apex $\left(\phi = 0\right)$ must approach the same limit, i.e.

$$-\bar{\sigma}_\theta = -\bar{\sigma}_\phi = 1, \text{ at the apex } \phi = 0 \text{ where } \bar{h} = 1 \tag{2.22}$$

By imposing the above limiting condition, Eq. (2.20) can be written as

$$\bar{p}_c \bar{R} = 2 - \bar{R}\left[1 + \bar{\gamma}_w\left(\bar{D} + \bar{R}\cos\alpha - \bar{R}\right)\right] \tag{2.23}$$

and by substituting $\bar{p}_c$ given in Eq. (2.22) into Eq. (2.17), we have

$$\bar{h}'\sin\phi + \bar{h}\left(2\cos\phi - \bar{R}\right) + \bar{\gamma}_w \bar{R}\left(\bar{D} + \bar{R}\cos\alpha\right)\left(1 - \cos\phi\right) - \bar{\gamma}_w \bar{R}^2\left(1 - \cos^2\phi\right) + \bar{R} - 2 = 0 \tag{2.24}$$

Equation (2.24) is the governing differential equation for determining the thickness variation of the submerged spherical dome of uniform strength.

Note that for the special case of zero hydrostatic pressure (i.e. $\bar{\gamma}_w = 0$), Eq. (2.24) reduces to

$$\bar{h}'\sin\phi + \bar{h}\left(2\cos\phi - \bar{R}\right) + \bar{R} - 2 = 0 \tag{2.25}$$

which corresponds to the expression derived by Prager and Rozvany (1980).

2.4 Results and discussions

2.4.1 Analytical solution using power series method

In order to solve the foregoing first-order ordinary differential equation (2.24), we represent the function $\bar{h}(\phi)$ in the form of a power series:

$$\bar{h}(\phi) = c_0 + c_1\phi^2 + c_2\phi^4 + c_3\phi^6 + \ldots + c_n\phi^{2n} = \sum_{i=0}^{n} c_i\phi^{2i} \tag{2.26}$$

The differentiation of the normalized dome thickness $\bar{h}(\phi)$ with respect to the meridian angle ϕ gives

$$\bar{h}'(\phi) = 2c_1\phi + 4c_2\phi^3 + 6c_3\phi^5 + \ldots + 2nc_n\phi^{2n-1} = \sum_{i=1}^{n} (2i)c_i\phi^{2i-1} \tag{2.27}$$

In order to facilitate the analytical solution, trigonometric functions of Eq. (2.24) are also expressed in the form of power series, i.e.

$$\sin\phi = \phi - \frac{\phi^3}{3!} + \frac{\phi^5}{5!} - \frac{\phi^7}{7!} + \ldots; \tag{2.28a}$$

$$\cos\phi = 1 - \frac{\phi^2}{2!} + \frac{\phi^4}{4!} - \frac{\phi^6}{6!} + \ldots \tag{2.28b}$$

By substituting the power series given in Eqs. (2.26) to (2.28) into Eq. (2.24) and then comparing the coefficients, one obtains the following recursive formula for the coefficients c_i

$$c_i = \left(\frac{1}{2i+2-\overline{R}}\right)\left[\frac{(-1)^i \overline{\gamma}_w \left(\overline{D}+\overline{R}\cos\alpha\right)\overline{R}}{(2i)!} + \frac{(-1)^{i+1} 2^{2i-1} \overline{\gamma}_w \overline{R}^2}{(2i)!} + \sum_{j=1}^{i} \frac{2(-1)^{j+1}(i+j+1)c_{i-j}}{(2j+1)!}\right] \tag{2.29}$$

with $c_0 = 1$. With these known coefficients c_i, the variation of normalized dome thickness $\overline{h}(\phi)$ is fully described by Eq. (2.26). For given values of σ_0, p_c, γ_a, γ_w, R, D and α, and noting that $\overline{p}_c = p_c/(\gamma_a h_0)$, we can use Eq. (2.23) to calculate the thickness of the dome at the apex h_0, as

$$h_0 = \frac{p_c R + \gamma_w R(D + R\cos\alpha - R)}{2\sigma_0 - R\gamma_a} = \frac{p_c R + \gamma_w R(D - H)}{2\sigma_0 - R\gamma_a} \tag{2.30}$$

2.4.2 Accuracy of Analytical Solution for Dome Thickness

The analytical solution for the normalized shell thickness is furnished by Eqs. (2.26) and (2.29). In order to check the correctness of the analytical solutions, we can solve the problem independently by integrating numerically the first-order ordinary differential equation (2.24) using the Runge-Kutta method (Kreyszig 1993). For this test, a dome with dimensions R = 500cm, D = 4000cm, α = 2.5 radians and material properties σ_0 = 75 kgf/cm^2, γ_a = 0.0024 kgf/cm^3, and the skin cover load $p_c = 0.5$ kgf/cm^2 are assumed. The analytical solution is computed using exponents of n = 5, 7 and 9 while a very small step size of $\Delta\phi = 0.0001$ *rad* is used for the fourth-order Runge-Kutta method to ensure a high accuracy.

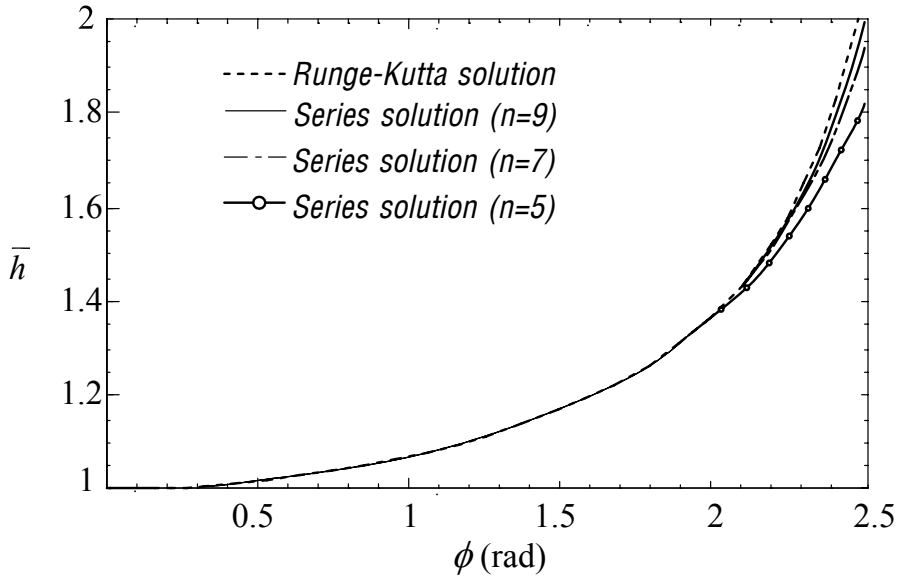

Fig. 2.7 Thickness variation obtained by series and numerical methods

The variations of normalized shell thickness $\bar{h}$ with respect to the meridian angle ϕ, obtained from both the analytical and numerical methods, are shown in Fig. 2.7. It can be seen that the thickness of the submerged dome is characterized by a fairly rapid increase in the large meridian angle range (e.g. $\phi > 2$ radians). The shell thickness at $\phi = 2.5$ radians is almost twice as thick as the shell at the apex. A comparison between the analytical and numerical solutions also indicates that the analytical solution agrees well with the numerical solution for all three exponents in the small meridian angle range i.e. $0 \le \phi < 2$ radians. A slight divergence of the analytical solution is noted in the large meridian angle range. However, an increasing order of the exponent gives rise to a better agreement with the numerical solution. For this example, an exponent of n = 9 gives an approximate solution that is sufficiently close to the numerical solution. This test establishes the correctness of the analytical solutions and for practical applications, it will be assumed that a power series with 9 terms is sufficient for estimating the shell thickness. This number of terms will thus be used for all calculations following.

2.4.3 Critical Value of Subtended Angle

In order to satisfy the stress state condition (2.16), we have to ensure that the condition $0 \le \beta \le 1$ is observed for the entire range $0 \le \phi \le \alpha$. This implies that for a given water depth D and base radius L (or dome radius R), there is a critical subtended angle α_{cr} (or a critical dome height $H_{cr} = R(1-\cos\alpha_{cr}) = L(1-\cos\alpha_{cr})/\sin\alpha_{cr}$). The α_{cr} value is evaluated by setting $\beta = 0$, $\phi = \alpha_{cr}$ and $\alpha = \alpha_{cr}$ in Eq. (2.24). This results in the transcendental equation:

$$\left(\overline{R}\cos\alpha_{cr} - 1\right)\left(\sum_{i=0}^{n} c_i \alpha_{cr}^{2i}\right) + \overline{p}_c \overline{R}\cos\alpha_{cr} + \overline{\gamma}_w \overline{R}\,\overline{D} = 0 \tag{2.31}$$

from which α_{cr} is to be evaluated.

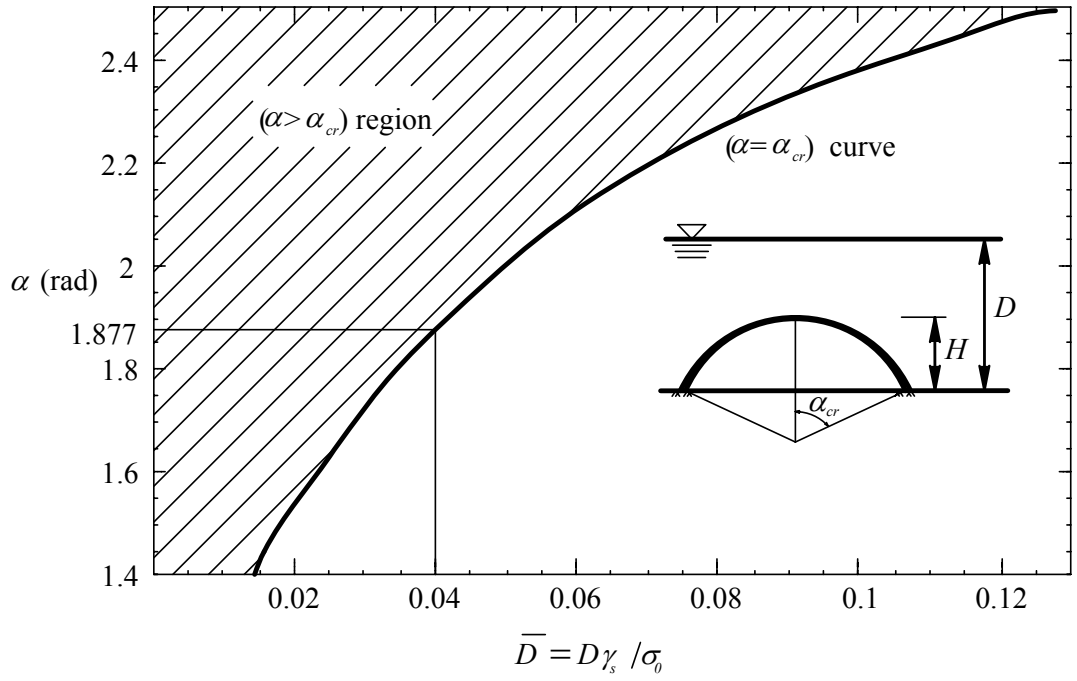

Fig. 2.8 Variation of α_{cr} with respect to water depth $\overline{D}$

As an example in finding α_{cr}, consider a spherical dome of R = 500 cm under various water depths D ranging from 625 cm to 4000 cm. The assumed material properties are σ_0 = 75 kgf/cm^2, γ_a = 0.0024 kgf/cm^3 and the skin cover load is taken as $p_c = 0.5$ kgf/cm^2. By solving Eq. (2.31), we obtain the variation of α_{cr} with respect to the non-dimensional water depth $\overline{D}$ as shown in Fig. 2.8. For a given water depth $\overline{D}$, the subtended angle α of the dome has a critical value $\alpha = \alpha_{cr}$ to ensure that there is no tensile stress region in the entire dome structure. Domes shapes with $\alpha > \alpha_{cr}$ in shaded region of Fig. 2.8 have the tensile stress region in the lower base of domes. For example, if the dome is submerged in a water depth of $\overline{D} = 0.04$, the maximum subtended angle that the dome can have is $\alpha_{cr} = 1.877$ radians. Beyond this α_{cr} value in the shaded area, a tensile stress region will appear in the lower base of the dome. It can be seen that as α_{cr} increases with water depth D, the dome is restricted to a flatter profile.

2.4.4 Effect of water depth on thickness variation

It is clear that the thickness variation of the submerged domes depends on the water depth, the selfweight and the skin cover load. In this section, we study the effect of the water depth $\overline{D}$ on the thickness variation when the dome shape is defined by a given subtended angle α. Figure 2.9 shows the normalized thickness $\overline{h} = h / h_0$ variations of submerged hemispherical domes with R = 500 cm and $\alpha = \pi / 2$ radians for various values of $\overline{D}$. It can be seen that the normalized thickness at the base of the dome is relatively sensitive to the water depth. A larger normalized thickness ratio at the base is associated with a shallow water depth.

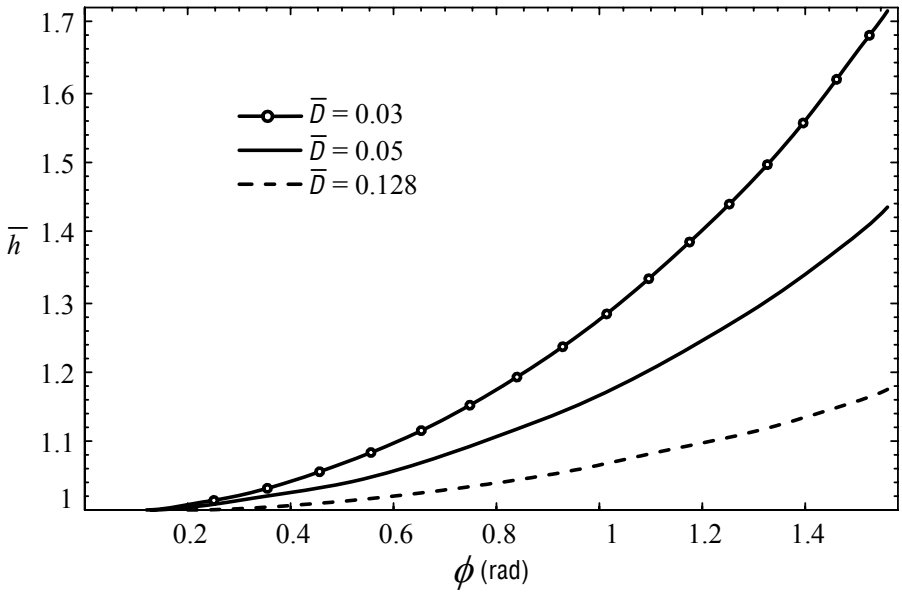

Fig. 2.9 Thickness variations of submerged domes for various water depths

2.4.5 Minimum weight design

For a given water depth D and a base radius L, there is a family of uniform strength designed domes. Each dome is associated with a subtended angle α (or dome height $H = L(1-\cos\alpha)/\sin\alpha$) as shown in Fig. 2.10. However, there is a minimum weight solution within this family of solutions that we want to seek because of its practical importance. This optimal solution is associated with the optimal subtended angle α_{opt}. For a given base radius, the non-dimensional optimal height $\overline{H}_{opt} = H_{opt}\gamma_a / \sigma_0$ of the submerged dome is related to α_{opt} by

$$\overline{H}_{opt} = \frac{\overline{L}}{\sin\alpha_{opt}}(1-\cos\alpha_{opt}) \tag{2.32}$$

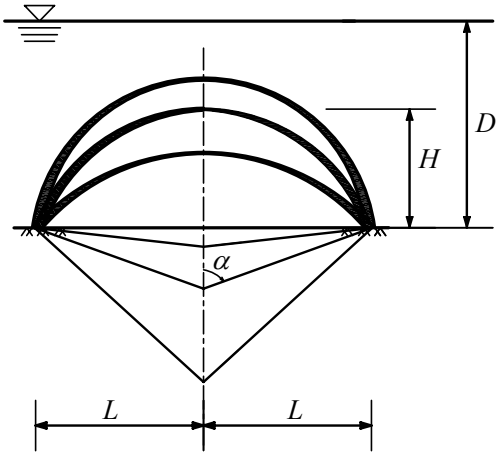

Fig. 2.10 Family of uniform strength designed domes for a given base radius L

The objective function of this optimization problem is defined by the selfweight of the dome. The selfweight W_0 can be calculated directly by integrating the product of $\bar{h}$ and the surface area of the dome, *i.e.*

$$W_0 = \gamma_a \int_0^{\alpha} h.2\pi R\sin\phi.Rd\phi \tag{2.33}$$

or in normalized form as

$$\overline{W}_0 = \frac{W_0}{\pi p_c L^2} = \frac{2}{\bar{p}_c \sin^2\alpha} \int_0^{\alpha} \bar{h}\sin\phi d\phi \tag{2.34}$$

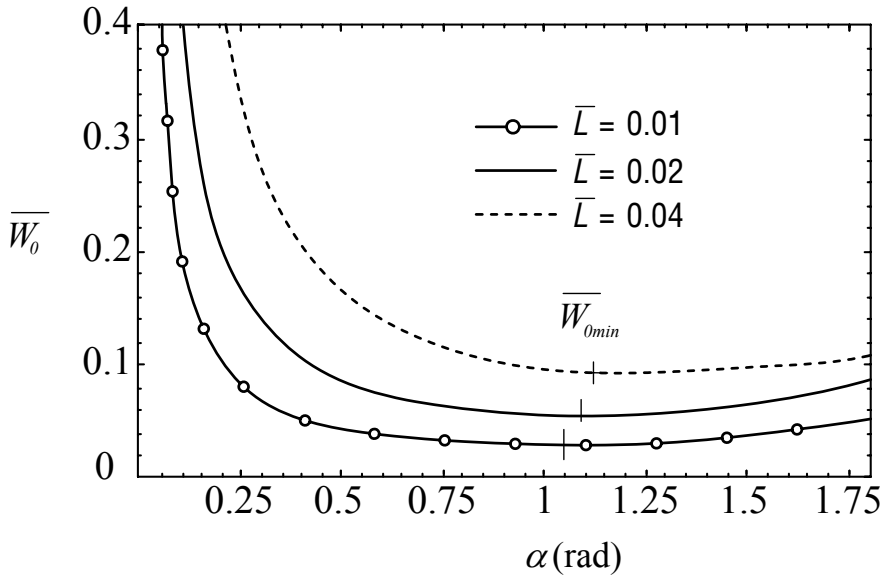

Fig. 2.11 Variations of weight $\overline{W}_0$ with respect to subtended angle α for $\overline{L} = 0.01,\ 0.02$ and 0.04

The variations of $\overline{W}_0$ with respect to the subtended angle α are shown in Fig. 2.11 for a given water depth D = 1500 cm for various base radii $\overline{L}$ = 0.01, 0.02 and 0.04. The variation of $\overline{W}_0$ is rather small over a wide range of α, especially when the base radius of the dome is small. The insensitivity of the dome weight for $1 \text{ radian} \le \alpha \le 1.25 \text{ radians}$ (which contains the optimal of subtended angle) is good news for engineers as it means that there is some flexibility when designing the dome shape without compromising too much on the optimum weight. It can be seen that the optimal subtended angle α_{opt} is about 1.1 radians.

Using the thickness variation $\overline{h}$, as given by Eq. (2.26), one can obtain the optimal value of the subtended angle α_{opt} for a minimum value of $\overline{W}_0$ by a simple minimization technique such as the Golden Section Search technique (Kreyszig 1993). Figure 2.12 shows the values of α_{opt} and W_{omin} with D = 5000 cm for a wide range

of practical base radii $\overline{L}$ (i.e. $0.01 \le \overline{L} \le 0.055$). It can be seen that α_{opt} varies in a narrow range of 1.04 radians $\le \alpha_{opt} \le$ 1.14 radians.

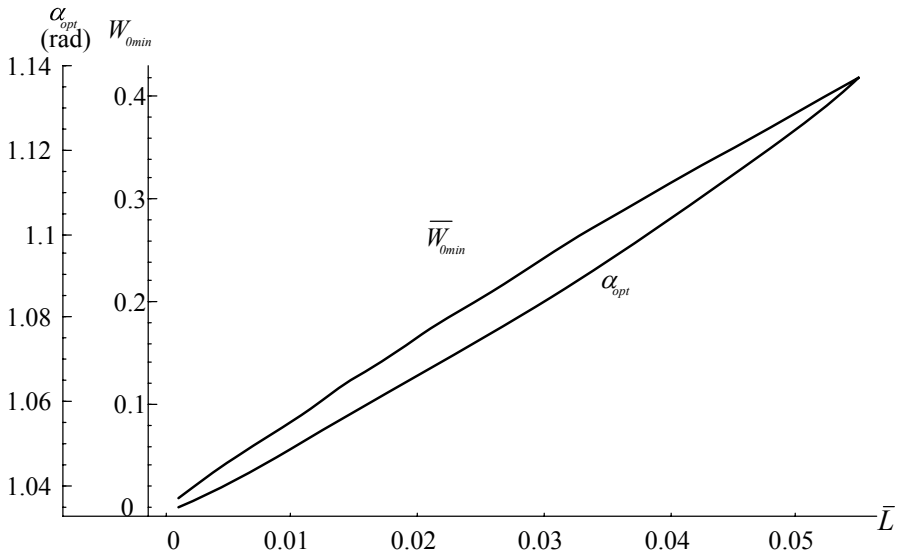

Fig. 2.12 Variations of minimum weight $\overline{W}_0$ and α_{opt} with respect to base radius $\overline{L}$

The relationship between the optimal dome height and water depth is also of interest in the minimum weight design of submerged domes. Figure 2.13 shows the variations of the optimal dome height to base radius ratio H_{opt}/L with respect to the water depth to base radius ratio D/L. It can be seen that the optimal shape of the spherical dome gets flatter with increasing water depth, but the optimal height to base radius ratio varies within a small range ($0.58 \le H_{opt}/L \le 0.61$) for a wide range of practical water depths ($5 \le D/L \le 30$). For very deep water, the optimal height of the dome is approximately $H_{opt}/L = 1/\sqrt{3}$ or $\alpha_{opt} = \pi/3$ radians.

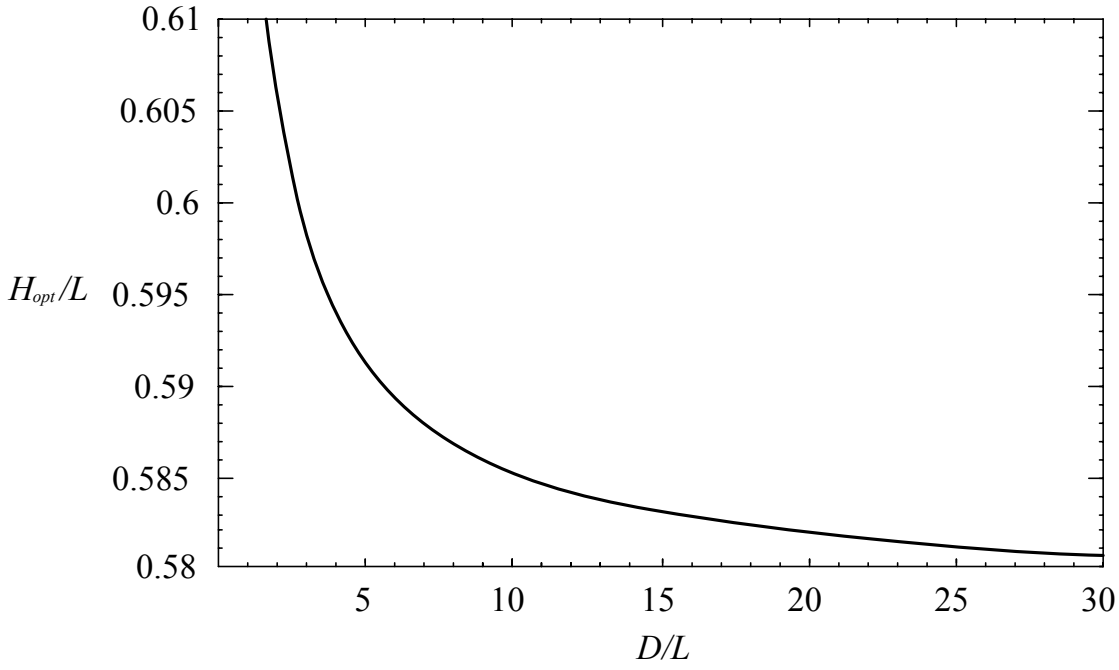

Fig. 2.13 Variation of optimal dome height H_{opt}/L with respect to water depth D/L

2.5 Concluding Remarks

In this chapter, we have derived an analytical expression in the form of a power series for the thickness variation of a submerged spherical dome in a uniform strength design as governed by the Tresca yield condition. Numerical examples show that the sum of the first 9 terms in the power series is sufficiently accurately for practical applications. Further, the optimal subtended angle α_{opt} (and the optimal dome height H_{opt}) for the minimum weight design of these domes have been determined. For very deep water, it was found that the optimal height of the dome is approximately $H_{opt}/L = 1/\sqrt{3}$ or $\alpha_{opt} = \pi/3$ radians.

Although the present chapter considers only spherical domes, the next chapter will treat non-spherical domes where the aim is to determine the optimal thickness variation as well as the shape of fully stressed submerged domes for minimum weight.

CHAPTER 3

CONSTANT STRENGTH DESIGNS OF SUBMERGED GENERAL DOMES

This chapter is concerned with the membrane analysis and optimal design of constant strength submerged domes. In addition to hydrostatic pressure, the domes are also subjected to selfweight and skin cover load, which are invariably present in this type of structure. Using membrane theory for thin shells and by adopting a fully stressed design, equations governing the meridional curve of submerged domes are derived with allowance for selfweight and skin cover load. The set of nonlinear differential equations, which correspond to a two-point boundary problem, is solved by the shooting-optimization method. Based on a family of fully stressed (constant strength) designs associated with a given water depth and dome height, the optimal dome shape for minimum weight is determined.

3.1 Introduction

In 1959, Timoshenko and Woinowsky-Krieger (1959) presented the optimal shape for domes under hydrostatic pressure only. Royles *et al.* (1980) pointed out that the optimal shape of submerged domes is similar to the shape of a sea urchin, which is a member of marine invertebrates in the phylum Echinodemata. Figure 3.1 shows the calcareous shell of a sea urchin after its spines have been removed. Due to their similarity, the optimal shape of fully stressed submerged domes under hydrostatic load has been referred to as an Echinodome by Royles *et al.* (1980). So far, little work has been done on the optimization of fully stressed submerged domes with allowance for selfweight. Prompted by this fact, we focus our study on the membrane analysis and the optimal shape of fully stressed domes under selfweight, hydrostatic pressure upon submergence in water and skin cover load arising from attachments on the domes.

Fig. 3.1 Calcareous shell of a sea urchin

3.2 Problem definition and basic equations

3.2.1 Problem definition

Consider a shell of revolution of height H and submerged under water at a depth D. Figure 3.2 shows the geometry of the submerged dome as defined by its meridian. Referring to the figure, r_0 is the distance from a point on the meridian to the vertical axis z, which is pointed in the gravity direction, and r_1 is the radius of curvature of the meridian. The principal radius r_2 generates the middle surface of the dome in the direction perpendicular to the tangent on the meridian. Only dome shapes involving positive values of r_1 and r_2 are considered. A second coordinate system, defined by the arc length s along the meridian angle ϕ, is also shown in Fig 3.2.

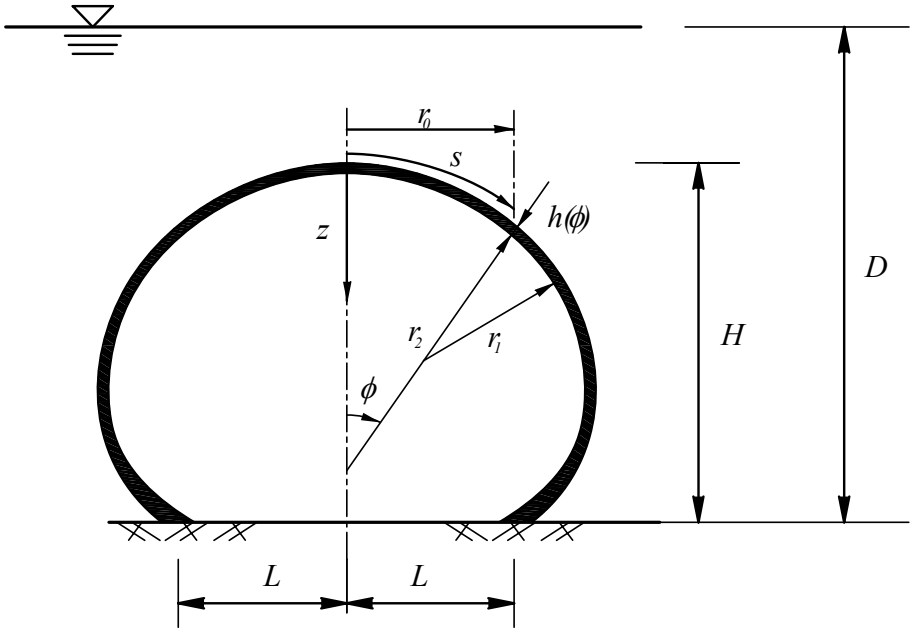

Fig. 3.2 Coordinate systems and parameters defining the shape of submerged dome

By adopting a fully stressed design, the problem at hand is to determine the thickness variation of the submerged dome under hydrostatic, selfweight and skin cover load. The optimal shape of submerged domes for least weight condition is sought as part of the solution.

3.2.2 Governing equations for membrane analysis of submerged domes

Consider a dome subjected to three types of loads: (i) hydrostatic pressure $p_h = \gamma_w(D - H + z)$, (ii) selfweight $p_a = \gamma_a h$ where h is thickness that varies with respect to the angle ϕ and (iii) skin cover load p_c. The positive direction of these loads and their distributions are shown in Fig. 3.3. Note that the skin cover load p_c in Fig 3.3(c) is defined as force per unit surface area and is assumed to be constant in this chapter. However, the skin cover load is indicated as varying in Fig. 3.3c due to the projection of the skin cover load on the horizontal plane. In deriving the governing equations for submerged domes, resolution of the forces normal and tangential to the middle surface is appropriate. In this case, net components of the load's normal p_n and tangential p_s to the middle surface are given by

$$p_n = (\gamma_a h + p_c)\cos\phi + \gamma_w(D - H + z) \tag{3.1}$$

$$p_s = (\gamma_a h + p_c)\sin\phi \tag{3.2}$$

respectively where γ_a is the specific weight of the dome material and γ_w is the specific weight of water.

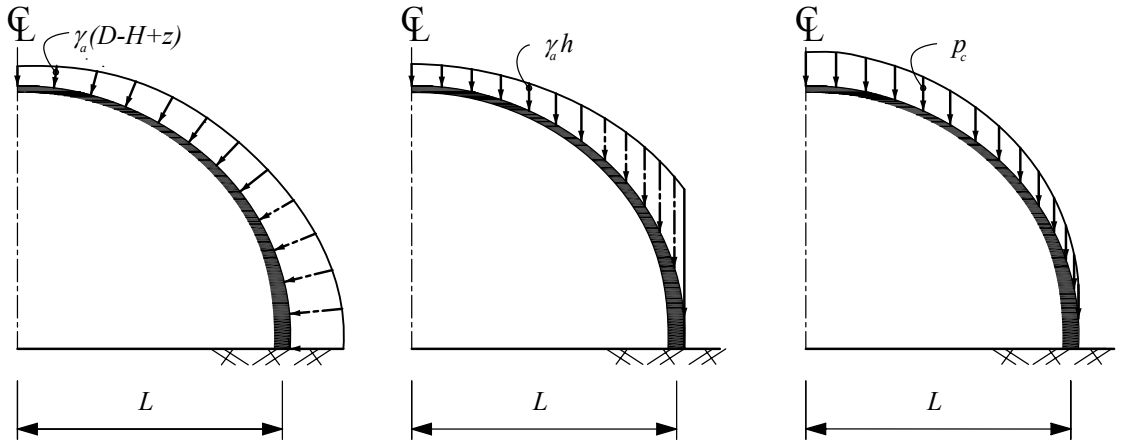

(a) Hydrostatic pressure **(b)** Selfweight **(c)** Skin cover load

Fig. 3.3 Load components on submerged domes

By considering equilibrium of forces in the shell of revolution in the normal ϕ-direction, one obtains the well known equation

$$\frac{N_\phi}{r_1} + \frac{N_\theta}{r_2} = -p_n \tag{3.3}$$

where $N_\phi = \sigma_\phi h$ and $N_\theta = \sigma_\theta h$ are the membrane forces in the meridional and circumferential directions, respectively. Note that unlike typical analyses, which involve the determination of membrane forces for a defined geometry of the dome, the task at hand corresponds to the inverse of the problem where the geometry of the dome is to be determined for prescribed stresses in the two principal directions.

To this end, consider the special case of a fully compressed dome where the meridian and circumferential stresses take on the same stress value

$$\sigma_\phi = \sigma_\theta = -\sigma_0 \tag{3.4}$$

in which σ_0 is the allowable compressive stress. It is thus implicitly assumed that buckling of the dome will not occur and that the stress condition defined by Eq. (3.4) can be achieved under the load combination.

By substituting Eq. (3.4) and Eq. (3.1) into Eq. (3.3), one obtains the condition for curvature variation of the dome i.e.

$$\frac{1}{r_1} = \frac{(\gamma_a h + p_c) r_2 \cos\phi + \gamma_w r_2 (D - H + z) - \sigma_0 h}{\sigma_0 h r_2} \tag{3.5}$$

In order to facilitate the solution of Eq. (3.5), the following geometrical relations for the shell of revolution are required

$$r_1 = \frac{ds}{d\phi} \tag{3.6a}$$

$$r_0 = r_2 \sin\phi \tag{3.6b}$$

$$dr_0 = ds \cos\phi \tag{3.6c}$$

$$dz = ds \sin\phi \tag{3.6d}$$

For generality, the following non-dimensional terms (denoted with over-bars) are introduced for the geometric and stress parameters

$$\overline{D} = \frac{D}{H},\ \overline{L} = \frac{L}{H}, \tag{3.7a-b}$$

$$\overline{r}_0 = \frac{r_0}{H},\ \overline{h} = \frac{h}{H}, \tag{3.7c-d}$$

$$\bar{l} = \frac{l}{H},\ \bar{z} = \frac{z}{H},\ \bar{s} = \frac{s}{l}, \tag{3.7e-g}$$

$$\bar{p}_c = \frac{p_c}{\sigma_0},\ \bar{\alpha} = \frac{\gamma_w H}{\sigma_0},\ \bar{\beta} = \frac{\gamma_a H}{\sigma_0} \tag{3.7g-i}$$

where l is the curve length for one-half of the meridian and s is the arc length along the meridian as measured from the apex of the dome (see Fig. 3.2). Using the geometrical relations of Eq. (3.6) and definitions in Eq. (3.7), the following differential equation governing the shape of the meridian in normalized form can be obtained

$$\frac{d\phi}{d\bar{s}} = \frac{\left[\left(\overline{\beta h} + \bar{p}_c\right)\bar{r}_0 \cos\phi + \overline{\alpha r}(\bar{D} - 1 + \bar{z}) - \bar{h}\sin\phi\right]\bar{l}}{\bar{h}\bar{r}} \tag{3.8}$$

In this case, the shape of the meridian, which is defined by the angular change of the middle surface with respect to the arc length, depends on all three load components.

Although Eq. (3.8) involves only a first-order differential equation, it must be solved in combination with the equilibrium condition of the shell in the meridian direction. To this end, the equation for equilibrium of forces in the s-direction, which is well known, is given by

$$\frac{d}{ds}\left(r_0 N_s\right) - N_\theta \cos\phi = -p_s r_0 \tag{3.9}$$

By substituting Eqs. (3.2), (3.4), (3.6) and (3.7) into Eq. (3.9), one obtains the variation of the meridian thickness in normalized form as

$$\frac{d\bar{h}}{d\bar{s}} = \left(\overline{\beta h} + \bar{p}_c\right)\bar{l}\sin\phi \tag{3.10}$$

Thus Eqs. (3.8) and (3.10) correspond to the equilibrium condition for the shell of revolution subjected to hydrostatic pressure, selfweight and skin cover load. The two equations may be solved in conjunction with the following normalized geometrical relations

$$\frac{d\bar{r}_0}{d\bar{s}} = \bar{l}\cos\phi \tag{3.11}$$

$$\frac{d\bar{z}}{d\bar{s}} = \bar{l}\sin\phi \tag{3.12}$$

which are obtained from Eqs. 3.6(c) and (d) using the definitions in Eq. (3.7). Note that the shape of the fully stressed submerged dome is characterized in terms of the Cartesian coordinates i.e. normalized $\bar{r}_0$ and $\bar{z}$, and is parameterized in terms of the normalized arc length $\bar{s}$, which is measured from the apex. An auxiliary result that forms a part of the solution includes the variation of the subtended angle ϕ and the variation of the dome thickness with respect to the normalized arc length $\bar{s}$.

3.2.3 Boundary conditions for membrane actions in fully stressed submerged domes

Because substantial forces are developed in the dome due to the combined effects of hydrostatic pressure, dome selfweight and skin cover load, an adequate foundation must be provided for the dome in order to ensure its integrity. Typically, domes are supported by a ring foundation at the base of the dome, where the loads are assumed to be transmitted to the ring foundation via membrane actions only. However, for the membrane theory to be valid for the aforementioned problem, the forces acting on the dome must be in equilibrium with the forces acting on the ring foundation, and the resulting deformation of the dome and ring foundation must be compatible at their boundary. In order to eliminate bending in the dome, which is pre-requisite for the membrane theory used here, the circumferential lengthening of the dome at the base must be equal to that of the supporting ring foundation (due to the horizontal component N_{rs} of meridian force N_s, see Fig. 3.4).

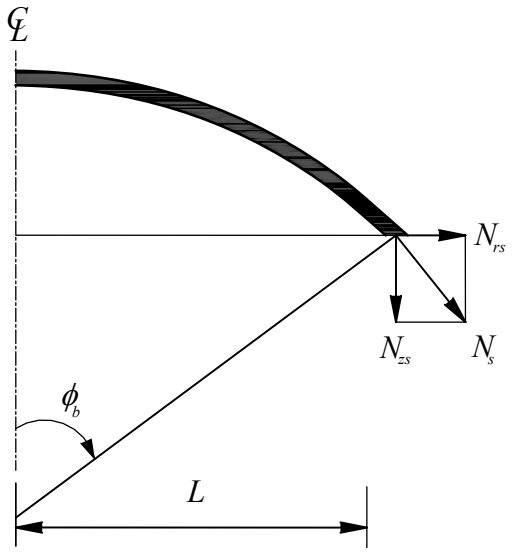

Fig. 3.4 Horizontal and vertical components of the meridian force N_s acting on the ring foundation

The stress in the supporting ring is given by Novozhilov (1970)

$$\sigma_k = \frac{N_{rs} r_0}{\Omega_k} = -\frac{N_s L}{\Omega_k} \cos\phi_b \tag{3.13}$$

where Ω_k is the cross-sectional area of the support ring, ϕ_b is the subtended angle at the dome base, L is the radius of the support ring, approximately equal to the radius at the dome base. The hoop stress at the dome base is equal to

$$\sigma_b = \frac{N_\theta}{h_b} \tag{3.14}$$

where h_b is the thickness at the dome base. By equating the hoop strain of the dome base to the extensional strain of the supporting ring, one obtains

$$-\frac{N_s L}{E_k \Omega_k} \cos\phi_b = \frac{N_\theta}{E h_b} \tag{3.15}$$

where E denotes the Young's modulus of the dome and E_k denotes the Young's modulus of the supporting ring and the Poisson ratio has been assumed to be equal to zero for both materials for simplicity. Therefore, the required cross-sectional area of the ring foundation may be calculated by the formula of Novozhilov (1970)

$$\Omega_k = -\frac{E}{E_k} \frac{N_s}{N_\theta} L h_b \cos\phi_b \tag{3.16}$$

Since the dome is assumed to be fully stressed, the circumferential stress and the meridian stress are equal to σ_0 and will have the same sign. Since the required area of the cross-section of the support ring has to be positive, Eq. (3.16) implies that in order for the dome to be in a fully stressed membrane state

$$\cos\phi_b < 0 \tag{3.17}$$

The inequality in Eq. (3.17) means that the subtended base angle ϕ_b of a fully stressed submerged dome has to be larger than $\pi/2$, or conversely, a dome with a subtended base angle ϕ_b of less than $\pi/2$ cannot be under a fully compressive stress state. Note that this condition is independent of the hydrostatic pressure, dome selfweight or imposed skin cover load.

3.3 Results and Discussions

In this section, numerical solutions for the dome thickness and shape are determined for two load cases. The first load case corresponds to purely hydrostatic pressure whereas the second load case consists of hydrostatic pressure, selfweight and skin cover load.

3.3.1 Weightless constant strength submerged domes

The thickness of the fully stressed dome can be represented as a function of elevation z by substituting the geometrical relation $dz = ds\sin\phi$ into Eq. (3.10). This leads to

$$\frac{d\bar{h}}{d\bar{z}} = \overline{\beta h} + \bar{p}_c \tag{3.18}$$

For the case of hydrostatic pressure only, the selfweight and skin cover load are zero leading to $\overline{\beta} = \bar{p}_c = 0$. Therefore, Eq. (3.18) reduces to

$$\frac{d\bar{h}}{d\bar{z}} = 0 \Rightarrow \bar{h} = \bar{h}_c = \frac{h_c}{D} = \text{constant} \tag{3.19}$$

Equation (3.19) implies that, for a fully stressed condition, a momentless dome has a constant thickness when subjected to hydrostatic pressure only.

In order to obtain the shape of such a submerged dome, one needs only to solve Eqs. (3.8), (3.11) and (3.12) since the thickness was determined to be constant. Therefore, the governing equations for this problem are

$$\frac{d\phi}{d\bar{s}} = \frac{\left[\overline{\alpha r_0}(\overline{D} - 1 + \bar{z}) - \bar{h}_c \sin\phi\right]\bar{l}}{\bar{h}_c \bar{r}} \tag{3-20 a}$$

$$\frac{d\bar{r}_0}{d\bar{s}} = \bar{l}\cos\phi \tag{3-20 b}$$

$$\frac{d\bar{z}}{d\bar{s}} = \bar{l}\sin\phi \tag{3.20 c}$$

For a given water depth D, specific weight of water γ_w, dome height *H*, constant thickness h_c, and an allowable compressive stress σ_0 (note that $\overline{\alpha} = \gamma_w H/\sigma_0$), there is a unique shape for the fully stressed submerged dome (Timoshenko and Woinowsky-Krieger, 1959 and Royles *et al.*, 1980). In order to determine this dome shape, the foregoing equations 3.20(a-c) are solved together with these boundary conditions that

$$\phi(0) = 0 \tag{3.21a}$$

$$\bar{r}_0(0) = 0 \tag{3.21b}$$

$$\bar{z}(0) = 0,\ \bar{z}(1) = 1 \tag{3.21c}$$

The set of nonlinear differential equations and boundary conditions i.e. Eqs. (3.20)-(3.21) constitute a two-point boundary value problem that can be solved using the shooting-optimization method as proposed by Wang and Kitipornchai (1992). In this method, the two-point boundary value problem is first converted into a set of initial value problems and the differential equations integrated forward by using the fourth-order Runge-Kutta algorithm (Kreyszig 1993). The only terminal boundary condition $\bar{z}(1) = 1$ to be satisfied can be taken care of by minimizing the objective function Φ with respect to the curved length $\bar{l}$, where Φ is defined by

$$\min_{\bar{l}} \Phi = \left|\bar{z}(1) - 1\right| \tag{3.22}$$

However, this optimization problem must be subjected to the inequality constraint

$$\phi(1) \geq \pi/2 \tag{3.23}$$

where $\bar{z}(1)$ and $\phi(1) = \phi_b$ are obtained from forward integration of the system of first order differential equations Eqs. 3.20(a-c). Note that the subtended angle at the base needs to satisfy the inequality $\phi_b \geq \pi/2$, as noted earlier, in order to ensure that the deformation of the dome at the base is compatible with the circumferential lengthening

of the ring foundation. The foregoing optimization problem can be solved using the generalized reduced gradient code GRG2 (Ladson *et al.* 1978). In this chapter, the accuracy of the solution is ensured by taking a very small step size $\Delta\bar{s} = 0.001$ in the forward integration in the Runge-Kutta algorithm (Kreyszig 1993)

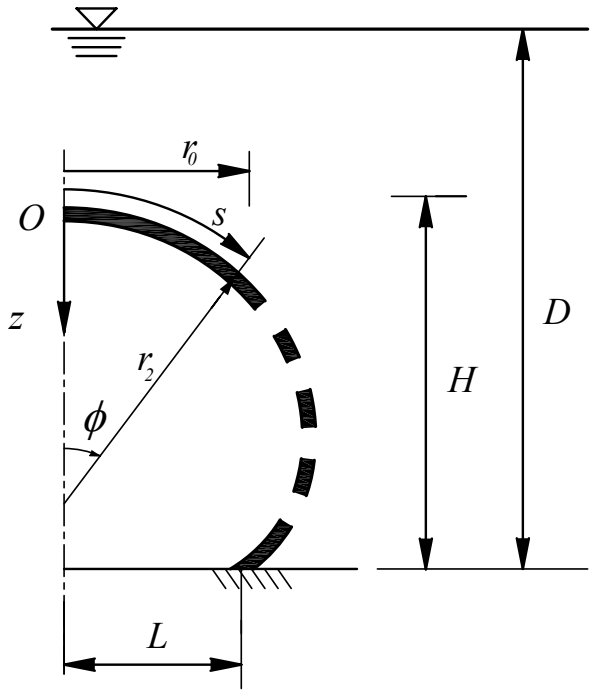

Fig. 3.5 Coordinate system for the Runge-Kutta forward integration

As an example, consider a dome of height $H = 1000$ cm and submerged at different water depths of $D = 2000$ cm, 2500 cm, 3000 cm and 3062 cm. The following values are assumed in the calculation: $h_c = 10$ cm, $\gamma_w = 1.10^{-3}$ kgf/cm^3 and $\sigma_0 = 75$ kgf/cm^2. These values give rise to $\alpha = 0.004$. Using the shooting optimization method, the shape of the submerged dome at different depths is plotted in the normalized coordinates $\bar{r}$ and $\bar{z}$ in Fig. 3.6. The final results indicated that the normalized curve length are $\bar{l}$ = 1.7240, 1.5355, 1.5071, 1.5732 for these depths. It can be seen from Fig. 3.6 that the submerged dome changes from a shape that is relatively

flat for shallow water to one that is highly curved for deep water. Note that the maximum water depth for this dome is $\overline{D} = 3.062$ and is associated with the limiting $\phi_b = \pi$ at its base. This limiting dome shape is often referred to as the Echinodome shape, which is easily understood by its remarkable resemblance to the shape of the sea urchin in Fig. 3.1 with the submerged dome shape at $\overline{D} = 3.3062$ in Fig. 3.6. Also note that for the case of $\overline{D} = 2$ the slope of the meridian is nearly vertical at the base of the dome with the angle ϕ_b slightly greater than $\pi/2$.

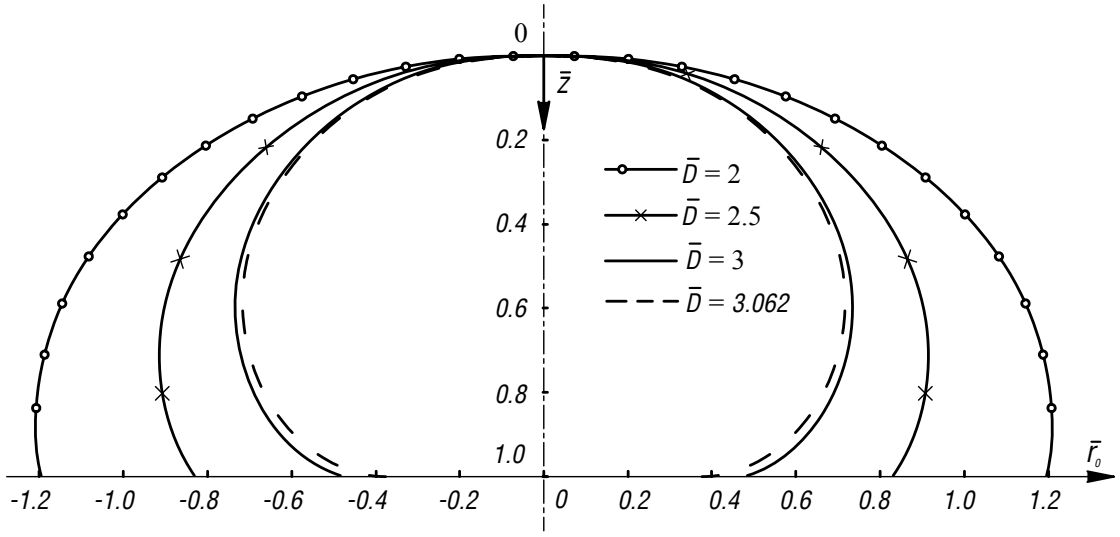

Fig. 3.6 Weightless fully stressed submerged dome shapes under various water depths

Although the above problem has been solved and well documented (see for example Timoshenko and Woinowsky-Krieger, 1959 and Royles *et al.*, 1980), it should be pointed out that our present formulation and solution technique have the following advantage. Owing to the complicated shape of the dome, Timoshenko and Woinowsky-Krieger (1959), Royles *et al.* (1980) and Sofoluwe *et al.* (1981) divided their calculations into three segments when integrating the dome shape in the *x* (or *z*) direction. The three segments, which depend on the value of the angle ϕ, were

necessary in order to avoid an infinite slope being encountered in the numerical solution. In the method proposed in this chapter, the entire shape of the dome can be determined without dividing the meridian into different segments since the integration is carried out using the arc length coordinate *s* and there is no difficulty in the solution for infinite slope. Although not explicitly shown in this chapter, the numerical solution for the shape of a submerged dome under hydrostatic pressure alone compares well with that presented by Timoshenko and Woinowsky-Krieger (1959) and Sofoluwe *et al.* (1981).

3.3.2 Constant strength of submerged general domes

For the second load case, the fully stressed dome is subjected to hydrostatic pressure, selfweight and a skin cover load. Unlike the case of hydrostatic pressure only, the dome thickness, which is defined by Eq. (3.10), cannot be uncoupled from the other three nonlinear equations. Consequently, one has to solve a set of four nonlinear ordinary differential equations as given by Eqs. (3.8), (3.10), (3.11) and (3.12)

$$\frac{d\phi}{d\bar{s}} = \frac{\left[\left(\overline{\beta h} + \bar{p}_c\right)\bar{r}\cos\phi + \overline{\alpha r}(\bar{D} - 1 + \bar{z}) - \bar{h}\sin\phi\right]\bar{l}}{\bar{h}\,\bar{r}} \tag{3.24a}$$

$$\frac{d\bar{h}}{d\bar{s}} = \left(\overline{\beta h} + \bar{p}_c\right)\bar{l}\sin\phi \tag{3.24b}$$

$$\frac{d\bar{r}_0}{d\bar{s}} = \bar{l}\cos\phi \tag{3.24c}$$

$$\frac{d\bar{z}}{d\bar{s}} = \bar{l}\sin\phi \tag{3.24d}$$

where $\phi, \bar{h}, \bar{r}_0, \bar{z}$ and $\bar{l}$ are the unknowns. This system of ordinary differential equations is solved in conjunction with these boundary conditions:

$$\phi(0) = 0 \tag{3.25a}$$

$$\bar{h}(0) = \bar{h}_0 \tag{3.25b}$$

$$\bar{r}(0) = 0 \tag{3.25c}$$

$$\bar{z}(0) = 0,\ \bar{z}(1) = 1 \tag{3.25d}$$

where $\bar{h}_0$ is the non-dimensional thickness at the apex of the dome. It should be noted that for this problem, the thickness is no longer constant but varying along the meridional curve.

Although the number of equations to be solved increases by one for the case of combined hydrostatic pressure, selfweight and skin cover load, these equations can also be treated as a two-point boundary value problem and solved using the same numerical technique described above for hydrostatic pressure only. The terminal boundary condition is satisfied by minimizing the objective function with respect to the curved length $\bar{l}$

$$\min_{\bar{l}} \Phi = \left|\bar{z}(1) - 1\right| \tag{3.26}$$

and the optimization problem is subjected to the inequality constraint given in (3.23). The values $\bar{z}(1)$ and $\phi(1)$ are obtained from forward integration of the system of first order differential equations Eq. 3.24(a-d). Since the shape of submerged domes subjected to combined hydrostatic pressure, selfweight and skin cover load has not been hitherto investigated, it is instructive to examine the influence of pertinent parameters on the shape of submerged domes.

3.3.2.1 Influence of water depth on dome shapes

Studies on submerged arches (Gavin and Reilly, 2000 and Chai and Kunnath, 2003) indicated that the shape of a momentless arch changes for a changing water depth. For deep water, the large hydrostatic pressure results in a funicular shape that tends to be circular, resulting in a small span length of the arch. On the other hand, shallow water results in a funicular shape that tends to be parabolic, resulting in a relatively long span. Although the observation was made on the basis of 2D structures, a shape change under different water depth is nonetheless expected of submerged domes.

In this section, the shape of a fully stressed submerged dome is investigated for three water depths, namely D = 2000 cm, 2500 cm and 3000 cm. The height of the dome is taken as H = 1000 cm and the thickness of the dome is taken as h_0 = 10 cm at the apex. The specific weight of water is taken as $\gamma_w = 1.10^{-3}$ kgf/cm^3 while the specific weight of the dome material is taken as $\gamma_a = 0.0024$ kgf/cm^3. The uniform skin cover load is assumed to be $p_c = 0.1$ kgf/cm^2, which is significant compared to the weight of the dome. The dome material is assumed to be uniformly compressed to an allowable stress of $\sigma_0 = 75$ kgf/cm^2. The shape of the meridian as obtained using the shooting optimization technique is plotted in Fig. 3.7 using the normalized Cartesian coordinates $\bar{r}_0$ and $\bar{z}$. The same step size of $\Delta\bar{s} = 0.001$ is used in this example.

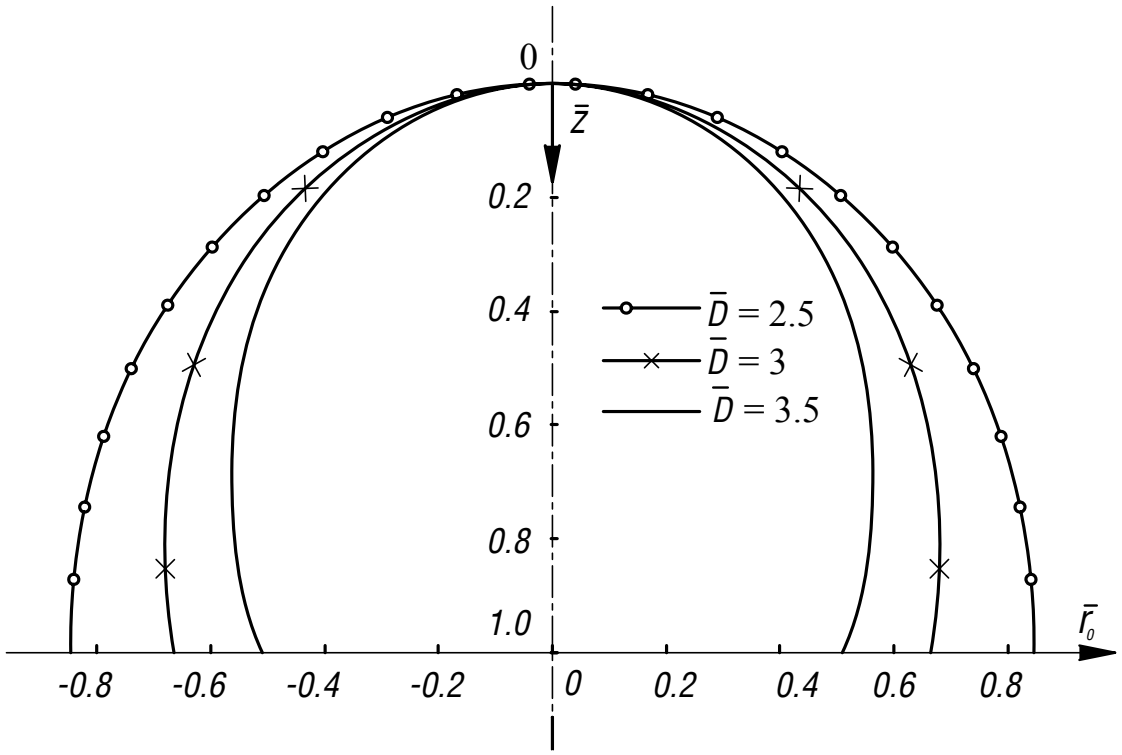

Fig. 3.7 Submerged dome shapes under selfweight and skin cover load for various water depths

It can be seen from Fig. 3.7 that the meridional shape of the dome changes under different water depths. Although the general shape of the dome under combined hydrostatic pressure, selfweight and skin cover load is similar to that under hydrostatic pressure alone, the base horizontal coordinate is smaller in the case of combined loading. For example, for the same normalized water depth of $\overline{D} = 3$, the base horizontal coordinate is $\bar{r}_b = 0.6636$ for the combined loading in Fig. 3.7, which is considerably larger than the base horizontal coordinate of $\bar{r}_b = 0.4291$ for hydrostatic pressure alone. The expansion in the base horizontal coordinate indicates the importance of including the effect of selfweight and skin cover load for determining the membrane (momentless) shape of the dome. It is also of interest to compare the dome shapes under different water depths but in combination with selfweight and skin

cover load. For the combined loads shown in Fig. 3.7, the base horizontal coordinate of the meridian reduces from $\bar{r}_b$= 0.8461 to $\bar{r}_b$= 0.6636 at the base as the water depth increases from $\overline{D} = 2.5$ to $\overline{D} = 3$. In contrast, the dome exhibits a more significant reduction in the base horizontal coordinate when subjected to hydrostatic pressure alone. For the same increment of water depths from $\overline{D} = 2.5$ to $\overline{D} = 3$, the horizontal coordinate at the base reduces from $\bar{r}_b$=0.7990 to $\bar{r}_b$=0.4291 as shown in Fig. 3.6. For the combined loads of hydrostatic pressure, selfweight and skin cover load, the change in the base horizontal coordinate is 21.6% as compared to 44.9% for the case of hydrostatic pressure alone. This comparison indicates that water depth exerts a lesser influence on the shape of fully stressed domes in the presence of selfweight and skin cover load. It can also be seen that the dome in Fig. 3.7 approaches an Echinodome-like shape with increasing water depth.

Although not explicitly shown in Fig. 3.7, the thickness of the dome increase from the apex to the base. The thickness variation with respect to $\bar{z}$, which is governed by Eq. (3.15), depends only on selftweight, skin cover load and dome height, but does not depend on hydrostatic pressure.

3.3.2.2 Effect of selfweight on dome shapes

In the application of submerged domes, various materials may be used for their construction. Since the weight of these materials is expected to have an influence on the membrane shape of the dome, the influence of selfweight is examined through a numerical example using the normalized selfweight parameter β which is defined as $\overline{\beta} = \gamma_a H / \sigma_0$.

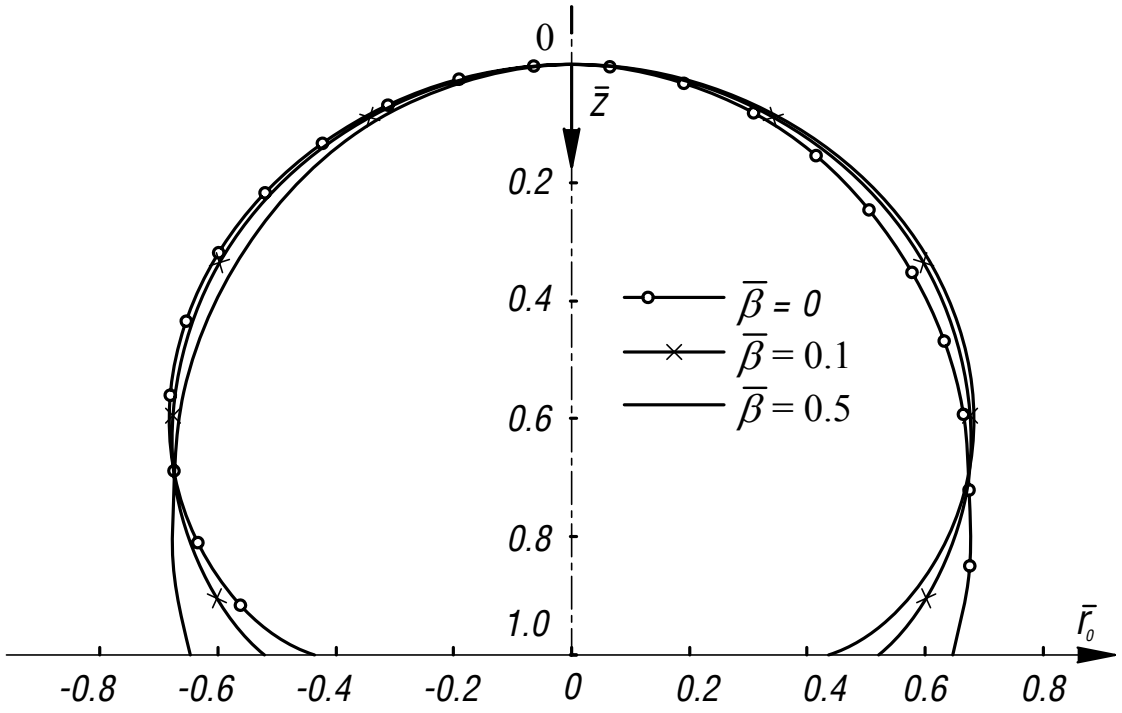

Fig. 3.8 Fully stressed submerged dome shapes with different selfweight parameter $\bar{\beta}$

Consider a fully stressed dome of height H = 1000 cm having an apex thickness h_0 = 10 cm submerged at the water depth D = 3000 cm. The allowable compressive stress of the dome material is assumed to be $\sigma_0 = 75$ kgf/cm^2. Three values are selected for the selfweight parameter for comparison, namely $\bar{\beta} = 0$ which corresponds to a weightless condition, $\bar{\beta} = 0.1$ and $\bar{\beta} = 0.5$. Note that the skin cover load skin is not included in this example i.e. p_c = 0 kgf/cm^2 so that the effect of selfweight on the dome shapes can be readily observed. The resulting dome shapes are plotted in Fig. 3.8, which indicates that the dome is characterized by a slight reduction in curvature of the meridian for increasing selfweight. In particular, the dome base radius increases with increased selfweight, which means that the dome shape deviates from that of the Echinodome shape as the selfweight parameter $\bar{\beta}$ increases. It is also evident from Fig. 3.8 there is a cross-over point where the coordinates of the meridian remains relatively constant despite the changing values of $\bar{\beta}$. For this example, the

cross-over point occurs in the vicinity of $\bar{r}_0 = 0.673$ and $\bar{z} = 0.690$.

3.3.2.3 Optimization of Submerged Domes

In characterizing the shape of fully stressed submerged domes, it is important to note that, for a given water depth and dome height, the shape of the domes is not unique but rather consists of a family of curves each of which is associated with a different value of the subtended base angle ϕ_b and dome apex thickness ho. Since each shape in the family of curves gives rise to a different overall weight of the dome, the variation of the dome weight with respect to base angle ϕ_b is important especially when the optimal shape of the dome is to be determined. To this end, the weight of the submerged dome is numerically integrated using the following expression in dimensionless form

$$\overline{W} = \frac{W}{2\pi\gamma_a H^3} = \bar{l}\int_0^1 \bar{h}\,\bar{r}_0\, d\bar{s} \tag{3.27}$$

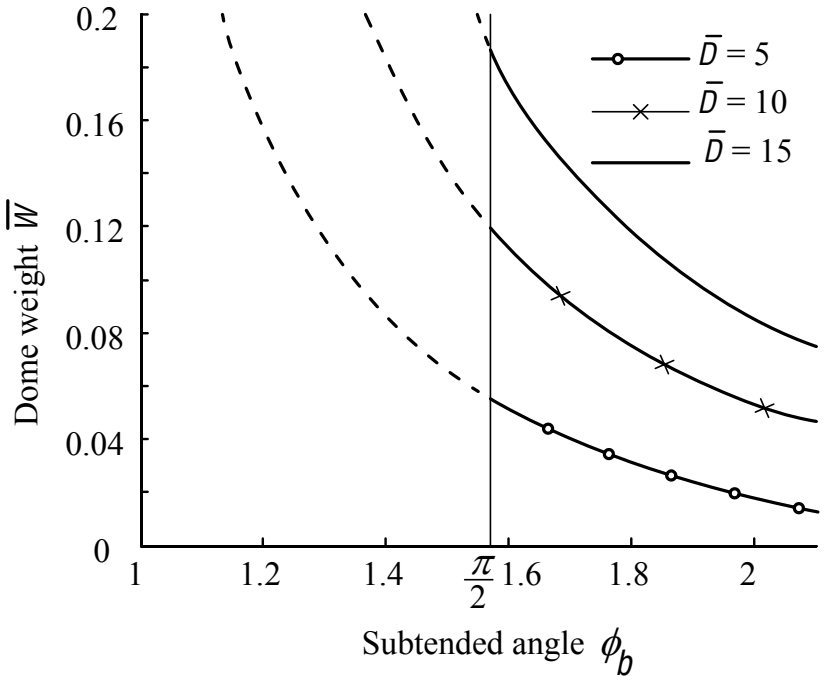

Fig. 3.9 Variation of submerged dome weight respect to subtended base angle ϕ_b

As an example, consider a dome height of H = 1000 cm, selfweight of $\gamma_a = 0.0024$ kgf/cm^3, skin cover load of p_c = 0.5 kgf/cm^2 and an allowable stress of $\sigma_0 = 75$ kgf/cm^2. The overall normalized weight of the dome is calculated for three normalized water depths of $\overline{D} = 5$, 10 and 15 and is plotted against the subtended base angle ϕ_b in Fig. 3.9. Note that, in order to ensure compatible deformation between the ring foundation and the base of the dome, the subtended angle at the base must satisfy $\phi_b \geq \pi/2$ as discussed earlier. The feasible solution space for the overall dome weight therefore lies to the right of the vertical line $\phi_b = \pi/2$ in Fig. 3.9. It can be seen from the figure that the normalized dome weight decreases monotonically with increasing values of the subtended base angle ϕ_b. Thus the problem of determining the optimal shape, which is defined by the minimum weight of the submerged dome, is equivalent to the problem of maximizing the subtended base angle ϕ_b. Note that even though the

size of the dome decreases with increasing water depth, as seen earlier in Fig. 3.7, the overall weight of the dome actually increases with increased water depth. The increase in overall dome weight is due to the increased thickness of the dome.

For a given water depth and dome height, the minimization of dome weight under the combined hydrostatic pressure, selfweight and skin cover load may be stated mathematically as

$$\max_{\bar{h}_0,\bar{l}} \Phi = \phi_b = \phi(1) \tag{3.28}$$

and subjected to the inequality constraints

$$\phi(1) \geq \pi/2 \tag{3.29}$$

$$\left|\bar{z}(1)-1\right| \leq 10^{-7} \tag{3.30}$$

The inequality in Eq. (3.29) is equivalent to Eq. (3.17) which is to ensure compatible deformations between the dome at the base and the ring foundation. The inequality condition in Eq. (3.30) ensures the satisfaction of the terminal boundary condition $\bar{z}(1)=1$. It should be noted that the decision variables in the optimization problem are the apex thickness $\bar{h}_0$ and the dome's curve length $\bar{l}$. The variation of the thickness is determined once these two decision variables are known.

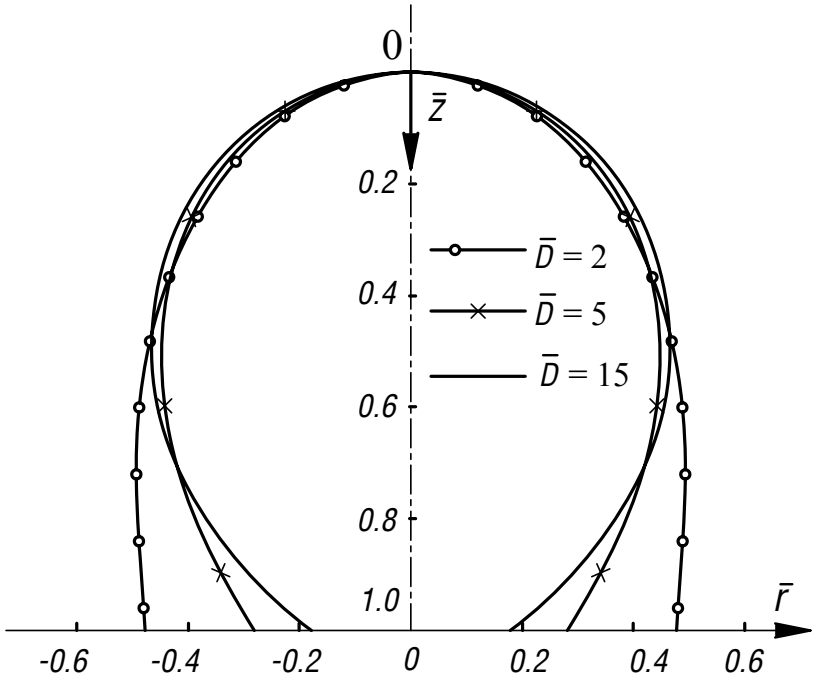

Fig. 3.10 Optimal shapes of submerged domes with respect to water depths

As an example of the optimal shape of submerged domes, the following parameters are assumed: dome height H = 1000 cm, selfweight $\gamma_a = 0.0024$ kgf/cm^3, skin cover load p_c = 0.5 kgf/cm^2 and allowable stress $\sigma_0 = 75$ kgf/cm^2. The optimal shape of the dome is shown in Fig. 3.10 for three normalized water depths of $\overline{D} = 2$, 5 and 15. It can be seen that the water depth affects the lower half of the dome i.e. $\bar{z} \geq 0.5$ more so than the upper half of the dome. The optimal shape of the submerged dome is also characterized by an increased curvature in the lower half of the dome for increased water depth. The increased curvature for domes submerged in deep water is accompanied by a reduced base radius. The increased water depth, however, has a diminishing influence of the optimal shape of the dome. For example, for a change of water depth from $\overline{D} = 2$ to 5 (2.5-folded increase), the base radius reduces from $\bar{r}_b$ = 0.4764 to 0.2808, which represents a 41.1% reduction. On the other hand, for the change in water depth from $\overline{D} = 5$ to 15 (threefold increase), the base radius reduces

from $\bar{r}_b$=0.2808 to 0.1698, which represents a smaller reduction of 39.5%. For completeness in the presentation of results, Table 3.1 shows the optimal value of the base angle $\phi_{b\,opt}$, apex dome thickness $h_{0\,opt}$, and curve length $\bar{\ell}_{opt}$ where the subscript opt is used to denote the optimal value. It can be seen that the optimal dome thickness is significantly increased for a large water depth. For the normalized water depth of $\overline{D} = 15$, the normalized dome thickness at the apex is $\bar{h}_{0\,opt}$ = 0.004364 as compared to the thickness of $\bar{h}_{0\,opt}$ = 0.000361 for the water depth of $\overline{D} = 2$. The increase in thickness is 12.1 times that of the thickness associated with $\overline{D} = 2$. The increased dome thickness however is accompanied by a slight reduction in the curve length of the dome. Although the variations of dome thickness may be different for different water depths, the thicker shells needed for fully stressed domes in deep water nonetheless results in an increase in the overall weight of the dome.

Table 3.1 Optimal values of base angle $\phi_{b\,opt}$, apex thickness $h_{0\,opt}$, and curved length $\bar{\ell}_{opt}$

Water depth $\overline{D}$	Subtended base angle $\phi_{b\,opt}$	Apex thickness $\bar{h}_{0\,opt}$	Curve length $\bar{\ell}_{opt}$
2	1.6942	0.000361	1.2446
5	2.1044	0.001225	1.2775
15	2.4610	0.004364	1.3603

3.4 Concluding remarks

Motivated by recent studies of funicular arches in submarine applications, this chapter extends the analysis to submerged domes where pure membrane actions are assumed. Equations governing the geometry of fully stressed submerged domes under combined hydrostatic pressure, selfweight and skin cover load are derived. These equations describe the curvature and thickness variation of the dome as well as the Cartesian coordinates of its meridian. For the special case of a weightless dome without skin cover load, the thickness of the dome was found to be constant when subjected to hydrostatic pressure only. The shape of the dome was also found to agree well with the shape currently reported in the literature.

Although the set of governing equations for submerged domes is highly nonlinear, the shooting optimization technique currently available in the literature was found to be well suited for solving this problem. A notable advantage of the equations derived in this chapter is the parameterization of the equations using the arc length s as measured from the apex of the dome. Such parameterization allows the entire shape of the submerged dome to be determined in a single integration process whereas previous methods cannot determine the Cartesian coordinates of the dome once vertical or infinite slope is encountered in the meridian. Parametric studies of dome shapes under different water depths and selfweight also led to an investigation of the optimal shape of submerged domes. Numerical examples indicated that the airspace enclosed by the optimal dome reduces in the presence of large hydrostatic pressure. The reduced airspace is accompanied by a significant increase in the dome thickness, which in turn results in an increased overall weight of the dome

.

CHAPTER 4

ENERGY FUNCTIONALS AND RITZ METHOD FOR BUCKLING ANALYSIS OF DOMES

This chapter is concerned with the elastic, axisymmetric buckling analysis of moderately thick domes under rotational loads. The domes have orthotropic properties which include the isotropic case as a specialized case. In order to capture the effect of transverse shear deformation, which is significant for moderately thick domes, Mindlin shell theory is used. Based on Mindlin shell theory, the energy functional is derived first. By using the Ritz method, the total potential energy functionals are minimized with respect to the parameterized admissible displacement functions to yield a system of homogenous equations. These equations forms the governing eigenvalue equation. With the aid of the commercial software package Mathematica (Wolfram, 1999), a computer code was written to solve the eigenvalue equation for the critical buckling pressure.

4.1. Introduction

The literature survey as reported in Chapter 1 provided the previous treatments of moderately thick domes. Most of these studies considered spherical domes and adopted shallow shell theory. The buckling formulation and analysis developed in this chapter are, however, applicable to domes of any meridional shape. Since the critical buckling pressure for moderately thick domes may be sensitive to the transverse shear deformation which depresses the buckling capacity, the effect of transverse shear deformation is included in the energy formulation.

The buckling analysis is carried out using the well accepted Ritz method, primarily for its simplicity and ease of implementation. The automation of the Ritz method for any boundary condition is achieved by approximating the shell displacement components as the product of one-dimensional polynomial functions with the boundary equations raised to appropriate powers so that the geometric boundary conditions are satisfied at the outset. By taking an appropriate number of Ritz function terms in the solution, the critical buckling pressure of rotational shells can be obtained accurately. This convergence characteristic of the solutions is demonstrated by comparing the results of spherical shells with existing solutions. Using a computer code developed in this study, new buckling solutions for moderately thick spherical and parabolic domes of various dimensions and boundary conditions are presented. These solutions are deemed useful to engineers engaged in the design of dome structures.

4.2 Governing Eigenvalue Equation

4.2.1 Geometrical properties of domes

In order to define the dome geometry, two principal radii of curvature: r_1 and r_2 have to be specified. The radius r_1 is the principal radius of curvature of the meridian whereas the principal radius r_2 generates the middle surface of the dome in the direction perpendicular to the tangent on the meridian. The principal radii of curvature, r_1 and r_2, which subsequently appear in the governing equations of shell buckling, may be determined from the generating curve $r_0 = f(z)$ using the following well known relations (Dym, 1974)

$$r_1 = -\frac{\left\{1+\left[\frac{df(z)}{dz}\right]^2\right\}^{\frac{3}{2}}}{\frac{d^2 f(z)}{dz^2}} \tag{4.1a}$$

$$r_2 = f(z)\left\{1+\left[\frac{df(z)}{dz}\right]^2\right\}^{\frac{1}{2}} \tag{4.1b}$$

Although the preceding equations are expressed in terms of the vertical coordinate, *z*, the deformation of rotational shells is often expressed in terms of the coordinate *s*, which is the arc length measured from the apex of the dome (see Fig. 4.1). In order to facilitate the transformation of functions associated with the problem, which include strains, one observes the following geometric relation between *ds* and *dz*, as indicated in Fig. 4.1,

$$(ds)^2 = (dz)^2 + (dr_0)^2 = \left[1 + \left(\frac{dr_0}{dz}\right)^2\right](dz)^2 = \left\{1 + \left[\frac{df(z)}{dz}\right]^2\right\}(dz)^2 \tag{4.2}$$

which leads to $$ds = \left\{1 + \left[\frac{df(z)}{dz}\right]^2\right\}^{\frac{1}{2}} dz \tag{4.3}$$

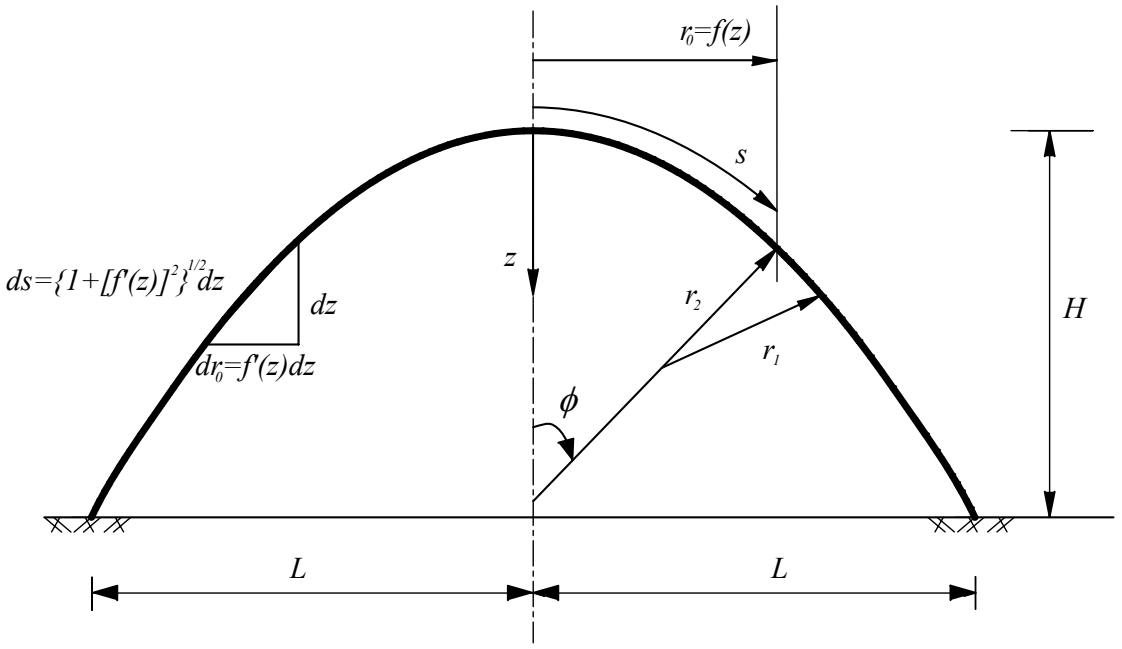

Fig. 4.1 Coordinate systems and parameters defining the shape of dome structures

Thus, for any function *g(z),* one may express its derivatives in either the *z* or *s* coordinates by the following transformation equation:

$$\frac{\partial g(z)}{\partial s} = \frac{\partial g(z)}{\partial z}\frac{\partial z}{\partial s} = \frac{1}{\left\{1 + \left[\frac{df(z)}{dz}\right]^2\right\}^{\frac{1}{2}}}\frac{\partial g(z)}{\partial z} = \frac{1}{\eta}\frac{\partial g(z)}{\partial z} \tag{4.4}$$

where $$\eta = \left\{1 + \left[\frac{df(z)}{dz}\right]^2\right\}^{\frac{1}{2}} \tag{4.5}$$

4.2.2 Mindlin Shell Theory

Generally, shell analyses are based on the classical thin shell theory (Aron 1874, Love 1888), in which the effect of transverse shear deformation is normally neglected. However, when dealing with moderately thick shells, the classical thin shell theory under-predicts the deflections and over-predicts the buckling loads and natural frequencies due to the effect of transverse shear deformations. As we are dealing with moderately thick shells, it is necessary to adopt a more refined shell theory such as Mindlin shell theory that will allow for the effects of transverse shear deformation.

4.2.2.1 Assumptions

In Mindlin shell theory, the following assumptions are made (Mindlin 1951, Reddy 2004):

- The transverse normal is inextensible.
- Normals to the reference surface of the shell before the deformation remain straight but not necessarily normal after the deformation.
- The shell deflections are small so that strains may be treated as infinitesimal.
- The transverse normal stress is negligible so that the plane stress assumptions can be invoked.
- The normals during bending undergo constant rotations about the middle surface while maintaining the straightness and thereby admitting a constant shear strain through the shell thickness. The constant rotations of the normals to the middle surface now become unknown independent variables and are denoted by $\psi(z)$.

The first four assumptions are the same as their classical thin shell counterparts. The last assumption that allows the constant rotation of normal is the main difference between Mindlin shell theory and the classical thin shell theory. The allowance of

constant rotation implies that transverse shear strain is constant through the thickness of the shell. This, however, contradicts the fact that the actual transverse shear strain distribution is parabolic through the thickness. As the constant strain (stress) violates the statical requirement of vanishing shear stress at the surface of the shell, a shear correction factor κ^2 was proposed by Mindlin (1951) to compensate for the error. He pointed out that for an isotropic plate, the shear correction factor κ^2 depends on Poisson's ratio v and it may vary from $\kappa^2 = 0.76$ for $v = 0.3$ to $\kappa^2 = 0.91$ for $v = 0.5$. On the other hand, by comparing the constitutive Mindlin shear force with the one proposed by Reissner (1945), who assumed a parabolic shear stress distribution at the outset of his plate theory formulation, the implicit shear correction factor becomes $\kappa^2 = 5/6$. This value of the shear correction factor has been commonly used for the analyses of Mindlin plates and shells (see for example, Liew *et al.* 2004 and Hou *et al.* 2005) and $\kappa^2 = 5/6$ will also be used in this study.

4.2.2.2 Displacement Components

Based on Mindlin shell theory, the displacement components of an arbitrary point at a distance ζ from the shell mid-surface are given by (Chao *et al.* 1988)

$$\tilde{u}(z,\zeta) = u(z) + \zeta\psi(z) \tag{4.6a}$$

$$\tilde{w}(z,\zeta) = w(z) \tag{4.6b}$$

where u is the meridional displacement, w is the radial displacement of the middle surface and ψ is the rotation of the middle-surface in the meridional direction. It should be apparent that Eq. (4.6a) assumes that the meridional displacement varies

linearly across the thickness of the shell. Note that by setting $\psi(z) = \frac{\partial \widetilde{w}}{\partial z}$, one recovers the displacement fields of classical thin shell theory.

4.2.3 Strain-Displacement Relations

According to Kraus (1967), the strain-displacement relations for small deformation of linearly elastic axisymmetric rotational shells are given by:

$$\varepsilon_\theta = \frac{1}{1+(\zeta / r_2)}\left(\frac{\partial r_0}{\partial s}\frac{u}{r_0} + \frac{w}{r_2} + \zeta \frac{\partial r_0}{\partial s}\frac{\psi}{r_0}\right) \tag{4.7a}$$

$$\varepsilon_s = \frac{1}{1+(\zeta / r_1)}\left(\frac{\partial u}{\partial s} + \frac{w}{r_1} + \zeta \frac{\partial \psi}{\partial s}\right) \tag{4.7b}$$

$$\gamma_{s\zeta} = \frac{1}{1+(\zeta / r_1)}\left(-\frac{u}{r_1} + \frac{\partial w}{\partial s} + \psi\right) \tag{4.7c}$$

where ε_θ is the normal strain in the direction of the parallel circles, ε_s is the normal strain in the meridional direction, and $\gamma_{s\zeta}$ is the transverse shear strain associated with rotation of the shell in the meridian direction.

By invoking Eq. (4.2), the kinematic equations of Eqs. (4.7a-c) may be re-written as:

$$\varepsilon_\theta = \frac{1}{1+(\zeta / r_2)}\left(\frac{\partial r_0}{\eta \partial z}\frac{u}{r_0} + \frac{w}{r_2} + \zeta \frac{\partial r_0}{\eta \partial z}\frac{\psi}{r_0}\right) \tag{4.8a}$$

$$\varepsilon_s = \frac{1}{1+(\zeta / r_1)}\left(\frac{\partial u}{\eta \partial z} + \frac{w}{r_1} + \zeta \frac{\partial \psi}{\eta \partial z}\right) \tag{4.8b}$$

$$\gamma_{s\zeta} = \frac{1}{1+(\zeta / r_1)}\left(-\frac{u}{r_1} + \frac{\partial w}{\eta \partial z} + \psi\right) \tag{4.8c}$$

where $\eta = \left\{1 + \left[\frac{df(z)}{dz}\right]^2\right\}^{\frac{1}{2}}$ (4.5)

4.2.4 Stress-Strain Relations

In order to accommodate a more general orthotropic shell, the stress-strain relation is assumed to follow the orthotropic Hooke's law in the form given by (Chao *et al.* 1988)

$$\begin{Bmatrix} \sigma_\theta \\ \sigma_s \\ \tau_{s\zeta} \end{Bmatrix} = \begin{bmatrix} Q_{11} & Q_{12} & 0 \\ Q_{12} & Q_{22} & 0 \\ 0 & 0 & Q_{44} \end{bmatrix} \begin{Bmatrix} \varepsilon_\theta \\ \varepsilon_s \\ \gamma_{s\zeta} \end{Bmatrix} \tag{4.9}$$

where σ_θ is the normal stress in the direction of the parallel circles, σ_s is the normal stress in the meridional direction, and $\tau_{s\zeta}$ is the transverse shear stress, and

$$Q_{11} = \frac{E_\theta}{1 - \nu_s \nu_\theta} \; ; \; Q_{22} = \frac{E_s}{1 - \nu_\phi \nu_\theta} ; \tag{4.10a}$$

$$Q_{12} = Q_{11}\nu_s \text{ and } \quad Q_{44} = \kappa^2 G_{s\varsigma} \tag{4.10b}$$

where E_s, E_θ, ν_s and ν_θ are the Young's moduli and Poisson's ratios in the direction of the meridian and parallel circle, respectively, and $G_{s\zeta}$ is the shear modulus in the $s-\zeta$ plane. The parameter κ^2 is a shear correction factor introduced to compensate for the error inherent in the assumption of a constant shear strain (stress) in Mindlin shell theory. The commonly accepted value of $\kappa^2 = 5/6$ is adopted for the correction factor in this chapter.

4.2.5 Derivation of Energy Functionals

For an assumed kinematically admissible displacement field for the middle surface, the elastic strain energy functional U of the rotational shell is defined as (Chao *et al*. 1988)

$$U = \frac{1}{2}\int_V \left(\sigma_\theta \varepsilon_\theta + \sigma_s \varepsilon_s + \tau_{s\zeta}\gamma_{s\zeta}\right) dV \tag{4.11}$$

In view of the stress and strain relations Eq. (4.9), one obtains

$$U = \frac{1}{2}\int_V \left(Q_{11}\varepsilon_\theta^2 + 2Q_{12}\varepsilon_\theta \varepsilon_s + Q_{22}\varepsilon_s^2 + Q_{44}\gamma_{s\zeta}^2\right) dV \tag{4.12a}$$

where the incremental volume dV is given by

$$dV = \left(1+\frac{\zeta}{r_1}\right)\left(1+\frac{\zeta}{r_2}\right) r_0 ds d\theta d\zeta = \left(1+\frac{\zeta}{r_1}\right)\left(1+\frac{\zeta}{r_2}\right)\eta r_0 dz d\theta d\zeta \tag{4.12b}$$

In view of Eqs. (4.8) and (4.12b) and after integrating Eq. (4.12) from θ = 0 through to 2π , and using the following parameters:

$$A_{11} = \left(\frac{1+\frac{\zeta}{r_1}}{1+\frac{\zeta}{r_2}}\right) Q_{11};$$

$$A_{22} = \left(\frac{1+\frac{\zeta}{r_2}}{1+\frac{\zeta}{r_1}}\right) Q_{22}; \tag{4.13a-d}$$

$$A_{12} = Q_{12}$$

$$A_{44} = \left(\frac{1+\frac{\zeta}{r_2}}{1+\frac{\zeta}{r_1}} \right) Q_{44}$$

one obtains the following expression for the elastic strain energy of the rotational shell

$$\begin{aligned} U = \pi \int_{-h/2}^{h/2} \int_{0}^{H} \Bigg\{ & A_{11}\left(\frac{\partial r_0}{\eta \partial z}\frac{u}{r_0} + \frac{w}{r_2} + \zeta \frac{\partial r_0}{\eta \partial z}\frac{\psi}{r_0} \right)^2 \\ & + 2A_{12}\left(\frac{\partial r_0}{\eta \partial z}\frac{u}{r_0} + \frac{w}{r_2} + \zeta \frac{\partial r_0}{\eta \partial z}\frac{\psi}{r_0} \right)\left(\frac{\partial u}{\eta \partial z} + \frac{w}{r_1} + \zeta \frac{\partial \psi}{\eta \partial z} \right) \\ & + A_{22}\left(\frac{\partial u}{\eta \partial z} + \frac{w}{r_1} + \zeta \frac{\partial \psi}{\eta \partial z} \right)^2 + A_{44}\left(-\frac{u}{r_1} + \frac{\partial w}{\eta \partial z} + \psi \right)^2 \Bigg\} \eta r_0 \, dz \, d\zeta \end{aligned} \tag{4.14}$$

In applying the Ritz method, the work done by the external forces in moving from one configuration to another configuration must be included in the estimation of the total potential energy. To that end, the work done by the buckling pressure, according to Kawai (1974) and Chao *et al*. (1998), is given by

$$\begin{aligned} W = \frac{1}{2} \int_{0}^{2\pi} \int_{0}^{H} & \left[N_\theta \left(l_{11}^2 + l_{21}^2 + l_{31}^2 \right) + \left[N_s \left(l_{12}^2 + l_{22}^2 + l_{32}^2 \right) \right. \right. \\ & \left. \left. + N_{\theta s} \left(l_{12} l_{11} + l_{21} l_{22} \right) \right] \eta r_0 \, d\theta \, dz \end{aligned} \tag{4.15}$$

where N_θ, N_s and $N_{\theta s}$ are taken as the initial membrane forces due to the critical buckling pressure (see Fig. 4.2). Note that by virtue of axisymmetry displacements in the assumed buckling mode of the dome, the in-plane shear force $N_{s\theta}$ vanishes i.e.

$$N_{s\theta} = 0 \tag{4.16}$$

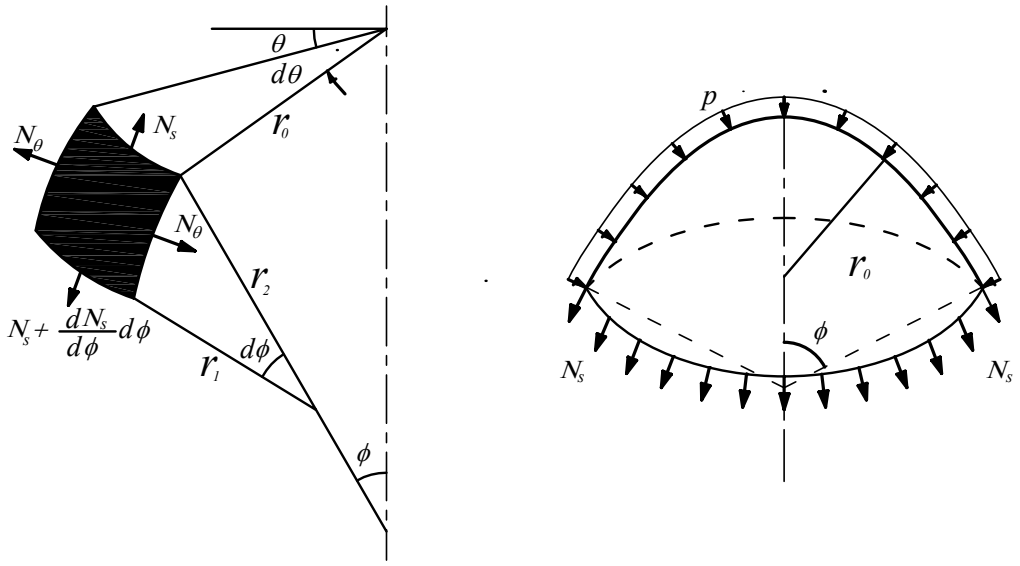

Fig. 4.2 Membrane forces in an axisymmetrically loaded domes

Furthermore, the initial membrane forces due to the critical buckling pressures can be defined in the form of:

$$N_\theta = pn_\theta,\ N_s = pn_s, \tag{4.17}$$

where p depends on the external loading conditions, and n_s, n_θ are parameters dependent on the geometry of the rotational shell, and

$$l_{11} = \frac{\partial r_0}{\eta \partial z}\frac{u}{r_0} + \frac{w}{r_2} \qquad l_{12} = 0$$

$$l_{21} = 0 \qquad l_{22} = \frac{\partial u}{\eta \partial z} + \frac{w}{r_1} \tag{4.18a-f}$$

$$l_{31} = 0 \qquad\qquad l_{32} = \frac{u}{r_1} - \frac{\partial w}{\eta \partial z}$$

By substituting Eqs. (4.16), (4.17) and (4.18a-f) into Eq. (4.15), one obtains the following functional for the work done by the buckling pressure

$$W = p\pi \int_0^H \left\{ n_\theta \left(\frac{\partial r_0}{\eta \partial z} \frac{u}{r_0} + \frac{w}{r_2} \right)^2 + n_s \left[\left(\frac{\partial u}{\eta \partial z} + \frac{w}{r_1} \right)^2 + \left(\frac{u}{r_1} - \frac{\partial w}{\eta \partial z} \right)^2 \right] \right\} \eta r_0 dz \quad (4.19)$$

For convenience, the coordinates and length parameters are normalized by a reference length *H,* which is the height, or by h, which is the thickness of the shell, and the critical pressure and material properties are normalized by an effective Young's modulus $\overline{E}$, which according to Tsai and Pagano (1968) may be taken as $\overline{E} = (3/8)E_s + (5/8)E_\theta$ for orthotropic composites, i.e.

$$\bar{z} = \frac{z}{H};\ \bar{r}_0 = \frac{r_0}{H};\ \bar{r}_1 = \frac{r_1}{H};\ \bar{r}_2 = \frac{r_2}{H};$$

$$\bar{u} = \frac{u}{h};\ \bar{w} = \frac{w}{h};\ \bar{\psi} = \frac{H\psi}{h};$$

$$\xi = \frac{h}{H};\ \bar{\zeta} = \frac{\zeta}{h}; \quad (4.20a\text{-}n)$$

$$\bar{n}_s = \frac{n_s}{H};\ \bar{n}_\theta = \frac{n_\theta}{H} \text{ and}$$

$$\lambda = \frac{pH(1 - \nu_s \nu_\theta)}{\overline{E}h}$$

By adopting the foregoing non-dimensional terms, the total potential energy functional Π of the rotational shell may be written in normalized form as

$$\overline{\Pi} = \overline{U} + \overline{W} \tag{4.21}$$

where

$$\begin{aligned}\overline{U} = \frac{U(1-\nu_s\nu_\theta)}{\pi\overline{E}h^3} = \int_{-1/2}^{1/2}\int_{0}^{1} \Bigg\{ & \overline{A}_{11}\left(\frac{\partial\overline{r}_0}{\eta\partial\overline{z}}\frac{\overline{u}}{\overline{r}_0} + \frac{\overline{w}}{\overline{r}_2} + \xi\overline{\zeta}\frac{\partial\overline{r}_0}{\eta\partial\overline{z}}\frac{\overline{\psi}}{\overline{r}_0}\right)^2 + \overline{A}_{22}\left(\frac{\partial\overline{u}}{\eta\partial\overline{z}} + \frac{\overline{w}}{\overline{r}_1} + \xi\overline{\zeta}\frac{\partial\overline{\psi}}{\eta\partial\overline{z}}\right)^2 \\ & + 2\overline{A}_{12}\left(\frac{\partial\overline{u}}{\eta\partial\overline{z}} + \frac{\overline{w}}{\overline{r}_1} + \xi\overline{\zeta}\frac{\partial\overline{\psi}}{\eta\partial\overline{z}}\right)\left(\frac{\partial\overline{r}_0}{\eta\partial\overline{z}}\frac{\overline{u}}{\overline{r}_0} + \frac{\overline{w}}{\overline{r}_2} + \xi\overline{\zeta}\frac{\partial\overline{r}_0}{\eta\partial\overline{z}}\frac{\overline{\psi}}{\overline{r}_0}\right) \\ & + \overline{A}_{44}\left(-\frac{\overline{u}}{\overline{r}_1} + \frac{\partial\overline{w}}{\eta\partial\overline{z}} + \overline{\psi}\right)^2 \Bigg\}\eta\overline{r}_0 d\overline{z}d\zeta\end{aligned} \tag{4.22}$$

and

$$\overline{W} = \frac{W(1-\nu_s\nu_\theta)}{\pi\overline{E}h^3} = \lambda\int_0^1 \left\{ \overline{n}_s\left[\left(\frac{\partial\overline{u}}{\eta\partial\overline{z}} + \frac{\overline{w}}{\overline{r}_1}\right)^2 + \left(\frac{\overline{u}}{\overline{r}_1} - \frac{\partial\overline{w}}{\eta\partial\overline{z}}\right)^2\right] + \overline{n}_\theta\left(\frac{\partial\overline{r}_0}{\eta\partial\overline{z}}\frac{\overline{u}}{\overline{r}_0} + \frac{\overline{w}}{\overline{r}_2}\right)^2 \right\}\eta\overline{r}_0 d\overline{z} \tag{4.23}$$

where non-zero terms $\overline{A_{ij}}$ are related to the material properties by:

$$\overline{A}_{11} = \left(\frac{1+\xi\frac{\overline{\zeta}}{\overline{r}_1}}{1+\xi\frac{\overline{\zeta}}{\overline{r}_2}}\right)\frac{Q_{11}(1-\nu_s\nu_\theta)}{\overline{E}} = \left(\frac{1+\xi\frac{\overline{\zeta}}{\overline{r}_1}}{1+\xi\frac{\overline{\zeta}}{\overline{r}_2}}\right)\frac{E_\theta}{\overline{E}} \tag{4.24a}$$

$$\overline{A}_{12} = \frac{\nu_s E_\theta}{\overline{E}} \tag{4.24b}$$

$$\overline{A}_{22} = \left(\frac{1+\xi\frac{\overline{\zeta}}{\overline{r}_2}}{1+\xi\frac{\overline{\zeta}}{\overline{r}_1}}\right)\frac{Q_{22}(1-\nu_s\nu_\theta)}{\overline{E}} = \left(\frac{1+\xi\frac{\overline{\zeta}}{\overline{r}_2}}{1+\xi\frac{\overline{\zeta}}{\overline{r}_1}}\right)\frac{E_s}{\overline{E}} \tag{4.24c}$$

$$\overline{A}_{44} = \left(\frac{1 + \xi \dfrac{\overline{\zeta}}{\overline{r}_1}}{1 + \xi \dfrac{\overline{\zeta}}{\overline{r}_2}} \right) \frac{\kappa^2 G_{s\zeta} \left(1 - \nu_s \nu_\theta\right)}{\overline{E}} \tag{4.24d}$$

The total potential energy, as expressed in terms of unknown normalized displacement and rotation components $\overline{u}$, $\overline{w}$ and $\overline{\psi}$ in Eqs. (4.22) to (4.24), is in a suitable form for buckling analysis where its stationary condition is sought to yield the critical buckling pressure.

4.3 Ritz method for buckling analysis

4.3.1 Introduction

In 1909, Walter Ritz published a paper that demonstrates his method for minimizing a functional, and determining the frequencies and mode shapes of structures. Since then, the Ritz method has been widely used because of its simplicity in implementation. Two years after Ritz's paper (1909), Rayleigh (1911) published a book where he complained that Ritz had not recognized his similar work (Rayleigh, 1877). Therefore it is sometime referred to as the Rayleigh-Ritz method. However, Leissa (2005) investigated carefully the historical works of Rayleigh and Ritz and arrived at the conclusion that Rayleigh's name should not be attached to the Ritz method.

In the Ritz method, the displacement function, $\Re(z)$ is approximated by a finite linear combination of trial functions in the form

$$\Re(z) \approx \sum_{i=1}^{N} c_i p_i(z) \tag{4.25}$$

in which $p_i(z)$ are the approximate functions which individually satisfy at least the geometric boundary conditions to ensure convergence to the correct solutions. The static boundary conditions need not be satisfied by these approximate functions. By minimizing the energy functional $\prod$ with respect to each of the unknown coefficients c_i, a set of homogeneous equations is obtained as follows

$$\frac{\partial \prod}{\partial c_i} = 0; \quad i = 1,2,....., N \tag{4.26}$$

For buckling and vibration problems, the above set of homogeneous equations is reduced to eigenvalue and eigenvector problems.

The exact solution is obtained if infinite terms are adopted in Eq. (4.25). However, it is impractical to use an infinite number of terms and so the number of terms is usually truncated to N terms in applications. The choice of the approximate functions is very important in order to simplify the calculations and to guarantee convergence to the exact solution. Some of the commonly used trial functions in the Ritz method for plates and shells analysis are orthogonal characteristic beam polynomials (Bhat 1985), spline and B-spline functions (Mizusawa 1986; Vermeulen and Heppler 1998); pb-2 Ritz formulation (Lim and Liew 1994, Liew *et al.* 1995 and Liew and Lim 1995); trigonometric functions (Lim *et al.* 2003) and two dimensional polynomial functions with appropriate basic functions (Liew 1990; Liew and Wang 1992, 1993; Geannakakes 1995). Among them, the latter trial functions can be

modified and used for the analysis of axisymmetric rotational shells with general shape and boundary conditions while the others may not be so convenient. Moreover, the computational accuracy may also be increased since the polynomial functions admit exact calculations of differentiation and integration of the functions (Liew *et al.* 1998). Therefore, in this study, mathematically complete, one-dimensional polynomial functions are adopted together with basic functions comprising boundary equations that are raised to appropriate powers in order to ensure the satisfaction of the geometric boundary conditions.

4.3.2 Ritz formulation

As noted earlier, buckling analysis of moderately thick shells of revolution when treated as an eigenvalue problem may be solved by the Ritz method where the method lends itself to yield reasonably accurate results. In using the Ritz method, kinematically admissible Ritz functions are assumed for the deflection and rotation components of the middle surface of the rotational shell. To that end, the normalized displacement and rotation components are approximated by polynomials as follows:

$$\overline{u}(\overline{z}) = \sum_{i=1}^{N_1} c_i p_i \tag{4.27a}$$

$$\overline{w}(\overline{z}) = \sum_{i=N_1+1}^{N_2} c_i p_i \tag{4.27b}$$

$$\overline{\psi}(\overline{z}) = \sum_{i=N_2+1}^{N_3} c_i p_i \tag{4.27c}$$

where N_1, $(N_2 - N_1)$ and $(N_3 - N_2)$ correspond to the number of the polynomial terms and c_i the unknown coefficients for the displacements and rotation and the functions p_i can be expressed in the following forms

$$p_i = \eta_u \bar{z}^{(i-1)} \qquad \text{for } i = 1 \text{ to } N_1, \tag{4.28a}$$

$$p_i = \eta_w \bar{z}^{(i-N_1-1)} \quad \text{for } i = N_1 \text{ to } N_2, \tag{4.28b}$$

$$p_i = \eta_\psi \bar{z}^{(i-N_2-1)} \quad \text{for } i = N_2 \text{ to } N_3. \tag{4.28c}$$

The terms η_u, η_w and η_ψ are the product of the boundary equations raised to an appropriate power so that the selected Ritz functions satisfy the geometric boundary conditions. More specifically, η_u, η_w, and η_ψ are given below for the following boundary conditions of domes.

In view of equations (4.22), after integrating Eq. (4.13) over the shell thickness h, one obtains the following coefficients

$$\widetilde{A}_{11} = \int_{-\frac{1}{2}}^{\frac{1}{2}} \overline{A}_{11} d\bar{\zeta} = \int_{-\frac{1}{2}}^{\frac{1}{2}} \left(\frac{1 + \xi \dfrac{\bar{\zeta}}{\bar{r}_1}}{1 + \xi \dfrac{\bar{\zeta}}{\bar{r}_2}} \right) \frac{E_\theta}{\overline{E}} d\bar{\zeta} \tag{4.29a}$$

$$\widetilde{A}_{22} = \int_{-\frac{1}{2}}^{\frac{1}{2}} \overline{A}_{22} d\bar{\zeta} = \int_{-\frac{1}{2}}^{\frac{1}{2}} \left(\frac{1 + \xi \dfrac{\bar{\zeta}}{\bar{r}_2}}{1 + \xi \dfrac{\bar{\zeta}}{\bar{r}_1}} \right) \frac{E_\theta}{\overline{E}} d\bar{\zeta} \tag{4.29b}$$

$$\widetilde{A}_{44} = \int_{-\frac{1}{2}}^{\frac{1}{2}} \overline{A}_{44} d\bar{\zeta} = \int_{-\frac{1}{2}}^{\frac{1}{2}} \left(\frac{1 + \xi \dfrac{\bar{\zeta}}{\bar{r}_2}}{1 + \xi \dfrac{\bar{\zeta}}{\bar{r}_1}} \right) \frac{\kappa^2 G_{s\zeta} \left(1 - v_\phi v_\theta\right)}{\overline{E}} d\bar{\zeta} \tag{4.29c}$$

$$\widetilde{B}_{12} = \int_{-\frac{1}{2}}^{\frac{1}{2}} \overline{A}_{12}\, \overline{\zeta}\, d\overline{\zeta} = \int_{-\frac{1}{2}}^{\frac{1}{2}} \frac{\nu_\theta E_s}{\overline{E}}\, \overline{\zeta}\, d\overline{\zeta} \tag{4.29d}$$

$$\widetilde{D}_{11} = \int_{-\frac{1}{2}}^{\frac{1}{2}} \overline{A}_{11} \overline{\zeta}^{\,2} d\overline{\zeta} = \int_{-\frac{1}{2}}^{\frac{1}{2}} \left(\frac{1+\xi \dfrac{\overline{\zeta}}{\overline{r}_1}}{1+\xi \dfrac{\overline{\zeta}}{\overline{r}_2}} \right) \frac{E_\theta}{\overline{E}} \overline{\zeta}^{\,2} d\overline{\zeta} \tag{4. 29e}$$

$$\widetilde{D}_{12} = \int_{-\frac{1}{2}}^{\frac{1}{2}} \overline{A}_{12}\, \overline{\zeta}^{\,2}\, d\overline{\zeta} = \int_{-\frac{1}{2}}^{\frac{1}{2}} \frac{\nu_\theta E_s}{\overline{E}}\, \overline{\zeta}^{\,2}\, d\overline{\zeta} \tag{4. 29f}$$

$$\widetilde{D}_{22} = \int_{-\frac{1}{2}}^{\frac{1}{2}} \overline{A}_{22} \overline{\zeta}^{\,2} d\overline{\zeta} = \int_{-\frac{1}{2}}^{\frac{1}{2}} \left(\frac{1+\xi \dfrac{\overline{\zeta}}{\overline{r}_2}}{1+\xi \dfrac{\overline{\zeta}}{\overline{r}_1}} \right) \frac{E_\theta}{\overline{E}} \overline{\zeta}^{\,2} d\overline{\zeta} \tag{4. 29g}$$

In view of Eqs. (4. 29a-g) and (4.28a-c), the energy functional $\overline{U}$ given by Eq. (4.22) may be written in matrix form as

$$\begin{aligned} \overline{U} = \sum_{i=1}^{N_3} \sum_{j=1}^{N_3} \int_{-1/2}^{1/2} \int_{0}^{1} \Big\{ & \Big[\widetilde{A}_{11} \widetilde{q}_i \widetilde{q}_j + \widetilde{D}_{11} \widetilde{w}_i \widetilde{w}_j + \widetilde{B}_{12} \left(\widetilde{w}_i \widetilde{q}_j + \widetilde{q}_i \widetilde{w}_j \right) \Big] + \\ & + \left[\widetilde{A}_{22} \widetilde{e}_i \widetilde{e}_j + \widetilde{D}_{11} \widetilde{r}_i \widetilde{r}_j + \widetilde{B}_{12} \left(\widetilde{e}_i \widetilde{r}_j + \widetilde{r}_i \widetilde{e}_j \right) \right] + \widetilde{A}_{12} \left(\widetilde{q}_i \widetilde{e}_j + \widetilde{q}_j \widetilde{e}_i \right) + \\ & + \widetilde{D}_{12} \left(\widetilde{w}_i \widetilde{r}_j + \widetilde{w}_j \widetilde{r}_i \right) + \widetilde{B}_{12} \left(\widetilde{q}_i \widetilde{r}_j + \widetilde{q}_j \widetilde{r}_i \right) + \widetilde{B}_{12} \left(\widetilde{w}_i \widetilde{e}_j + \widetilde{w}_j \widetilde{e}_i \right) + \overline{A}_{44} \widetilde{t}_i \widetilde{t}_j \Big\} c_i c_j \eta \overline{r}_0 d\overline{z} d\overline{\zeta} \end{aligned} \tag{4.30}$$

where the terms in Eq. (4.30) can be expressed as

(a) $$\frac{\partial \overline{r}_0}{\eta \partial \overline{z}} \frac{\overline{u}}{\overline{r}_0} + \frac{\overline{w}}{\overline{r}_2} = \sum_{i=1}^{N_3} c_i \widetilde{q}_i \tag{4.31}$$

and $\tilde{q}_i = \frac{\partial \bar{r}_0}{\eta \partial \bar{z}} \frac{p_i}{\bar{r}_0}$ for $i = 1$ to N_1, $\tilde{q}_i = \frac{p_i}{\bar{r}_2}$ for $i = N_1 + 1$ to N_2 and $\tilde{q}_i = 0$ for $i = N_2 + 1$ to N_3

(b) $$\bar{\zeta} \frac{\partial \bar{r}_0}{\eta \partial \bar{z}} \frac{\overline{\psi}}{\bar{r}_0} = \sum_{i=1}^{N_3} c_i \tilde{w}_i \tag{4.32}$$

and $\tilde{w}_i = 0$ for $i = 1$ to N_1, $\tilde{w}_i = 0$ for $i = N_1 + 1$ to N_2 and $\tilde{w}_i = \xi \bar{\zeta} \frac{\partial \bar{r}_0}{\eta \partial \bar{z}} \frac{p_i}{\bar{r}_0}$ for $i = N_2 + 1$ to N_3

(c) $$\frac{\partial \bar{u}}{\eta \partial \bar{z}} + \frac{\overline{w}}{\bar{r}_1} + = \sum_{i=1}^{N_3} c_i \tilde{e}_i \tag{4.33}$$

and $\tilde{e}_i = \frac{1}{\eta} \frac{\partial p_i}{\partial \bar{z}}$ for $i = 1$ to N_1, $\tilde{e}_i = \frac{p_i}{\bar{r}_1}$ for $i = N_1 + 1$ to N_2 and $\tilde{e}_i = 0$ for $i = N_2 + 1$ to N_3

(d) $$\xi \frac{\partial \overline{\psi}}{\eta \partial \bar{z}} = \sum_{i=1}^{N_3} c_i \tilde{r}_i \tag{4.34}$$

and $\tilde{r}_i = 0$ for $i = 1$ to N_1, $\tilde{r}_i = 0$ for $i = N_1 + 1$ to N_2 and $\tilde{r}_i = \frac{\xi}{\eta} \frac{\partial p_i}{\partial \bar{z}}$ for $i = N_2 + 1$ to N_3

(e) $$-\frac{\bar{u}}{\bar{r}_1} + \frac{\partial \overline{w}}{\eta \partial \bar{z}} + \overline{\psi} = \sum_{i=1}^{N_3} c_i \tilde{t}_i \tag{4.35}$$

and $\tilde{t}_i = -\frac{p_i}{\bar{r}_1}$ for $i = 1$ to N_1, $\tilde{t}_i = \frac{1}{\eta} \frac{\partial p_i}{\partial \bar{z}}$ for $i = N_1 + 1$ to N_2 and $\tilde{t}_i = p_i$ for $i = N_2 + 1$ to N_3

Similarly, the work done by the external forces (Eq. 4.23) can be expressed as

$$\overline{W} = \sum_{i=1}^{N_3}\sum_{j=1}^{N_3} \lambda \int_0^1 \left\{ \overline{n}_s \left(\widetilde{u}_i \widetilde{u}_j + \widetilde{g}_i \widetilde{g}_j \right) + \overline{n}_\theta \widetilde{y}_i \widetilde{y}_j \right\} \eta \overline{r}_0 \, d\overline{z} \tag{4.36}$$

where the terms in Eq. (4.36) may be expressed as

(f) $$\frac{\partial \overline{r}_0}{\eta \partial \overline{z}} \frac{\overline{u}}{\overline{r}_0} + \frac{\overline{w}}{\overline{r}_2} = \sum_{i=1}^{N_3} c_i \widetilde{y}_i \tag{4.37}$$

and $\widetilde{y}_i = \frac{1}{\eta} \frac{\partial \overline{r}_0}{\partial \overline{z}} \frac{p_i}{\overline{r}_0}$ for i = 1 to N_1, $\widetilde{y}_i = \frac{p_i}{\overline{r}_2}$ for $i = N_1 + 1$ to N_2 and $\widetilde{y}_i = 0$ for $i = N_2 + 1$ to N_3

(g) $$\frac{\partial \overline{u}}{\eta \partial \overline{z}} + \frac{\overline{w}}{\overline{r}_1} = \sum_{i=1}^{N_3} c_i \widetilde{u}_i \tag{4.38}$$

and $\widetilde{u}_i = \frac{1}{\eta} \frac{\partial p_i}{\partial \overline{z}}$ for i = 1 to N_1, $\widetilde{u}_i = \frac{p_i}{\overline{r}_1}$ for $i = N_1 + 1$ to N_2 and $\widetilde{u}_i = 0$ for $i = N_2 + 1$ to N_3

(h) $$\frac{\overline{u}}{\overline{r}_1} - \frac{\partial \overline{w}}{\eta \partial \overline{z}} = \sum_{i=1}^{N_3} c_i \widetilde{g}_i \tag{4.39}$$

and $\widetilde{g}_i = \frac{p_i}{\overline{r}_1}$ for i = 1 to N_1, $\widetilde{g}_i = -\frac{1}{\eta} \frac{\partial p_i}{\partial \overline{z}}$ for $i = N_1 + 1$ to N_2 and $\widetilde{g}_i = 0$ for $i = N_2 + 1$ to N_3

The total potential energy functional given by Eqs. (4.21) (with (4.30) and (4.36)) is expressed in terms of displacements, the material stiffness, and external loads. Following the standard procedure for the Ritz method, the unknown coefficients c_i are obtained by extremizing the total potential energy functional $\overline{\Pi}$, i.e.

$$\left\langle \frac{\partial \overline{\Pi}}{\partial c_i} \right\rangle = \langle 0 \rangle; \quad i = 1, 2, ..., N_3 \tag{4.40}$$

which yields a set of homogeneous equations that can be conveniently expressed in a matrix form containing the unknown coefficients c_i

$$([K] + \lambda [M])\{c\} = \{0\} \tag{4.41}$$

where [K] and [M] are (N_3 x N_3) square matrices and $\{c\}$ is a column vector consisting of the coefficients c_i.

The elastic buckling pressure parameter λ is obtained by solving eigenvalue of the governing equation. With the aid of the commercial software package Mathematica (Wolfram, 1999), this eigenvalue problem is solved using built-in function **Eigenvalues**.

4.3.3 Boundary conditions

Two edge supporting conditions are considered, namely the clamped support and the simply supported as shown in Fig. 4.3.

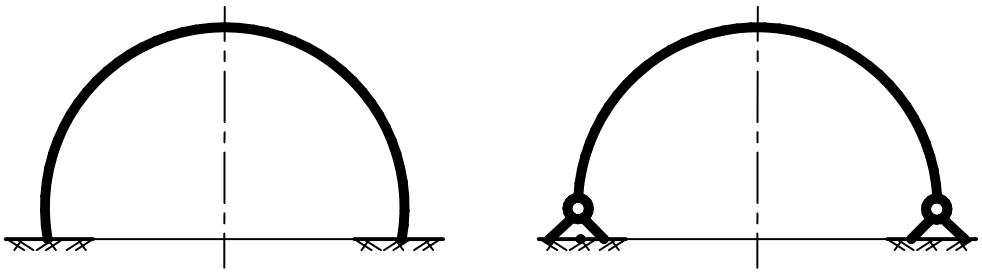

(a) Clamped **(b)** Simply supported

Fig. 4.3 Boundary conditions

For a clamped edge, the boundary conditions are $\overline{u}(1)=\overline{w}(1)=\overline{\psi}(1)=0$. In view of these boundary conditions, the basis functions are given by

$$\begin{aligned}\eta_u &= (\bar{z}-1)\bar{z}\\ \eta_w &= (\bar{z}-1)\\ \eta_\psi &= (\bar{z}-1)\bar{z}\end{aligned} \tag{4.42}$$

For a simply supported edge, the boundary conditions are $\overline{u}(1)=\overline{w}(1)=0$ but $\overline{\psi}(1)\neq 0$. In view of these boundary conditions, the basis functions are given by

$$\begin{aligned}\eta_u &= (\bar{z}-1)\bar{z}\\ \eta_w &= (\bar{z}-1)\\ \eta_\psi &= \bar{z}\end{aligned} \tag{4.43}$$

4.3.4 Mathematica for solving eigenvalue problem

Modern computer algebra systems especially Mathematica (Wolfram 1999) are very powerful not only in symbolic computations, but in numerical computations as well. Among other things, Mathematica (Wolfram 1999) allows its user to manipulate symbols, numbers, data, and graphics. Such computing environments are already used quite extensively by researchers for a wide range of serious scientific calculations. In 1990, Beltzer (1990) gave a comprehensive review of symbolic computation packages and analytical applications in engineering analysis. Ioakimidis (1992a, 1992b, 1992c) has demonstrated the use of Mathematica(Wolfram 1999) in semi-analytical numerical structural applications, particularly those involving energy methods.

A system such as Mathematica (Wolfram 1999) is ideally suited for many analytical applications in small engineering energy problems. The eigenvalue problem is solved using built-in function **Eigenvalues** in the software package Mathematica (Wolfram, 1999). In Mathematica, ***Eigenvalues*** function used the function DSYEVR in LAPACK<www.netlib.org/lapack/> routines to calculate the numerical eigen values and vectors of a real and symmetric matrice. The Mathematica code to obtain buckling strength of rotational shells is presented in the Appendix.

4.4 Concluding remarks

Although buckling of shells under compressive loading is of practical significance in the design of these structures, most of the studies thus far focused on rotational shells of spherical shape using a thin shell theory. An attempt is made in this chapter to formulate a methodology for predicting the critical buckling pressure of moderately thick rotational shells generated by any meridional shape under external uniform pressure. The effect of transverse shear deformation is included in the formulation using Mindlin shell theory so that the critical buckling pressure will not be excessively overestimated when the shell is relatively thick.

The critical buckling pressure of thick shells under uniform pressure, formulated as an eigenvalue problem, is derived using the well accepted Ritz method. Numerical results, obtained from a computer program, were shown to be in close agreement with existing buckling solutions for isotropic and orthotropic spherical shells. One feature of the proposed method is that highly accurate solutions can be ensured by including an appropriate number of terms in the Ritz functions. The formulation is also capable of handling different support conditions, by raising the boundary equations to the appropriate power so that the geometric boundary conditions are satisfied *a priori*. New solutions for the buckling pressure of moderately thick spherical and parabolic shells of various dimensions and boundary conditions are presented and, although these results are limited by the material properties assumed in this chapter, they are nonetheless useful for preliminary design of shell structures.

CHAPTER 5

BUCKLING OF DOMES UNDER UNIFORM PRESSURE

This chapter is concerned with the elastic, axisymmetric buckling of moderately thick, orthotropic domes under a uniform external pressure. For the buckling analysis, we apply the Ritz method presented in Chapter 4. The validity of the developed Ritz method as well as the convergence and accuracy of the buckling solutions are demonstrated using examples of spherical domes (a special case of generic dome structures) where closed-form solutions exist. Upon establishment of the validity of the method and its ability to furnish accurate results, we generate extensive buckling solutions for moderately thick spherical and parabolic domes of various dimensions and boundary conditions. These new results, presented in tabulated form, are deemed useful to engineers engaged in the design of shell structures.

5.1 Problem definition

Consider a dome, also known as a synclastic shell of revolution, of height *H,* base radius *L*, and uniform thickness *h*. The dome is formed by rotating a curve defined by $r_0 = f(z)$ with $(df/dz)_{z=0} = 0$, about the vertical *z* axis as shown in Fig. 5.1. The dome is subjected to a static uniform external pressure *p*, and is free of geometric and material imperfections. The problem at hand is to determine the critical pressure p_{cr} for axisymmetric buckling of domes under the uniform external pressure *p*.

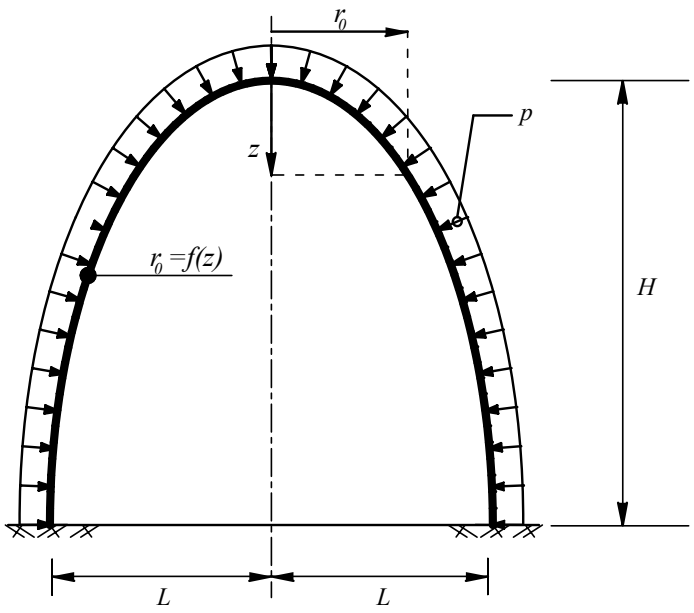

Fig 5.1 Dome under uniform pressure

5.2 Geometrical parameters

To consider the aforementioned buckling problem, one needs to first evaluate the parameters for general energy functionals given by Eqs. (4.21), (4.22) and (4.23) in Chapter 4. From statical considerations, the membrane force N_s acting in the meridian direction is given by

$$N_s = -\frac{1}{r_2 \sin^2 \phi} \int_0^{\phi} p \cos\phi \sin\phi \; r_1 r_2 d\phi \tag{5.1}$$

In view of the following geometric relations for rotational shells

$$r_0 = r_2 \sin\phi \; ; \tag{5.2a}$$

$$dr_0 = ds \cos\phi = r_1 \cos\phi d\phi \tag{5.2b}$$

Eq. (5.1) may be expressed as

$$N_s = -\frac{1}{r_2 \sin^2 \phi} \int_0^{r_0} p r_0 dr_0 = -\frac{p r_0^2}{2 r_2 \sin^2 \phi} = -\frac{p r_2}{2} \tag{5.3}$$

Similarly, from statical considerations, the membrane force N_θ acting in the circumferential direction is given by

$$N_\theta = -r_2 \left(p + \frac{N_\phi}{r_1} \right) = -p r_2 \left(1 - \frac{r_2}{2 r_1} \right) \tag{5.4}$$

By comparing the definitions of Eq. (4.17) with Eqs. (5.1) and (5.4), one can deduce that

$$n_s = -\frac{r_2}{2} \; ; \; n_\theta = -r_2 \left(1 - \frac{r_2}{2 r_1} \right) \tag{5.5}$$

5.3. Results and discussions

5.3.1 Spherical domes

For the spherical dome, the meridional curve is defined by (see Fig. 5.2)

$$r_0 = f(z) = \sqrt{2Rz - z^2} \tag{5.6}$$

In view of the non-dimensional parameters in Eq. (4.20), one can obtain

$$\bar{r}_0 = \sqrt{2\bar{R}\bar{z} - \bar{z}^2} \tag{5.7}$$

where $\bar{R} = R/H$ and $\bar{z} = z/H$.

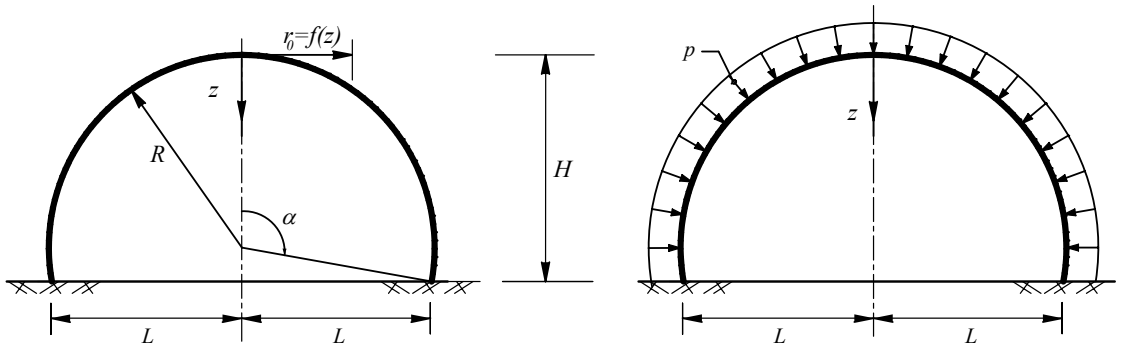

(a) **(b)**

Fig 5.2 Spherical domes under uniform pressure

By substituting Eqs. (5.5) and (5.7) into Eq.(4.1) and (4.20), one can obtain the geometrical properties of the spherical dome

$$\bar{r}_1 = \bar{r}_2 = \bar{R} \tag{5.8}$$

$$\bar{n}_s = \bar{n}_\theta = -\frac{\bar{R}}{2} \tag{5.9}$$

For a given spherical dome with a subtended angle α (see Fig. 5.2a) and thickness to radius ratio *h/R*, the non-dimensional terms $\overline{R}, \xi$ that appear in the energy functionals are defined as

$$\overline{R} = \frac{R}{H} = \frac{1}{(1-\cos\alpha)} \tag{5.10a}$$

$$\xi = \frac{h}{H} = \frac{h}{R}.\frac{R}{H} = \frac{T}{(1-\cos\alpha)} \tag{5.10b}$$

By substitution of the foregoing geometrical parameters into the eigenvalue equation (4.41) in Chapter 4, and upon solving the equation, one obtains the critical buckling pressure parameter $\lambda = \frac{p_{cr} H(1-\nu_s \nu_\theta)}{\overline{E}h}$ of spherical domes. Results for spherical domes with different thickness-to-radius ratios will be given in the next section.

Convergence and comparison studies

To study the convergence of the Ritz solutions with respect to the number of polynomial terms used to approximate the displacements, we consider hemispherical domes with radius-to-thickness ratios ranging from *R/h* = 10 to 1000 and with different boundary conditions, namely, clamped and simply supported. Tables 5.1 and 5.2 show the convergence studies of the critical buckling pressure parameter λ. It can be seen that the Ritz solutions converge monotonically with increasing degrees of the polynomials for all radius-to-thickness ratios. In order to obtain accurate buckling solutions (within 0.05% error), the number of polynomial terms required for each

displacement function is 40. This number of terms will be assumed to suffice for generating accurate results for other spherical dome shapes in this chapter.

For comparison purposes, numerical solutions for clamped domes obtained by Uddin (1987, 1993) who used the multi segment method of integration of Kalnins and Lestingi (1967) to solve the governing shell equations are included in Table 5.1. By comparing Uddin's results with the present Ritz solutions, it can be seen that for the large radius-to-thickness ratios (e.g. R/h = 300), the converged results are found to be in good agreement. However, for relatively small radius-to-thickness ratios (i.e. thicker shells), the Ritz solutions are slightly lower than those presented by Uddin (1987). For example, for R/h = 25, the difference between the converged Ritz solution and that of Uddin (1987) is about 1.2% lower. This difference is due to neglect of the effect of transverse shear deformation in Uddin's analysis.

Table 5.1 Convergence of critical buckling pressure parameter λ of a clamped hemispherical dome

λ x10^3		Radius over thickness ratio *R/h*				
		10	25	100	300	1000
Number of terms	3	222.41039	194.03803	188.27774	187.92796	187.88811
	6	118.54395	55.67167	27.17262	25.13063	24.89573
	9	112.83077	46.57039	14.33367	7.43311	6.39213
	12	110.93703	45.69036	11.66922	5.23093	2.64581
	15	109.84001	45.26218	11.27922	4.23114	1.77093
	18	109.15098	44.95244	11.19395	3.88616	1.46390
	21	108.69171	44.71732	11.16818	3.75452	1.31493
	24	108.36999	44.53604	11.15321	3.70952	1.20982
	27	108.13490	44.39430	11.14080	3.69693	1.16335
	30	107.95671	44.28166	11.12910	3.69448	1.13873
	33	107.81719	44.19041	11.11740	3.69317	1.12215
	36	107.70465	44.11488	11.10527	3.69199	1.11328
	39	107.61129	44.05082	11.09222	3.69081	1.10788
	40	107.58348	44.03143	11.08757	3.69039	1.10670
Uddin 1987)		……..	44.6469	11.0423	3.6364	…..

Table 5.2. Convergence of critical buckling pressure parameter λ of a simply supported hemispherical dome

λ x10^3		Radius over thickness ratio *R/h*				
		10	25	100	300	1000
Number of terms	3	159.45770	102.99050	88.55159	87.63990	87.53578
	6	106.57882	46.48155	16.72819	9.38351	8.46736
	9	105.95376	43.91228	11.96595	5.71284	2.42462
	12	105.63408	43.55971	11.23972	4.10419	1.77645
	15	105.38689	43.41658	11.03587	3.83347	1.38606
	18	105.19826	43.31454	11.00392	3.72957	1.22685
	21	105.05506	43.23428	11.00054	3.69173	1.15762
	24	104.94536	43.16959	10.99926	3.67563	1.13439
	27	104.85989	43.11685	10.99842	3.67253	1.11983
	30	104.79192	43.07337	10.99769	3.67146	1.11122
	33	104.73669	43.03703	10.99696	3.67090	1.10711
	36	104.69077	43.00614	10.99616	3.67050	1.10441
	39	104.65169	42.97931	10.99521	3.67014	1.10293
	40	104.63986	42.97107	10.99484	3.67002	1.10249

Although a clamped spherical dome with a 90^o meridian angle differs geometrically from that of a complete spherical shell, the critical buckling pressure of the clamped spherical shell is nonetheless of the same order of magnitude when compared to that of a complete shell with the same radius. For comparison of the results obtained from the various methods, it is convenient to express the critical buckling pressure of incomplete shells as a fraction of that of complete shells. To that end, it is instructive to note that the classical buckling pressure of complete isotropic spherical shells, first established by Zoelly (1915), is

$$p_{cl} = \frac{2E}{\sqrt{3\left(1-\nu^2\right)}}\left(\frac{h}{R}\right)^2 \tag{5.11}$$

Recall from the definition in Eq. (4.20) that,

$$\lambda = \frac{p_{cr} H\left(1-\nu^2\right)}{\bar{E}h} \tag{5.12}$$

and in view of Eqs. (5.11) and (5.12), the solution for incomplete shells can be expressed as a fraction of the classical buckling pressure of a complete spherical shell by the following ratio

$$\frac{p_{cr}}{p_{cl}} = \lambda \frac{2}{\sqrt{3}} \frac{1}{\left(1-\nu^2\right)^{3/2}} \frac{R}{h} \frac{R}{H} \tag{5.13}$$

The ratio of critical buckling pressures in Eq. (5.13) will be used as the basis for comparison of available solutions in the literature. Table 5.3 shows the comparison of critical buckling pressures of the 90^0 clamped spherical domes with solutions by various researchers for a small radius-to-thickness ratio of R/h = 25. Among these researchers, only Uddin (1987) calculated the buckling pressure without adopting the shallowness assumptions of shell structures. It can seen from Table 5.3 that the present result, expressed as a ratio in Eq. (5.13), is less than that of Uddin (1987) due to the effect of transverse shear deformation. Note that the current formulation may be used to furnish the critical buckling pressure associated with the corresponding result based on classical thin shell theory by setting a large value for the shear correction factor, say κ^2 =1000. By doing so, the current formulation yields a ratio of p_{cr}/p_{cl} =1.120 which is relatively close to Uddin's ratio of p_{cr}/p_{cl} =1.127.

Table 5.3 Comparison of critical buckling pressure ratio p_{cr}/p_{cl} of a 90^0 clamped spherical dome (R/h = 25)

Present result (p_{cr}/p_{cl})	Uddin (1987)	Huang (1964)	Archer (1958)	Dumir *et al.* (1984)	Budiansky (1959)	Thurston (1961)
1.076	1.127	1.057	0.750	1.035	1.058	1.067

It can be seen from Table 5.3 that the prediction of the critical buckling pressure of hemispherical domes with R/h = 25 varies among different researchers. The value varies from a low ratio of 0.75 by Archer (1958) to a high ratio of 1.067 by Thurston (1961). It should be noted that a shallow shell theory was assumed in the studies by Huang (1964), Archer (1958), Dumir *et al*. (1984), Budiansky (1959) and Thurston (1961). Their results are therefore expected to be lower than the results based on the

non-shallow shell theory, which is adopted herein. Also interestingly, their analyses, which neglect the effect of transverse shear deformation and employ shallow shell theory, yield critical buckling pressures that are comparable with the present result for moderately thick shells. The good prediction is, in part, because the shallow shell assumption lowers the critical buckling pressure whilst the neglect of transverse shear deformation raises the critical buckling pressure. These are compensating effects that have effectively canceled each other out for the considered shell problem.

Effects of radius-to-thickness ratio and transverse shear deformation

As the critical buckling pressure may be sensitive to the amount of transverse shear deformation that occurs during buckling, the influence of shear deformation is examined in moderately thick shells by varying the radius-to-thickness ratio. The sensitivity study is made for isotropic hemispherical shells that are simply supported at their edges. Table 5.4 presents the critical buckling pressure normalized by the Young's modulus i.e. p_{cr}/E for radius-to-thickness ratios R/h ranging from 10 to 1000. The assessment is made for hemispherical domes with simply-supported boundary conditions. Critical buckling pressures obtained using classical thin shell theory are also included in the table so as to observe the effect of transverse shear deformation on the buckling pressure.

Table 5.4 Effect of transverse shear deformation on the buckling pressures p_{cr}/E of simply supported hemispherical domes

R/h	Thin shell theory (Muc 1992)	Mindlin shell theory	Difference (%)
10	12104.5507	11507.0859	-5.1921
25	1936.7281	1890.5567	-2.4422
50	484.1820	480.5784	-0.7499
100	121.0455	120.8434	-0.1673
200	30.2614	30.2318	-0.0977
300	13.4495	13.4441	-0.0400
400	7.5653	7.5637	-0.0220
500	4.8418	4.8412	-0.0119
600	3.3624	3.3622	-0.0064
700	2.4703	2.4705	0.0071
800	1.8913	1.8917	0.0198
900	1.4944	1.4951	0.0475
1000	1.2105	1.2115	0.0901

It can be seen from the results in Table 5.4 that, for a small shell thickness, as reflected by a large radius-to-thickness ratio e.g. $R/h > 100$, the buckling pressure p_{cr}/E is close to the result obtained using thin shell theory (Muc 1992). However, for a large shell thickness e.g. $R/h < 100$, the buckling pressure p_{cr}/E based on Mindlin shell theory is somewhat lower than their thin shell theory counterparts due to the shear deformation effect. At a radius-to-thickness ratio of $R/h = 10$, the difference between the Mindlin and thin shell theories is approximately 5%.

Orthotropic Spherical Domes under uniform pressure p

The versatility of the proposed method in this chapter will now be demonstrated using an orthotropic dome when subjected to uniform external pressure. According to an earlier study by Muc (1992), the critical buckling pressure of a simply supported orthotropic spherical shell is given by

$$p_{cr} = 4\left(\frac{t}{R}\right)^2 \sqrt{\frac{A_{11}A_{22} - A_{12}^2}{12}} \tag{5.14}$$

We shall assess the accuracy of this formula by comparing it with our Ritz results. For the subsequent numerical calculations, the orthotropic dome is assumed to be made from a graphite/epoxy material with values of E_s = 120 GPa, E_θ = 4.8 GPa, $G_{s\zeta}$ = 2.4 GPa and $\nu_{s\theta}$ = 0.25 taken from Chao *et al* (1988). Table 5.5 furnishes the results by the present Ritz results based on Mindlin shell theory and its comparison with the thin shell theory by Muc (1992). The results indicate that the normalized buckling pressure as obtained by Mindlin shell theory may be noticeably smaller than that of thin shell theory, depending on the thickness of the shell. In the case of thin shells (*R/h* > 200), both results are in good agreement, which is expected. However, the difference between the two theories increases in thick shells as characterized by *R/h* <200. In the case of *R/h* = 25, the difference in critical buckling pressure is as high as 8%. The tendency of Eq. (5.14) to over-estimate the critical buckling pressure of moderately thick shells is likely due to the neglecting of the transverse shear deformation.

Table 5.5 Buckling pressures $p_{cr}/\overline{E}$ of orthotropic hemispherical domes

R/h	Thin shell theory (Muc 1992)	Mindlin shell theory	Difference (%)
25	924.917	855.6495	-8.0953
100	57.8073	57.2088	-1.0461
200	14.4518	14.4346	-0.1197
300	6.42304	6.4159	-0.1118
500	2.31229	2.3112	-0.0482
1000	0.57807	0.5780	-0.0085

5.3.2 Parabolic Domes

For parabolic domes, the meridional curve is defined by (See Fig. 5.3)

$$r_0 = \sqrt{4az} \tag{5.15}$$

where $a = L^2/(4H)$.

In view of the non-dimensional parameters in Eq. (4.20), one can obtain

$$\bar{r}_0 = \sqrt{4\bar{a}\bar{z}} \tag{5.16}$$

where $\bar{a} = \dfrac{a}{H} = \dfrac{L^2}{4H^2} = \dfrac{\bar{L}^2}{4}$ and $\bar{z} = \dfrac{z}{H}$

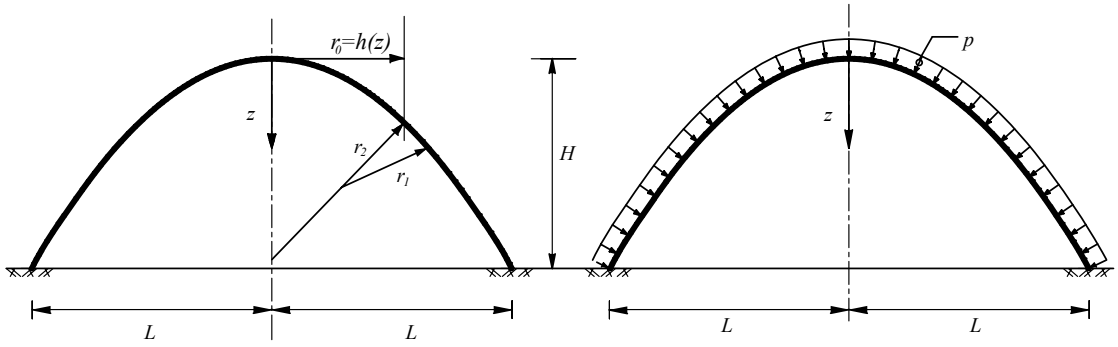

Fig 5.3 Parabolic domes under uniform pressure

By substituting Eqs. (5.15) and (5.16) to Eq. (4.1) and (4.20), one can obtain the geometry properties of parabolic domes

$$\bar{r}_1 = \frac{2\bar{a}(\bar{a}+\bar{z})^{\frac{3}{2}}}{\bar{a}^2} \tag{5.17}$$

$$\bar{r}_2 = 2\sqrt{\bar{a}(\bar{a}+\bar{z})} \tag{5.18}$$

$$\bar{n}_s = -\sqrt{\bar{a}\left(\bar{a}+\bar{z}\right)} \tag{5.19}$$

$$\bar{n}_\theta = -\frac{\bar{a}\left(\bar{a}+2\bar{z}\right)}{\sqrt{\bar{a}\left(\bar{a}+1\right)}} \tag{5.20}$$

By substituting of the foregoing geometrical parameters into the eigenvalue equation (4.41) in Chapter 4, and upon solving the equation, one obtains the critical buckling pressure parameter $\lambda = \frac{p_{cr} H\left(1-\nu_s \nu_\theta\right)}{\bar{E}h}$ of parabolic domes. Results for parabolic domes with different height-to-base radius ratios and base radius-to-thickness ratios will be given in the next section.

Convergence study

Table 5.6 shows the convergence of the critical buckling pressure for an isotropic parabolic dome of equal base radius and height, and clamped at the base. Results were generated for domes with base-radius-to-thickness ratio from *L/h* = 50 to 300. It can be seen from the table that the solutions from the Ritz method converge monotonically when the number of terms in the polynomials is increased. The convergence criterion for parabolic domes was also taken as 0.05%. It is of interest to note that the rate of convergence differs for different base-radius-to-thickness ratios. For the case of parabolic domes with a smaller *L/h* ratio, the critical buckling pressure converges faster than that of large *L*/*h* ratios. Unlike the case for clamped hemispherical domes where 40 terms are needed in the power series, only 30 terms are needed to satisfy the convergence criterion of 0.05% in clamped parabolic domes. This number of terms is assumed to be sufficient for yielding accurate results in parabolic domes of different height-to-base-radius ratios, base-radius-to-thickness ratios and support conditions.

Table 5.6 Convergence of critical buckling pressure parameter λ of a clamped parabolic dome with normalized base radius $\overline{L} = 1$

λ x10^3		Base radius over thickness ratio *L/h*				
		10	25	100	300	1000
Number of terms	3	306.24159	268.34711	260.36352	259.87675	259.82128
	6	160.04376	65.69875	37.59424	35.75372	35.54293
	9	151.57371	57.11352	15.62226	8.55188	7.69817
	12	151.52923	56.52362	12.71975	5.10587	2.78505
	15	151.52875	56.51417	12.27600	4.07852	1.62731
	18	151.52852	56.51386	12.21165	3.80622	1.43103
	21	151.52839	56.51366	12.20937	3.72199	1.16553
	24	151.52831	56.51353	12.20936	3.70724	1.09714
	27	151.52826	56.51343	12.20935	3.70623	1.06598
	30	151.52822	56.51336	12.20935	3.70617	1.04336

Table 5.7 Convergence of critical buckling pressure parameter λ of a simply supported parabolic dome with normalized base radius $\overline{L} = 1$

λ x10^3		Base radius over thickness ratio *L/h*				
		10	25	100	300	1000
Number of terms	3	163.11313	117.33128	106.67237	106.00877	105.93304
	6	110.63181	48.44707	15.19676	9.54045	8.85377
	9	110.08303	43.41861	11.15899	4.92409	2.22540
	12	110.06928	43.34664	10.31764	3.64115	1.47504
	15	110.06330	43.34458	10.21054	3.39915	1.22387
	18	110.05964	43.34344	10.20759	3.28913	1.02073
	21	110.05722	43.34270	10.20750	3.26611	0.98596
	24	110.05554	43.34218	10.20746	3.26337	0.96253
	27	110.05432	43.34180	10.20743	3.26322	0.94995
	30	110.05340	43.34151	10.20740	3.26321	0.94706

The methodology is readily adaptable to parabolic domes of different height, thickness, material properties and support conditions. Tables 5.8 presents the critical buckling pressures for parabolic domes of isotropic properties for both clamped and simply supported edge conditions.

Orthotropic Parabolic Domes under Uniform Pressure p

For the case of orthotropic parabolic domes, the same material properties with E_s = 120 GPa, E_θ = 4.8 GPa, $G_{s\xi}$ = 2.4 GPa and $v_{s\theta}$ = 0.25 for a graphite/epoxy composite are assumed. Base radius-to-height ratios in the range of $1/3 \le L/H \le 3$ and base radius-to-thickness ratios of $10 \le L/h \le 1000$ are considered.

The critical axisymmetric buckling pressure $\overline{p}_{cr}$ are presented in Table 5.9 for the domes with simply supported edge and fixed edge. It can be seen from this two tables that the critical buckling pressure $\overline{p}_{cr}$ is sensitive to the edge support conditions. For instance, for a base radius-to-thickness ratio of *L/h* =1/100 and base radius-to-height ratio of *L/H* = 1 the critical buckling pressure increases from p_{cr} = 5.6758 for the simply-supported edge condition to 7.5879 for the fixed edge condition. This shows that the critical buckling pressure increases by 1.34 times from the case of simply supported domes to fixed edge domes in this particular dome dimensions. Similarly, large increases in the critical buckling pressure are observed for other base radius-to-thickness and base radius-to-height ratios.

In order to check our results, we employ the finite element package SAP2000 (Computers and Structures, Inc, 2007) to analyze the above parabolic dome example. The type of shell element used is the thick shell element and the mesh design adopted for the analysis is shown in Fig. 5.4. The critical buckling pressures furnished by SAP2000 are $p_{cr} = 5.60892$ for simply supported dome and $p_{cr} = 7.7375$ for fixed edge dome. These finite element results are in good agreement with our results (within 2%), thereby confirming the correctness of our solutions.

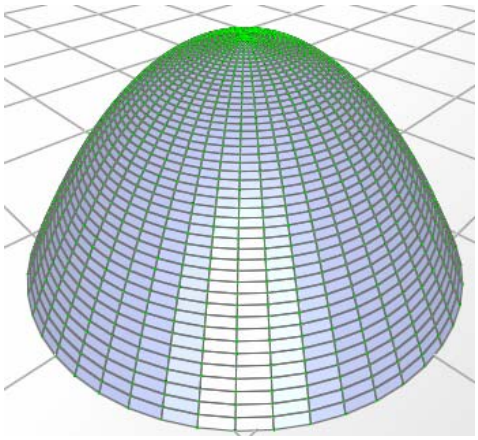

Fig 5.4 SAP2000 model of parabolic dome (50x50 elements)

Table 5.8 Buckling pressure parameter λ of isotropic parabolic domes

$\lambda .10^3$			Base radius over thickness ratio *L/h*			
			10	25	100	1000
Simply supported	*L/H*	1/3	882.07863	407.69691	105.74235	10.42014
		1/2	437.41458	188.47243	46.71385	4.45216
		1	110.05340	43.34151	10.20740	0.94706
		2	17.56449	6.70454	1.56722	0.14638
		3	4.52483	1.75368	0.41569	0.03946
Clamped	*L/H*	1/3	1085.90030	498.99744	122.36784	12.11705
		1/2	567.40922	238.32228	55.02010	4.98820
		1	151.52822	56.51336	12.20935	1.04336
		2	22.46878	8.30881	1.81417	0.15776
		3	5.29120	2.03606	0.46225	0.04177

Table 5.9 Buckling pressure parameter λ of orthotropic parabolic domes

$\lambda .10^3$			Base radius over thickness ratio *L/h*			
			10	25	100	1000
Simply supported	*L/H*	1/3	223.31297	154.46551	53.15067	5.48792
		1/2	133.90936	81.35266	24.64222	2.39820
		1	45.74201	22.25162	5.67579	0.51788
		2	8.93617	3.75169	0.87637	0.07961
		3	2.41126	0.99661	0.22899	0.02125
Clamped	*L/H*	1/3	231.13316	189.75079	66.17285	6.18249
		1/2	150.08675	107.14368	31.80184	2.73826
		1	62.41928	32.28857	7.58789	0.59871
		2	12.82840	5.34474	1.11203	0.08978
		3	3.39914	1.31463	0.27230	0.02323

5.4 Concluding remarks

The applicability of the Ritz method for various kinds of domes is demonstrated by solving the buckling problems of spherical and parabolic domes. The results are verified by comparing them with limited existing solutions. Based on these examples, it can be concluded that the developed Ritz method can be readily applied for the buckling analyses of arbitrarily shaped domes. In the next chapter, results for buckling of domes under hydrostatic pressure and selfweight will be presented.

CHAPTER 6

BUCKLING OF SUBMERGED DOMES

This chapter is concerned with the elastic, axisymmetric buckling of submerged moderately thick domes. In addition to the water pressure, the domes are also subjected to selfweight, which is invariably present in this type of structure. Applying the Ritz method presented in Chapter 4, new buckling solutions for moderately thick spherical and parabolic domes with various dimensions and boundary conditions are presented. The validity of the method, convergence and accuracy of solutions are also demonstrated.

6.1 Problem definition

Consider a dome of height *H,* base radius *L*, and uniform thickness *h*. The dome is formed by rotating a curve, defined by $r_0 = f(z)$ with $f'(0) = 0$, about the vertical *z* axis as shown in Fig. 6.1. The dome is subjected to hydrostatic pressure $p_h = \gamma_w(D - H + z)$ where γ_w is the specific weight of water and its selfweight $p_a = \gamma_a h$ where h is thickness of the dome and γ_a the specific weight of dome material.

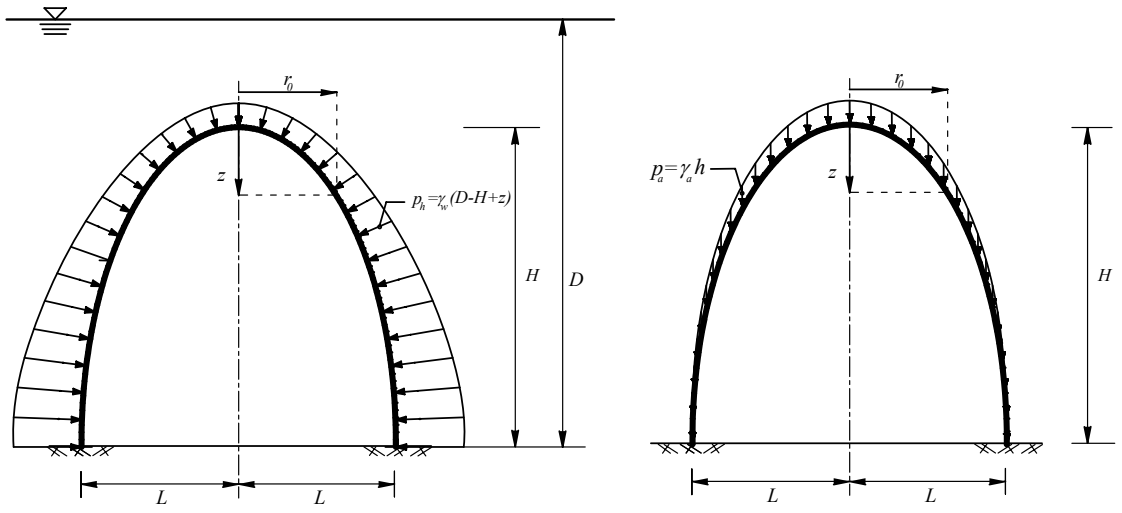

(a) Hydrostatic pressure (b) Selfweight

Fig 6.1 Domes under selfweight and hydrostatic pressure

The dome is also assumed to be free of geometrical and material imperfections. For a given dome height *H*, the problem at hand is to determine the critical pressure p_{cr}, for axisymmetric buckling of this submerged dome. This critical pressure will

provide information on the maximum height of water depth (or critical water depth) D_{cr} for which the dome can be constructed without premature buckling failure.

6.2 Governing equations and Ritz method

6.2.1 Geometrical and loading properties

Consider a dome subjected to hydrostatic pressure $p_h = \gamma_w(D-H)+\gamma_w z$ and its selfweight $p_a = \gamma_a h$. The positive direction of these loads and their distributions are shown in Figs. 6.2 and 6.3.

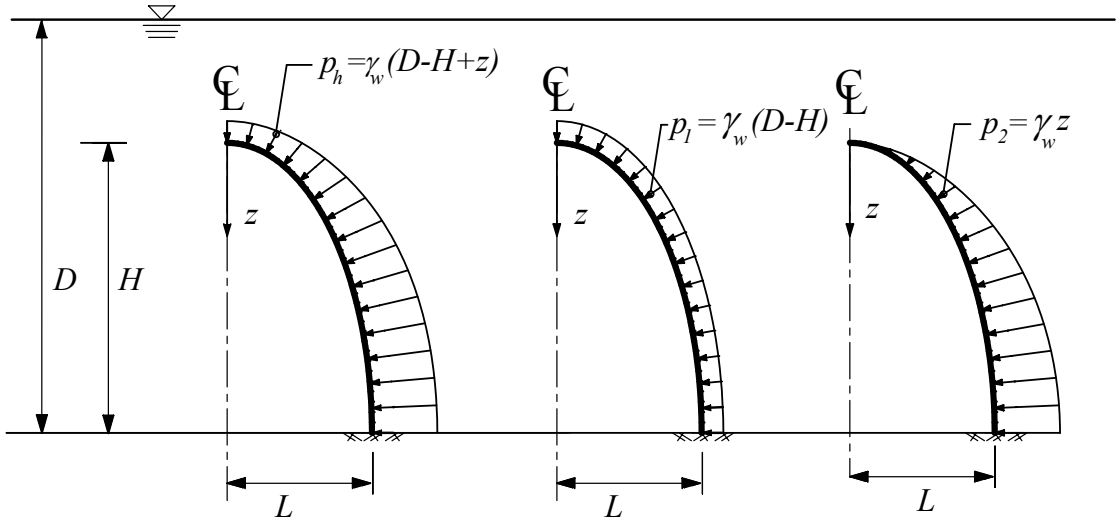

(a) Hydrostatic pressure (b) Pressure p_1 (c) Pressure p_2

Fig. 6.2 Hydrostatic pressure components

In the case of hydrostatic pressure (see Fig. 6.2a), we can separate the hydrostatic pressure p_h into two components p_1 and p_2. The pressure p_1 is constant over the surface of the dome (see Fig. 6.2b) and is calculated by the product of the distance from the water level to the apex of the dome $(D-H)$ and the specific weight of the water γ_w, i.e.

$$p_1 = \gamma_w(D-H) \tag{6.1}$$

According to Eqs. (5.3) and (5.4) in Chapter 5, we obtain the internal forces of the dome under uniform pressure p_1 as

$$N_{s1} = -\frac{p_1 r_2}{2} \tag{6.2}$$

$$N_{\theta 1} = -r_2\left(p_1 + \frac{N_{s1}}{r_1}\right) \tag{6.3}$$

Recall Eq. (4.17)

$$N_s = pn_s$$

$$N_\theta = pn_\theta \tag{4.17}$$

From Eqs. (6.1), (6.2) and (6.3), one obtains

$$p_{h1} = p_1 = \gamma_w (D - H) \tag{6.4}$$

$$n_{s1} = -\frac{r_2}{2} \tag{6.5a}$$

$$n_{\theta 1} = -r_2\left(1 + \frac{n_{s1}}{r_1}\right) \tag{6.5b}$$

On the other hand, the pressure p_2 is linearly dependent on the distance z from the apex of the dome (see Fig. 6.2c). We can see that z only varies for 0 to the dome height H. Therefore, for a given dome height, the pressure p_2 does not depend on the

water depth D and is given by

$$p_2 = \gamma_w z \tag{6.6}$$

From statical considerations, the membrane force N_s acting in the meridian direction is given by

$$N_{s2} = -\frac{1}{r_2 \sin^2 \phi} \int_0^{\phi} p_2 \cos\phi r_1 r_0 d\phi \tag{6.7}$$

In view of the following geometric relations for rotational shells

$$\begin{aligned} r_0 &= f(z) \\ r_0 &= r_2 \sin\phi \\ dr_0 &= ds\cos\phi = r_1 \cos\phi d\phi \end{aligned} \tag{6.8}$$

Eq. (6.7) may be expressed as

$$N_{s2} = -\gamma_w \frac{r_2}{r_0^2} \int_0^z z\, f(z) f'(z) dz \tag{6.9}$$

In view of Eq.(5.4), one obtains

$$N_{\theta 2} = -r_2 \left(\gamma_w z + \frac{N_{s2}}{r_1} \right) \tag{6.10}$$

Similar to the above case, one can obtain the loading parameters of rotational shells

$$p_{h2} = \gamma_w H \tag{6.11}$$

$$n_{s2} = -\frac{r_2}{Hr_0^2}\int_0^z z\, f(z) f'(z) dz \tag{6.12a}$$

$$n_{\theta 2} = -r_2\left(\frac{z}{H} + \frac{n_{s2}}{r_1}\right) \tag{6.12b}$$

In the case of selfweight (see Fig. 6.3), the internal membrane force is given by

$$N_{sa} = -\frac{1}{r_2 \sin^2\phi}\int_0^\phi p_a r_1 r_0 d\phi \tag{6.13}$$

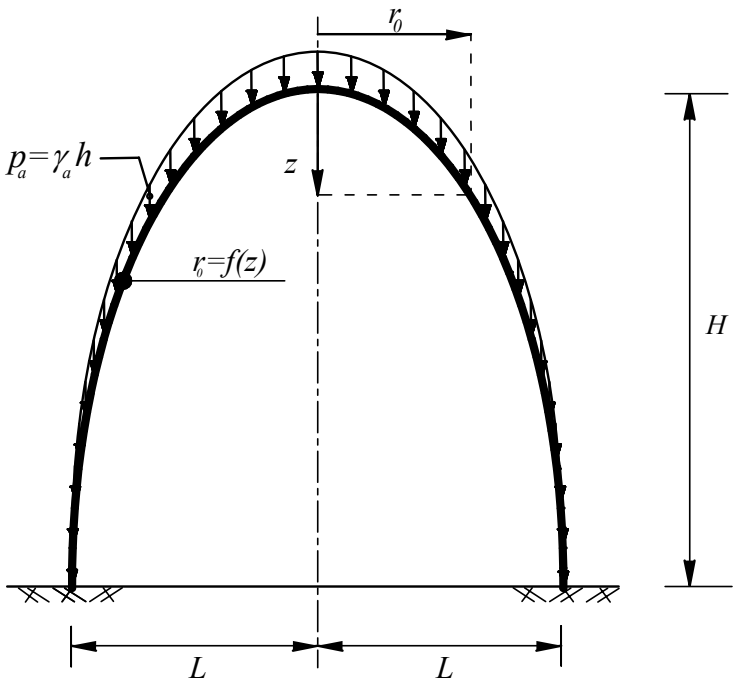

Fig. 6.3 Selfweight of the dome

In view of the geometric relations for rotational shells given in Eq. (6.8), Eq. (6.13) may be expressed as

$$N_{sa} = -\gamma_a h \frac{r_2}{r_0^2} \int_0^z f(z)\eta dz \tag{6.14}$$

where $\eta = \left\{1 + \left[\frac{df(z)}{dz}\right]^2\right\}^{\frac{1}{2}}$. In view of Eq. (5.4), one obtains

$$N_{\theta a} = -r_2 \left(\gamma_a h \frac{f'(z)}{\eta} + \frac{N_{sa}}{r_1} \right) \tag{6.15}$$

In view of Eq. (4.17) , one can obtain the geometrical and loading parameters of the domes as

$$p_a = \gamma_a h \tag{6.16}$$

$$n_{sa} = -\frac{r_2}{r_0^2} \int_0^z f(z)\eta dz \tag{6.17a}$$

$$n_{\theta a} = -r_2 \left(\frac{f'(z)}{\eta} + \frac{n_{sa}}{r_1} \right) \tag{6.17b}$$

6.2.2 Energy functionals and Ritz method

The elastic strain energy of the dome was derived in Eq.(4.22) as

$$\overline{U} = \int_{-1/2}^{1/2}\int_{0}^{1} \left\{ \overline{A}_{11}\left(\frac{\partial \overline{r}_0}{\eta \partial \overline{z}}\frac{\overline{u}}{\overline{r}_0} + \frac{\overline{w}}{\overline{r}_2} + \xi\overline{\zeta}\frac{\partial \overline{r}_0}{\eta\partial\overline{z}}\frac{\overline{\psi}}{\overline{r}_0}\right)^2 + \overline{A}_{22}\left(\frac{\partial \overline{u}}{\eta\partial\overline{z}} + \frac{\overline{w}}{\overline{r}_1} + \xi\overline{\zeta}\frac{\partial\overline{\psi}}{\eta\partial\overline{z}}\right)^2 \right.$$
$$+ 2\overline{A}_{12}\left(\frac{\partial \overline{u}}{\eta\partial\overline{z}} + \frac{\overline{w}}{\overline{r}_1} + \xi\overline{\zeta}\frac{\partial\overline{\psi}}{\eta\partial\overline{z}}\right)\left(\frac{\partial \overline{r}_0}{\eta\partial\overline{z}}\frac{\overline{u}}{\overline{r}_0} + \frac{\overline{w}}{\overline{r}_2} + \xi\overline{\zeta}\frac{\partial\overline{r}_0}{\eta\partial\overline{z}}\frac{\overline{\psi}}{\overline{r}_0}\right) \tag{4.22}$$
$$\left. + \overline{A}_{44}\left(-\frac{\overline{u}}{\overline{r}_1} + \frac{\partial\overline{w}}{\eta\partial\overline{z}} + \overline{\psi}\right)^2 \right\} \eta\overline{r}_0 d\overline{z}d\zeta$$

Note that the work done by the hydrostatic pressure is the sum of the work done by each load component p_1 and p_2. The work done by the hydrostatic pressure and selfweight is thus given by

$$\overline{W} = \overline{W}_1 + \overline{W}_2 + \overline{W}_a \tag{6.18}$$

In view of Eq.(4.23), one obtains

$$\overline{W}_1 = \lambda_1 \int_0^1 \left\{ \overline{n}_{s1}\left[\left(\frac{\partial\overline{u}}{\eta\partial\overline{z}} + \frac{\overline{w}}{\overline{r}_1}\right)^2 + \left(\frac{\overline{u}}{\overline{r}_1} - \frac{\partial\overline{w}}{\eta\partial\overline{z}}\right)^2\right] + \overline{n}_{\theta 1}\left(\frac{\partial\overline{r}_0}{\eta\partial\overline{z}}\frac{\overline{u}}{\overline{r}_0} + \frac{\overline{w}}{\overline{r}_2}\right)^2 \right\} \eta\overline{r}_0 d\overline{z} \tag{6.19}$$

$$\overline{W}_2 = \lambda_2 \int_0^1 \left\{ \overline{n}_{s2}\left[\left(\frac{\partial\overline{u}}{\eta\partial\overline{z}} + \frac{\overline{w}}{\overline{r}_1}\right)^2 + \left(\frac{\overline{u}}{\overline{r}_1} - \frac{\partial\overline{w}}{\eta\partial\overline{z}}\right)^2\right] + \overline{n}_{\theta 2}\left(\frac{\partial\overline{r}_0}{\eta\partial\overline{z}}\frac{\overline{u}}{\overline{r}_0} + \frac{\overline{w}}{\overline{r}_2}\right)^2 \right\} \eta\overline{r}_0 d\overline{z} \tag{6.20}$$

$$\overline{W}_a = \lambda_a \int_0^1 \left\{ \overline{n}_{sa}\left[\left(\frac{\partial\overline{u}}{\eta\partial\overline{z}} + \frac{\overline{w}}{\overline{r}_1}\right)^2 + \left(\frac{\overline{u}}{\overline{r}_1} - \frac{\partial\overline{w}}{\eta\partial\overline{z}}\right)^2\right] + \overline{n}_{\theta a}\left(\frac{\partial\overline{r}_0}{\eta\partial\overline{z}}\frac{\overline{u}}{\overline{r}_0} + \frac{\overline{w}}{\overline{r}_2}\right)^2 \right\} \eta\overline{r}_0 d\overline{z} \tag{6.21}$$

where the non-dimensional terms are defined as

$$\overline{n}_{s1} = \frac{n_{\phi 1}}{H};\ \ \overline{n}_{\theta 1} = \frac{n_{\theta 1}}{H}$$

$$\lambda_1 = \frac{p_{h1}(1-\nu_s\nu_\theta)}{\overline{E}\xi} = \frac{\gamma_w(D-H)(1-\nu_s\nu_\theta)}{\overline{E}\xi}; \tag{6.22a-c}$$

$$\overline{n}_{s2} = \frac{n_{s2}}{H};\ \overline{n}_{\theta 2} = \frac{n_{\theta 2}}{H}$$

$$\lambda_2 = \frac{p_{h2}(1-\nu_s\nu_\theta)}{\overline{E}\xi} = \frac{\gamma_w H(1-\nu_s\nu_\theta)}{\overline{E}\xi} \tag{6.23a-c}$$

$$\overline{n}_{sa} = \frac{n_{sa}}{H};\ \overline{n}_{\theta a} = \frac{n_{\theta a}}{H}$$

$$\lambda_a = \frac{p_a(1-\nu_s\nu_\theta)}{\overline{E}\xi} = \frac{\gamma_a h(1-\nu_s\nu_\theta)}{\overline{E}\xi} \tag{6.24a-c}$$

The total potential energy functional $\overline{\Pi}$ of the dome under uniform pressure may be written as

$$\overline{\Pi} = \overline{U} + \overline{W} \tag{6.25}$$

Following the standard procedure for the Ritz method in Chapter 4, the unknown coefficients c_i are obtained by extremizing the total potential energy functional Π, i.e.

$$\left\langle \frac{\partial \Pi}{\partial c_i} \right\rangle = \langle 0 \rangle; \quad i = 1,2,...,N_3 \tag{6.26}$$

which yields a set of homogeneous equations that can be conveniently expressed in a matrix form containing the unknown coefficients c_i

$$\left([K] + \lambda_1[M_1] + \lambda_2[M_2] + \lambda_a[M_a]\right)\{c\} = \{0\} \tag{6.27}$$

where [K] is stiffness matrix; [M_1], [M_2] and [M_a] are work matrices by the pressure p_1, p_2 and p_a and $\{c\}$ is a column vector consisting of the coefficients c_i. It is to be

noted that λ_2 and λ_a are known from the information given on the dome height *H*, dome thickness *h*, specific weight of water γ_w and specific weight of dome material γ_a. Therefore, λ_1 becomes the unknown eigenvalue of the governing equation. The eigenvalue problem is solved using built-in function **Eigenvalues** in the software package Mathematica (Wolfram, 1999). Recall the critical buckling pressure parameter λ_1 is defined as (see Eq. 6.13c)

$$\lambda_1 = \frac{\gamma_w (D-H)(1-\nu_s \nu_\theta)}{\overline{E}\xi} \tag{6.28}$$

The critical water depth in which the submerged dome will buckle is given by

$$D = \lambda_1 \frac{\overline{E}\xi}{\gamma_w (1-\nu_s \nu_\theta)} + H \tag{6.29}$$

In the subsequent sections, we present new buckling solutions for moderately thick spherical and parabolic domes with various dimensions and boundary conditions under their own selfweight and hydrostatic pressure. The validity of the method, convergence and accuracy of solutions are also demonstrated.

6.3 Results and discussions

As an example, consider a dome of height *H*=3000cm submerged at the water depth *D*. For the subsequent numerical calculations, the dome is assumed to be made from a material with values of $E_s = E_\theta = 30.10^4$ kgf/cm^2, $\nu_{s\theta} =$ 0.3 and $\gamma_a = 2.4 \times 10^{-3}$ kgf/cm^3. The specific weight of water is assumed in the calculation $\gamma_w = 1x10^{-3}$ kgf/cm^3. These values give rise to

$$\lambda_2 = \frac{\gamma_w H(1-\nu_s\nu_\theta)}{\overline{E}\xi} = \frac{4.55x10^{-7}}{\xi} \tag{6.30}$$

$$\lambda_a = \frac{\gamma_a h(1-\nu_s\nu_\theta)}{\overline{E}\xi} = \frac{\gamma_a H(1-\nu_s\nu_\theta)}{\overline{E}} = 1.092x10^{-6} \tag{6.31}$$

With the given value of normalized thickness ξ, substituting Eqs. (6.30) and (6.31) to Eq.(6.16), one obtains the critical buckling parameter λ_1. Therefore, the critical buckling water depth can also obtained from Eq. (6.29)

$$D = \lambda_1 \frac{\overline{E}\xi}{\gamma_w(1-\nu_s\nu_\theta)} + H \tag{6.32}$$

Note that, in case of γ_a = 0, one obtains the critical buckling of domes under hydrostatic force only.

6.3.1 Spherical Domes

Similarly to part 5.3.1 of chapter 5, for spherical domes, the meridional curve is defined by (see Fig. 6.4)

$$\bar{r}_0 = \sqrt{2\bar{R}\bar{z} - \bar{z}^2} \tag{6.33}$$

where $\bar{R} = \dfrac{R}{H}$ and $\bar{z} = \dfrac{z}{H}$

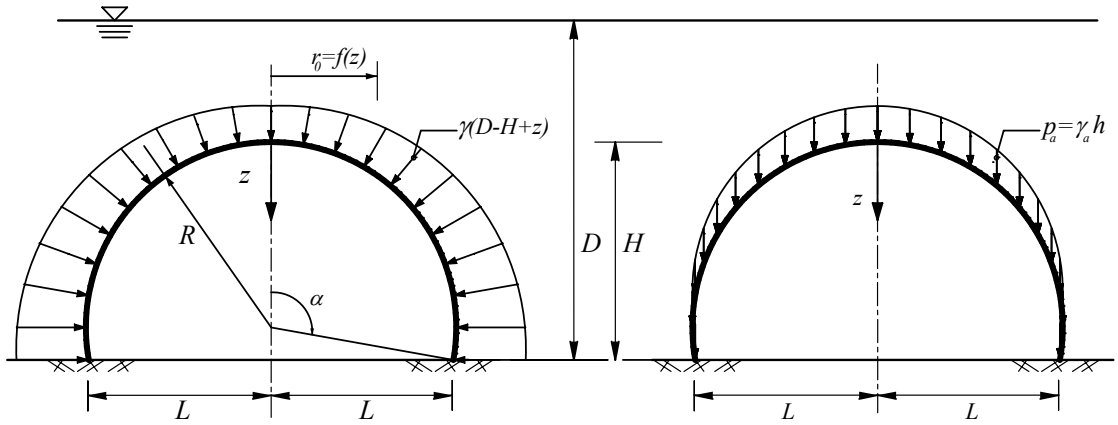

Fig 6.4 Spherical dome under its own selfweight and hydrostatic pressure

By substituting Eq. (6.30) to Eq.(4.1), one can obtain the geometric properties of spherical shells

$$\bar{r}_1 = \bar{r}_2 = \bar{R} \tag{6.34}$$

In view of Eqs. (6.4) and (6.5), the parameters of the hydrostatic component p_1 are given by

$$\bar{n}_{s1} = \bar{n}_{\theta 1} = -\frac{\bar{R}}{2} \tag{6.35}$$

By substituting Eq. (6.34) to Eqs. (6.11) and (6.12), one obtains the parameters of hydrostatic component p_2

$$\overline{n}_{s2} = -\frac{\overline{R}\left(3\overline{R} - 2\overline{z}\right)\overline{z}}{12\overline{R} - 6\overline{z}} \tag{6.36}$$

$$\overline{n}_{\theta 2} = -\frac{\overline{R}\overline{z}\left(4\overline{z} - 9\overline{R}\right)}{12\overline{R} - 6\overline{z}} \tag{6.37}$$

Similarly, by substituting Eq. (6.34) to Eqs. (6.16) and (6.17), the selfweight parameters is given by

$$\overline{n}_{sa} = -\frac{\overline{R}^2}{2\overline{R} - \overline{z}} \tag{6.38}$$

$$\overline{n}_{\theta a} = -\frac{\overline{R}^2 - 3\overline{z}\overline{R} + z^2}{2\overline{R} - \overline{z}} \tag{6.39}$$

By substituting all the above geometric parameters into the eigenvalue equation (6.27), one can obtain the buckling pressure parameters λ_1 and the critical water depth in which the submerged dome will buckle.

Convergence study

Tables 6.1 and 6.2 show the convergence of the critical buckling pressure parameter λ_1 for weightless hemispherical domes under hydrostatic forces by setting the specific weight of the dome material as $\gamma_a = 0$.

Table 6.3 and 6.4 show the convergence of the critical buckling pressure parameter λ_1 of hemispherical domes under their own selfweight and hydrostatic pressure with radius-to-thickness ratio from R/h = 10 to R/h = 300 with different boundary conditions: clamped, simply supported.

The same as for the uniform pressure case, in order to obtain an accurate solution, the number of terms in the power series is increased until the difference in the result is less than or equal to 0.05%. It can be seen from the tabulated results that the critical buckling pressure parameter λ_1 achieves the required 0.05% accuracy when 40 terms were taken in the polynomial functions. This number of terms is assumed to be sufficient for accurate results of other spherical shells generated in this chapter.

Table 6.1 Convergence of critical buckling pressure parameter λ_1 of clamped hemispherical domes under hydrostatic pressure only

$\lambda_1 \times 10^3$		Radius over thickness ratio *R/h*			
		10	25	100	300
Number of terms	3	222.39639	194.00132	188.12904	187.48133
	6	118.52774	55.62063	26.93537	24.41495
	9	112.81965	46.53730	14.11276	6.62415
	12	110.92726	45.66285	11.46389	4.44392
	15	109.83091	45.23730	11.11006	3.42276
	18	109.14228	44.92945	11.04762	3.14028
	21	108.68325	44.69574	11.03112	3.03240
	24	108.36170	44.51550	11.02182	3.02392
	27	108.12673	44.37456	11.01425	3.02328
	30	107.94863	44.26252	11.00714	3.02328
	33	107.80918	44.17175	11.00002	3.02328
	36	107.69669	44.09661	10.99257	3.02328
	39	107.60338	44.03287	10.98448	3.02328
	40	107.57558	44.01358	10.98157	3.02328

Table 6.2 Convergence of critical buckling pressure parameter λ_1 of a simply supported hemispherical domes under hydrostatic pressure only

$\lambda_1 \times 10^3$		Radius over thickness ratio *R/h*			
		10	25	100	300
Number of terms	3	159.42869	102.91870	88.26668	86.78558
	6	106.55644	46.41693	16.43394	8.50931
	9	105.93322	43.85519	11.68065	4.81828
	12	105.61462	43.50903	10.97080	3.21768
	15	105.36832	43.36872	10.79344	2.96056
	18	105.18038	43.26883	10.77757	2.86980
	21	105.03771	43.19032	10.77643	2.85274
	24	104.92840	43.12707	10.77605	2.85023
	27	104.84323	43.07552	10.77583	2.85018
	30	104.77550	43.03301	10.77566	2.85017
	33	104.72046	42.99749	10.77551	2.85017
	36	104.67470	42.96728	10.77537	2.85017
	39	104.63575	42.94105	10.77523	2.85016
	40	104.62397	42.93300	10.77517	2.85016

Table 6.3 Convergence of critical buckling pressure parameter λ_1 of a clamped spherical hemispherical under its own selfweight and hydrostatic pressure

$\lambda_1 \times 10^3$		Radius over thickness ratio *R/h*			
		10	25	100	300
Number of terms	3	222.37027	193.97458	188.10213	187.45440
	6	118.50084	55.59072	26.90317	24.38265
	9	112.79475	46.51126	14.08138	6.58786
	12	110.90279	45.63755	11.43356	4.40858
	15	109.80665	45.21236	11.08176	3.38647
	18	109.11814	44.90478	11.02027	3.10635
	21	108.65919	44.67126	11.00410	2.99859
	24	108.33768	44.49116	10.99500	2.99022
	27	108.10275	44.35033	10.98760	2.98961
	30	107.92467	44.23838	10.98065	2.98960
	33	107.78525	44.14767	10.97368	2.98960
	36	107.67278	44.07258	10.96640	2.98960
	39	107.57948	44.00889	10.95849	2.98960
	40	107.55168	43.98961	10.95564	2.98960

Table 6.4 Convergence of critical buckling pressure parameter λ_1 of a simply supported hemispherical domes under its own selfweight and hydrostatic pressure

$\lambda_1 \times 10^3$		Radius over thickness ratio *R/h*			
		10	25	100	300
Number of terms	3	159.39456	102.88405	88.23202	86.75092
	6	106.52590	46.38259	16.39416	8.46966
	9	105.90364	43.82325	11.64241	4.77710
	12	105.58557	43.47845	10.93461	3.17736
	15	105.33969	43.33871	10.75953	2.92116
	18	105.15208	43.23924	10.74441	2.83112
	21	105.00965	43.16109	10.74334	2.81446
	24	104.90052	43.09812	10.74298	2.81209
	27	104.81549	43.04679	10.74278	2.81204
	30	104.74787	43.00448	10.74263	2.81204
	33	104.69291	42.96911	10.74249	2.81203
	36	104.64722	42.93903	10.74236	2.81203
	39	104.60833	42.91292	10.74223	2.81203
	40	104.59657	42.90490	10.74218	2.81203

Figure 6.5 shows the variation of the critical water depth $\overline{D}_{cr} = D/H$ for which that the dome can be constructed without buckling failure. Results were generated for a spherical dome with a normalized base radius $\overline{L}$ = 1,2 and 3. It can be seen that, for a same value of normalized thickness ξ, the normalized critical water depth $\overline{D}_{cr}$ of the dome has the smaller base radius $\overline{L}$ much larger. For example, for the same normalized thickness ξ = 0.01, the critical water depth $\overline{D}_{cr}$ =13.039 for the dome with a normalized base radius $\overline{L}$ =3, which is considerably larger than the critical water depth $\overline{D}_{cr}$ =1.19 of the dome with a normalized base radius $\overline{L}$ =1.

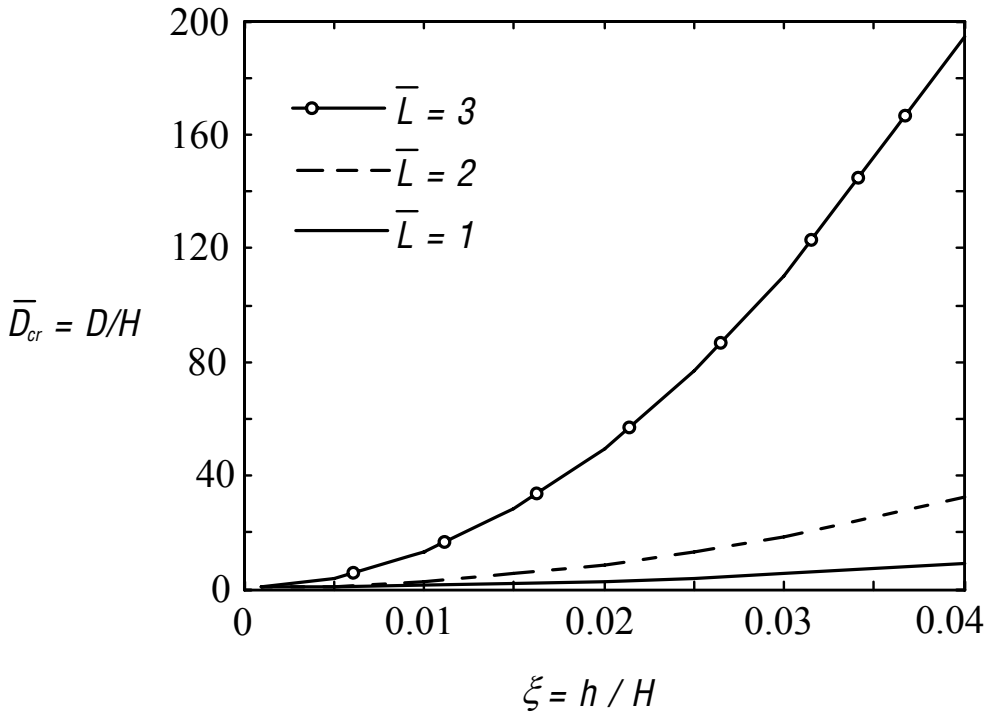

Fig 6.5 Variations of critical water depth $\overline{D}_{cr} = D/H$ with respect to normalized thickness $\xi = h/H$ of a hemispherical dome

6.3.2 Parabolic Domes

Similar to part 5.3.2 of chapter 5, for parabolic domes, the meridional curve is defined by (see Fig. 6.6)

$$\bar{r}_0 = \sqrt{4\bar{a}\bar{z}} \tag{6.40}$$

where $\bar{a} = \dfrac{a}{H} = \dfrac{L^2}{4H^2} = \dfrac{\bar{L}^2}{4}$

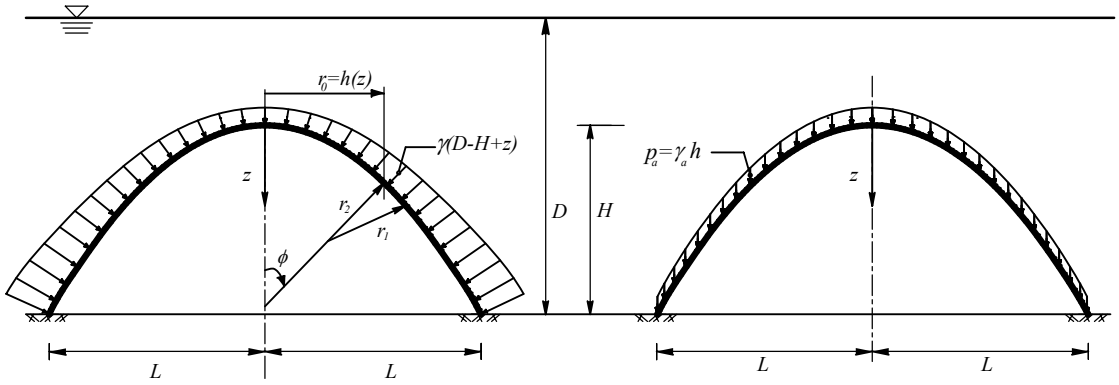

Fig 6.6 Parabolic dome under its own selfweight and hydrostatic pressure

Similarly the above spherical case, by substituting Eqs.(6.41) to Eqs (6.4), (6.5), (6.11), (6.12), (6.16) and (6.17), one can obtain the geometric properties of parabolic domes

- Meridional and circumference radii

$$\bar{r}_1 = \frac{2\bar{a}\left(\bar{a}+\bar{z}\right)^{\frac{3}{2}}}{\bar{a}^2} \tag{6.41}$$

$$\bar{r}_2 = 2\sqrt{\bar{a}\left(\bar{a}+\bar{z}\right)} \tag{6.42}$$

- Hydrostatic component p_1

$$\bar{n}_{s1} = -\sqrt{\bar{a}\left(\bar{a}+\bar{z}\right)} \tag{6.43}$$

$$\bar{n}_{\theta 1} = -\frac{\bar{a}(\bar{a}+2\bar{z})}{\sqrt{\bar{a}(\bar{a}+\bar{z})}} \tag{6.44}$$

- Hydrostatic component p_2

$$\bar{n}_{s2} = -\frac{1}{2}\bar{z}\sqrt{\bar{a}(\bar{a}-\bar{z})} \tag{6.45}$$

$$\bar{n}_{\theta 2} = -2\bar{z}\sqrt{\bar{a}(\bar{a}-\bar{z})}\left(\bar{z}-\frac{\bar{a}\bar{z}}{4(\bar{a}+\bar{z})}\right) \tag{6.46}$$

- Selfweight parameters:

$$\bar{n}_{sa} = -\frac{2\sqrt{\bar{a}(\bar{a}+\bar{z})}\left(-\bar{a}^2+\bar{z}\sqrt{\bar{a}(\bar{a}+\bar{z})}+\sqrt{\bar{a}^3(\bar{a}+\bar{z})}\right)}{3\bar{a}\bar{z}} \tag{6.47}$$

$$\bar{n}_{\theta a} = -\frac{2\bar{a}\left(\bar{a}^2-\left(\bar{z}+\sqrt{\bar{a}(\bar{a}+\bar{z})}\right)\bar{a}-2\bar{z}^2\right)}{3\bar{z}(\bar{a}+\bar{z})} \tag{6.58}$$

Tables 6.5 and 6.6 show the convergence of the critical buckling pressure parameter λ_1 for weightless parabolic domes with $\bar{L}=1$ under hydrostatic forces by setting specific weight of the dome material as γ_a = 0. Tables 6.7 and 6.8 show the convergence of the critical buckling pressure parameter λ_1 of parabolic domes with $\bar{L}=1$ under their own selfweight and hydrostatic pressure with height-to-thickness ratios from *H/h* = 10 to *H/h* = 300 with different boundary conditions: clamped, simply supported.

The same for the uniform pressure case, in order to obtain an accurate solution, the number of polynomial terms is increased until the difference in the result is less than or equal to 0.05%. It can be seen from the tabulated results that the critical buckling pressure parameter λ_1 achieves the required 0.05% accuracy when 30 terms were

taken in the polynomial function. This number of terms is assumed to be sufficient for accurate results of other parabolic shells generated in this chapter.

Table 6.5 Convergence of critical buckling pressure parameter λ_1 of clamped parabolic domes with normalized base radius $\overline{L} = 1$ under hydrostatic pressure only

$\lambda_1 \text{x} 10^3$		Height-over-thickness ratio *H/h*			
		10	25	100	300
Number of terms	3	306.20544	268.25757	260.00589	258.80373
	6	160.01226	65.61563	37.26095	34.75325
	9	151.54276	57.03116	15.24487	7.40797
	12	151.49825	56.44285	12.35274	3.89063
	15	151.49777	56.43338	11.91667	2.90081
	18	151.49754	56.43308	11.85564	2.65044
	21	151.49741	56.43287	11.85336	2.57042
	24	151.49733	56.43274	11.85334	2.55510
	27	151.49727	56.43264	11.85333	2.55401
	30	151.49724	56.43257	11.85333	2.55399

Table 6.6 Convergence of critical buckling pressure parameter λ_1 of a simply supported parabolic domes with normalized base radius $\overline{L} = 1$ under hydrostatic pressure only

$\lambda_1 \text{x} 10^3$		Height-over-thickness ratio *H/h*			
		10	25	100	300
Number of terms	3	163.07327	117.23260	106.27888	104.82850
	6	110.59318	48.35053	14.77523	8.28281
	9	110.04449	43.32113	10.75227	3.61208
	12	110.03074	43.24899	9.91127	2.36965
	15	110.02476	43.24692	9.80371	2.12465
	18	110.02109	43.24579	9.80068	2.01849
	21	110.01868	43.24504	9.80060	2.00114
	24	110.01699	43.24452	9.80055	1.99960
	27	110.01577	43.24414	9.80052	1.99952
	30	110.01485	43.24386	9.80049	1.99951

Table 6.7 Convergence of critical buckling pressure parameter λ_1 of a clamped parabolic domes with normalized base radius $\overline{L} = 1$ under its own selfweight and hydrostatic pressure

$\lambda_1 \text{x} 10^3$		Height-over-thickness ratio *H/h*			
		10	25	100	300
Number of terms	3	306.17307	268.22526	259.97358	258.77143
	6	159.98111	65.58308	37.22836	34.72065
	9	151.51145	56.99835	15.21022	7.37320
	12	151.46692	56.41022	12.31829	3.85500
	15	151.46644	56.40074	11.88241	2.86550
	18	151.46621	56.40044	11.82147	2.61528
	21	151.46608	56.40023	11.81918	2.53525
	24	151.46600	56.40010	11.81916	2.51992
	27	151.46595	56.40000	11.81916	2.51882
	30	151.46591	56.39993	11.81915	2.51880

Table 6.8 Convergence of critical buckling pressure parameter λ_1 of a simply supported parabolic domes with normalized base radius $\overline{L} = 1$ under its own selfweight and hydrostatic pressure

$\lambda_1 \text{x} 10^3$		Height-over-thickness ratio *H/h*			
		10	25	100	300
Number of terms	3	163.04084	117.20001	106.24627	104.79588
	6	110.55973	48.31640	14.73944	8.24706
	9	110.01104	43.28662	10.71679	3.57560
	12	109.99729	43.21445	9.87573	2.33351
	15	109.99131	43.21238	9.76814	2.08843
	18	109.98764	43.21125	9.76511	1.98229
	21	109.98522	43.21050	9.76502	1.96499
	24	109.98354	43.20998	9.76498	1.96345
	27	109.98232	43.20960	9.76494	1.96337
	30	109.98139	43.20931	9.76492	1.96337

Figure 6.7 shows the variation of the critical water depth $\overline{D}_{cr} = D/H$ for which the dome can be constructed without buckling failure. Results were generated for parabolic domes with normalized base radius $\overline{L}$ = 1,2 and 3. It can be seen that, for a same value of the normalized thickness ξ, the normalized critical water depth $\overline{D}_{cr}$ of the dome has the smaller base radius $\overline{L}$ much larger. For example, for the same normalized thickness ξ = 0.01, the critical water depth $\overline{D}_{cr}$ =13.398 for the dome with normalized base radius $\overline{L}$ =3, which is considerably larger than the critical water depth $\overline{D}_{cr}$ =1.137 of the dome with a normalized base radius $\overline{L}$ =1.

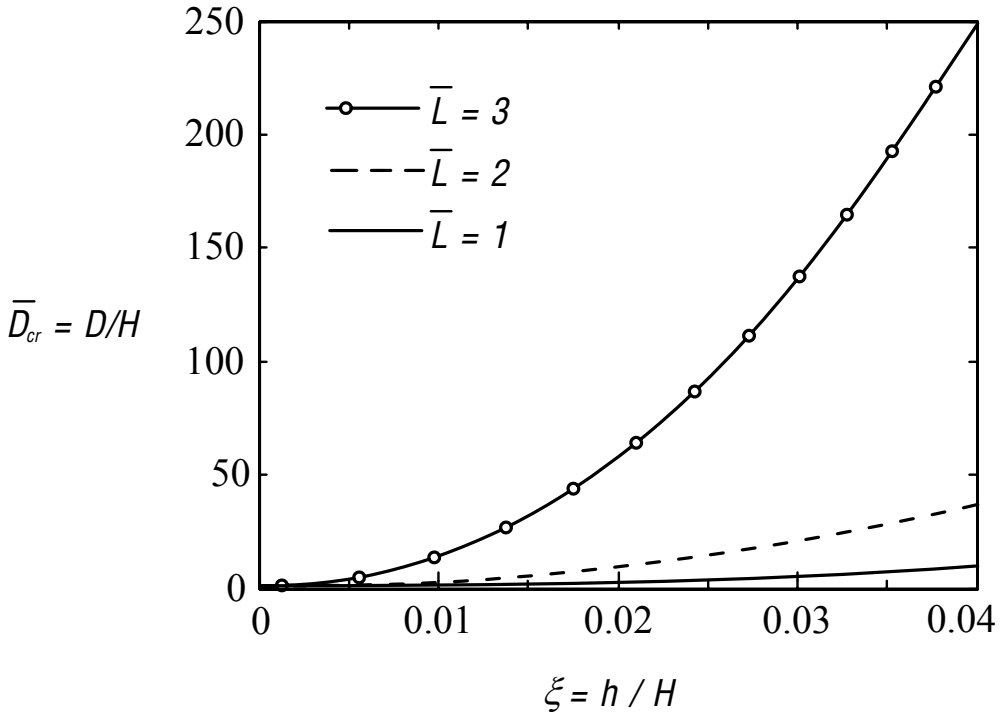

Fig 6.7 Variation of critical water depth $\overline{D}_{cr} = D/H$ with respect to normalized thickness $\xi = h/H$ of parabolic dome

6.4 Concluding remarks

The applicability of the Ritz method for various kinds of domes is demonstrated by solving the buckling problems of spherical and parabolic domes under selfweight and hydrostatic pressure. Based on these examples, it can be concluded that the developed Ritz method can be readily applied for the buckling analyses of arbitrarily shaped rotational shells under their own selfweight and hydrostatic pressure.

CHAPTER 7

OPTIMAL DESIGNS OF SUBMERGED DOMES AGAINST BUCKLING

This chapter is concerned with the optimal design of moderately thick submerged domes. In addition to the water pressure, we also take into consideration the selfweight, which is a significant load for such long span structures. For a given dome height, based on a family of domes that is defined by the meridian curve $r_0 = f(z)$ with $f'(0) = 0$ and submerged in a given water depth, we seek the dome design for minimum weight as well as maximum enclosed airspace whereby the dome will not buckle under the hydrostatic pressure and its own weight. The performance index of the optimization is formulated as the weighted sum of individual objectives in order to obtain Pareto optimal solutions. The buckling analysis of the submerged dome is carried out using the Ritz method that was presented in Chapter 6.

.

7.1 Problem definition

Consider a dome of height H and uniform thickness h. The dome is formed by rotating a curve, defined by $r_0 = f(z)$ with $f'(0) = 0$, about the vertical z axis as shown in Fig. 7.1. The dome is deployed under a water depth of D and thus it is subjected to a hydrostatic pressure $p_h = \gamma_w(D - H + z)$ as shown in Fig. 7.1a where γ_w is the specific weight of water. The loading due to its selfweight is $p_a = \gamma_a h$ as shown in Fig. 7.1b where h is the thickness of the dome and γ_a the specific weight of the dome material. The dome is also assumed to be free of geometrical and material imperfections.

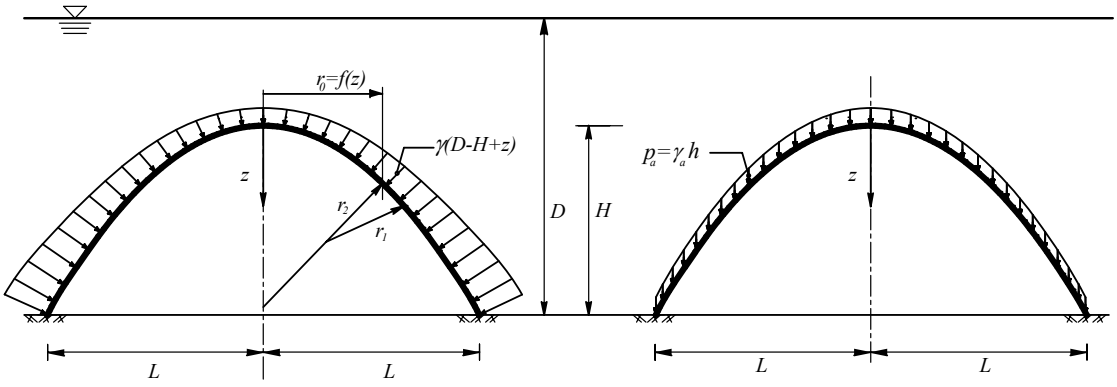

(a) Hydrostatic pressure **(b)** Selfweight

Fig 7.1 Dome under selfweight and hydrostatic pressure

For a given dome height H and water depth D_{rc0}, there is a family of domes defined by $r_0 = f(z)$ (see Fig. 7.2) that will not buckle when deployed in a given water depth D_{cr0}. Based on this family of domes, we seek the dome with the maximum enclosed airspace S_a and minimum weight W_a. The problem will be specialized for the optimization of a family of spherical domes (Fig. 7.2) and parabolic domes (Fig 7.3) and extensive results are presented in this chapter.

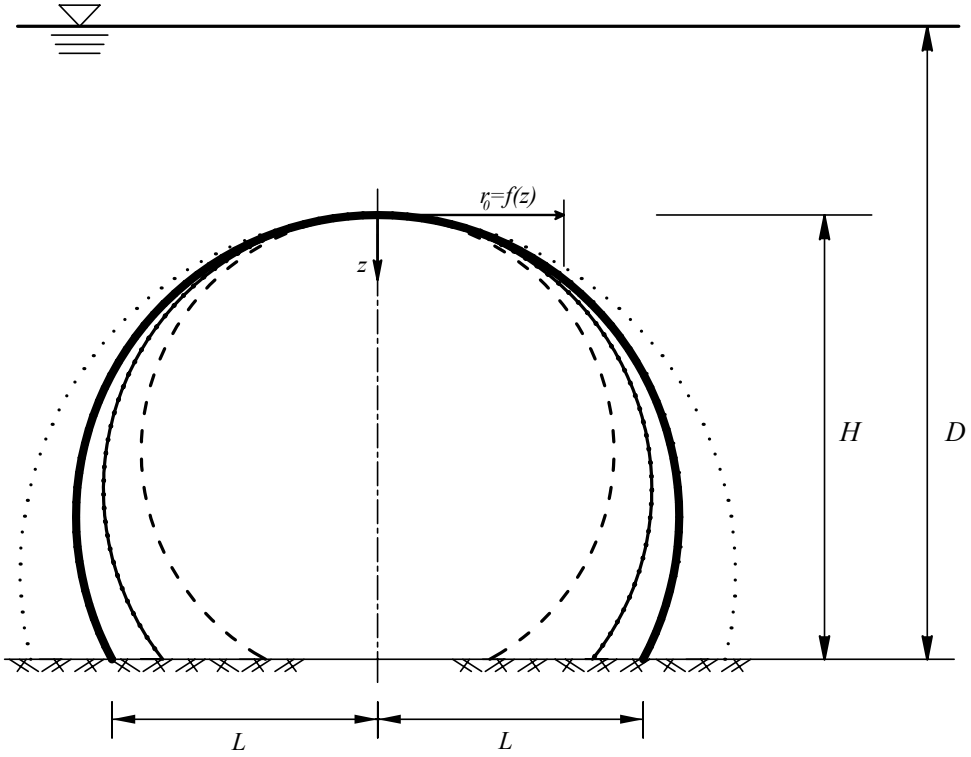

Fig. 7.2 Family of spherical domes for a given dome height H

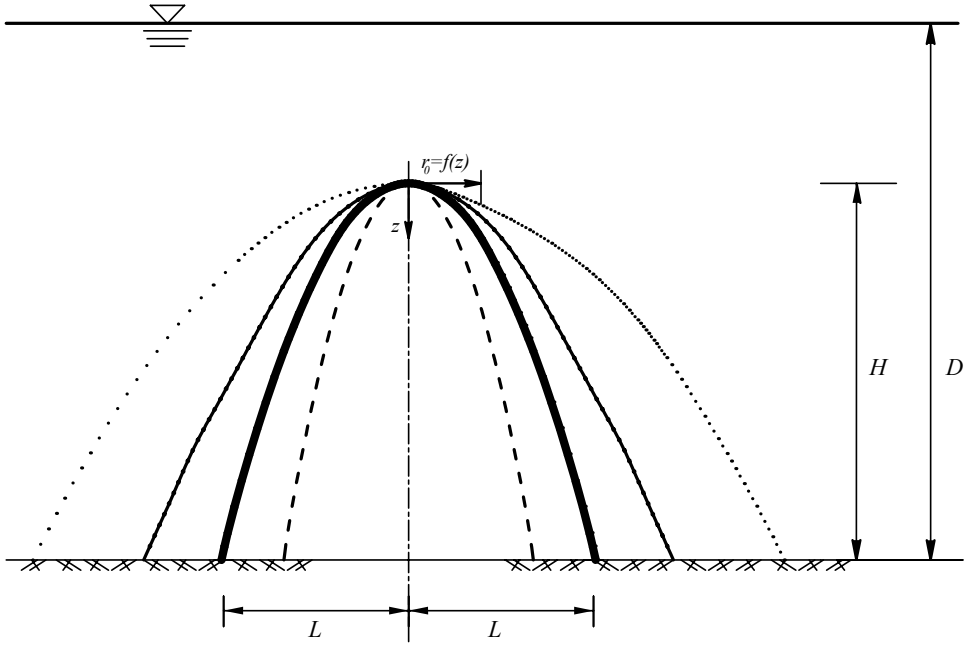

Fig 7.3 Family of parabolic domes for a given dome height H

7.2 Method of Optimization

The weight W_a of a uniform thickness dome, defined by $r_0 = f(z)$ with $f'(0) = 0$, can be calculated as follows

$$W_a = 2\gamma_a \pi h \int_0^H f(z)\sqrt{1 + f'(z)^2}\, dz \tag{7.1}$$

The enclosed airspace S_a of the dome is given by

$$S_a = \pi \int_0^H [f(z)]^2 dz \tag{7.2}$$

Although Eqs. (7.1) and (7.2) are valid for any function $f(z)$, we first restrict our study to a family of spherical domes for which the meridional curves is defined by

$$r_0 = f(z) = \sqrt{2Rz - z^2} \tag{7.3}$$

In view of the non-dimensional parameters in Eq. (4.20), Eq. (7.3) may be expressed as

$$\bar{r}_0 = \sqrt{2\bar{R}\bar{z} - \bar{z}^2} \tag{7.4}$$

where $\bar{R} = R/H$ and $\bar{z} = z/H$.

By substituting Eq. (7.4) into Eq. (7.1) and in view of Eq. (4.20), one obtains the weight of a spherical dome as

$$\overline{W}_{ap} = \frac{W_{ap}}{H^3} = \pi\xi\left(\overline{L}^2 + 1\right) \tag{7.5}$$

Similarly, by substituting Eq. (7.5) into Eq. (7.2), one obtains the non-dimensional enclosed airspace of a spherical dome as

$$\overline{S}_{ap} = \frac{S_{ap}}{H^3} = \left(\frac{\overline{L}^2}{2} + \frac{1}{6}\right)\pi \tag{7.6}$$

For a given dome height *H*, we can apply the Ritz method presented in Chapter 5 and the Bisection method (Kreyszig 1993) to seek for a family of spherical domes that have the critical water depth $D = D_{cr0}$. In view of Eqs. (7.1) to (7.6), it can be easily seen that, the spherical dome shape is defined by the dome height *H* and dome base radius *L*. The dome weight and enclosed airspace increase with increasing base radius *L* for a given dome height.

However, the objective function of this optimal design involves the maximum enclosed airspace and the minimum the material weight. In general, for a given dome height and water depth, these aforementioned objectives are in conflict with each other. We have a bi-criterion optimization problem to deal with.

As the dome height is prescribed, the dome base radius *L* (which will be confined to $\frac{H}{3} \le L \le 3H$ from practical considerations) is taken as the decision variable. The performance index is formulated as the weighted sum of individual

objectives in order to obtain Pareto optimal solutions for the bi-criterion optimization problem.

One introduces $S'_a = \frac{1}{S_a}$ as the objective function for the enclosed space. Thus, seeking the maximum of enclosed space S_a is tantamount to seeking the minimum enclosed space parameter S_a'.

In order to get a better result in the Pareto optimization, one restricts each criterion to be bounded in range [0,1] by using the following normalizations

$$\hat{W}_a = \frac{W_a - W_{a\min}}{W_{a\max} - W_{a\min}} \tag{7.7a}$$

$$\hat{S}'_a = \frac{S'_a - S'_{a\min}}{S'_{a\max} - S'_{a\min}} \tag{7.7b}$$

where $W_{a\min}$, $W_{a\min}$, $S'_{a\min}$, $S'_{a\max}$ are the maximum and minimum values of the weight and enclosed airspace parameters of the dome in prescribed range of $\overline{L}$, i.e. $\frac{1}{3} \le \overline{L} \le 3$

The performance index $J(\hat{\alpha}, \hat{\beta}; \overline{L})$ of the problem is given by

$$J(\hat{\alpha}, \overline{L}) = \hat{\alpha}\hat{W}_a + (1-\hat{\alpha})\hat{S}'_a \tag{7.8}$$

where $0 \le \hat{\alpha} \le 1$ is the weighting factor of the material weight $\hat{W}_a$ and $0 \le (1-\hat{\alpha}) \le 1$ denotes the weighting factor of the enclosed airspace parameter $\hat{S}'_a$.

The bi-criterion optimization problem can be mathematically stated as

$$J = \min_{\bar{L}}[J(\hat{\alpha}, \bar{L})] = \min_{\bar{L}}\left[\hat{\alpha}\hat{W}_a + (1-\hat{\alpha})\hat{S}'_a\right] \tag{7.9a}$$

$$\text{subject to } \frac{1}{3} \le \bar{L} \le 3 \text{ and } \bar{D}_{cr} = \bar{D}_{cr0} \tag{7.9b}$$

A simple minimum weight optimization problem is obtained by setting $\hat{\alpha} = 1$ for minimum weight whereas $\hat{\alpha} = 0$ corresponds to the optimization problem which maximizes the enclosed airspace. For $0 < \hat{\alpha} < 1$, the base radius $\bar{L}$ minimizing $J(\hat{\alpha}, \bar{L})$ gives the Pareto optimal solution.

In the optimization stages, one applied the Golden Section Search technique (Kreyszig 1993) to determine the minimum value of the performance index *J*.

7.3 Results and Discussions

7.3.1 Spherical domes

As an example, one considers a spherical dome of height H = 3000cm. For the subsequent numerical calculations, the dome is assumed to be made from a material with $E_s = E_\theta = 30x10^4$ kgf/cm^2, $\nu_{s\theta} = 0.3$ and $\gamma_a = 2.4 \times 10^{-3}$ kgf/cm^3. The specific weight of water is assumed to be $\gamma_w = 1x10^{-3}$ kgf/cm^3.

Results for the single objective optimization are presented first. Figure 7.4 shows the variations of performance index J in the case of $\hat{\alpha} = 1$ and $\hat{\alpha} = 0$. In the case of $\hat{\alpha} = 1$, one obtains $J(\hat{\alpha}, \bar{L}) = \hat{W}_a$, i.e. the performance index is the normalized dome weight $\tilde{W}_a$. It is clear that the performance index J reaches the minimum value at the boundary value of $\bar{L} = 1/3$, i.e. the minimum weight of the dome is obtained at the lowest value of the normalized base radius $\bar{L}$.

In the case of $\alpha = 0$, one obtains $J(\hat{\alpha}, \overline{L}) = \hat{S}'_a$, i.e. the performance index is the normalized enclosed airspace parameter S'_a. It is clear that the performance index J reaches the minimum value at the boundary value of $\overline{L} = 3$, i.e. the maximum enclosed airspace is obtained at the largest value of the normalized base radius $\overline{L}$ in the given practical range $\frac{1}{3} \le \overline{L} \le 3$.

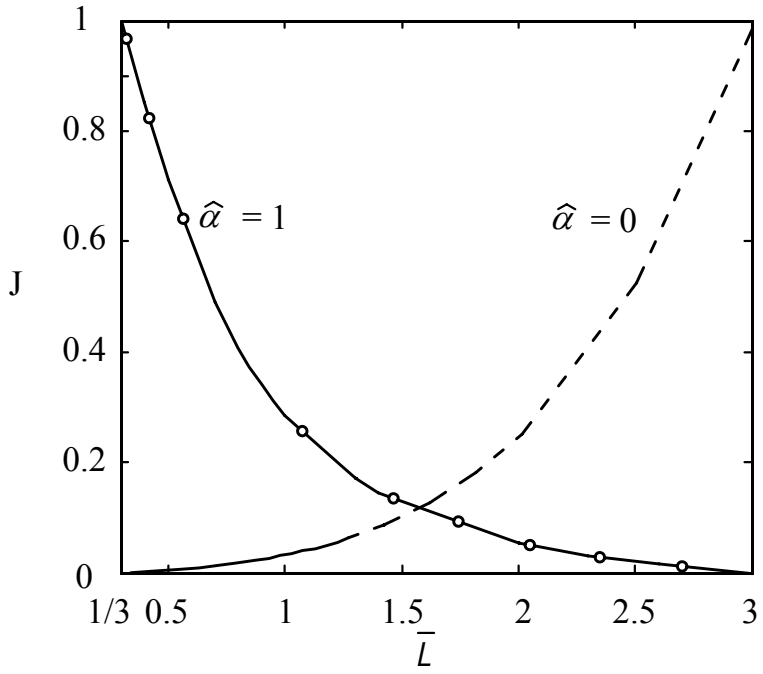

Fig. 7.4 Variations of performance index J of spherical domes with respect to normalized base radius $\overline{L}$ in case of $\hat{\alpha} = 0$ and $\hat{\alpha} = 1$.

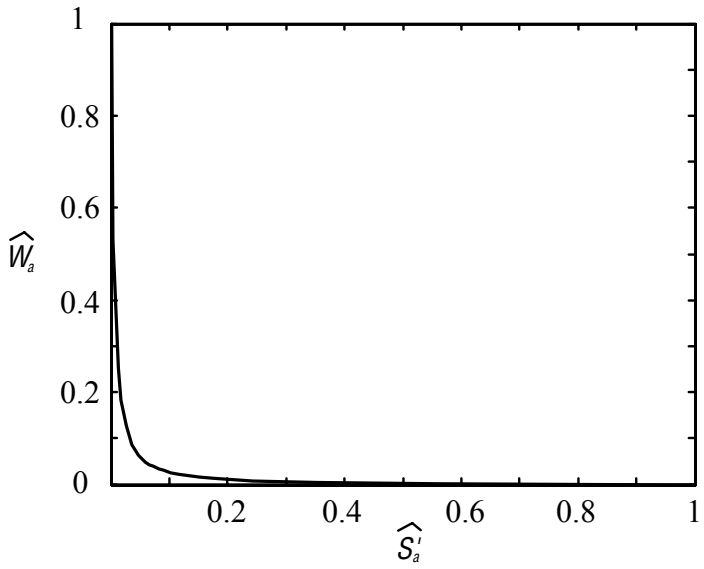

Fig 7.5 Trade-off curve of normalized dome weight $\hat{W}_a$ and normalized enclosed airspace parameter $\hat{S}'_a$ of spherical domes

Figure 7.5 shows the trade-off curve of normalized dome weight $\hat{W}_a$ and normalized enclosed airspace parameter $\hat{S}'_a$. The contributions these criteria are plotted against each other to give the trade-off between the weightings $\hat{\alpha}$=1 and $\hat{\alpha}$=0.

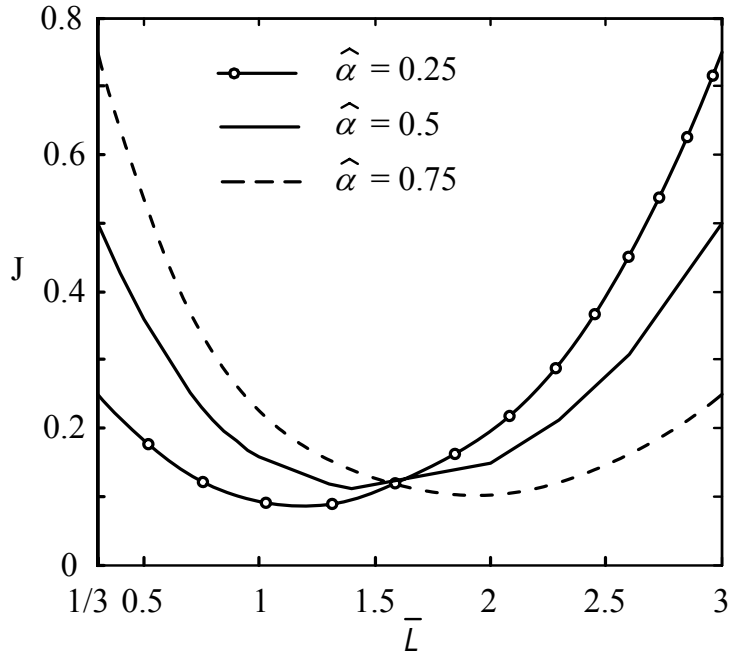

Fig 7.6 Variations of performance index J of spherical domes with respect to normalized base radius L in case of $\hat{\alpha}$ = 0.25; 0.5 and 0.75

Figure 7.6 shows the variations of the performance index J in the case of α =0.25; 0.5 and 0.75. In the case of $\hat{\alpha}$ = 0.25, one obtains the minimum value of the performance index J at $\overline{L}$ =1.2. For $\hat{\alpha}$ =0.5 and 0.75, the performance index reaches the minimum value at $\overline{L}$ =1.5 and $\overline{L}$ = 1.9. It can be seen that the Pareto optimal result is highly dependent on the weight coefficient $\hat{\alpha}$ which the design engineer has to decide in consultation with the client.

7.3.2 Parabolic domes

Extending our research on optimal designs of submerged domes, we investigate the optimal design of parabolic domes for which the meridional curve is defined by

$$r_0 = \sqrt{4az} \tag{7.10}$$

where $a = L^2/(4H)$.

In view of the non-dimensional parameters in Eq. (4.20), Eq. (7.10) may be expressed as

$$\bar{r}_0 = \sqrt{4\bar{a}\bar{z}} \tag{7.11}$$

where $\bar{a} = \dfrac{a}{H} = \dfrac{L^2}{4H^2} = \dfrac{\bar{L}^2}{4}$ and $\bar{z} = \dfrac{z}{H}$. By substituting Eq. (7.11) into Eq. (7.1) and in view of Eq. (4.20), one obtains the weight of a parabolic dome as

$$\overline{W}_{ap} = \frac{W_{ap}}{H^3} = \frac{\pi\xi\bar{L}}{6}\left(\bar{L}^2\left(\sqrt{\bar{L}^2+4}-\bar{L}\right)+4\sqrt{\bar{L}^2+4}\right) \tag{7.12}$$

Similarly, by substituting Eq. (7.5) into Eq. (7.2), one obtains the non-dimensional enclosed airspace of a parabolic dome as

$$\overline{S}_{ap} = \frac{S_{ap}}{H^3} = \frac{\pi\bar{L}^2}{2} \tag{7.13}$$

As an example, one considers a parabolic dome of height H = 3000cm. For the subsequent numerical calculations, the dome is assumed to be made from a material with $E_s = E_\theta = 30x10^4$ kgf/cm^2, $\nu_{s\theta} = 0.3$ and $\gamma_a = 2.4 \times 10^{-3}$ kgf/cm^3. The specific weight of water is assumed to be $\gamma_w = 1x10^{-3}$ kgf/cm^3.

Results for the single objective optimization are presented first. Figure 7.7 shows the variations of performance index J in the case of $\hat{\alpha} = 1$ and $\hat{\alpha} = 0$. Similarly for the spherical domes, the minimum weight of the dome is obtained at the lowest value of the normalized base radius $\overline{L} = 1/3$ and the maximum enclosed airspace is obtained at the largest value of the normalized base radius $\overline{L} = 3$

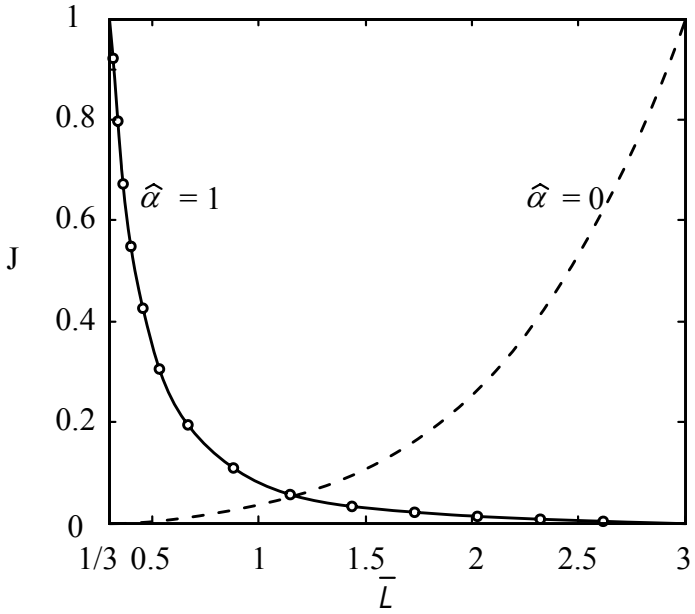

Fig. 7.7 Variations of performance index J of parabolic domes with respect to normalized base radius $\overline{L}$ in case of $\hat{\alpha} = 0$ and $\hat{\alpha} = 1$.

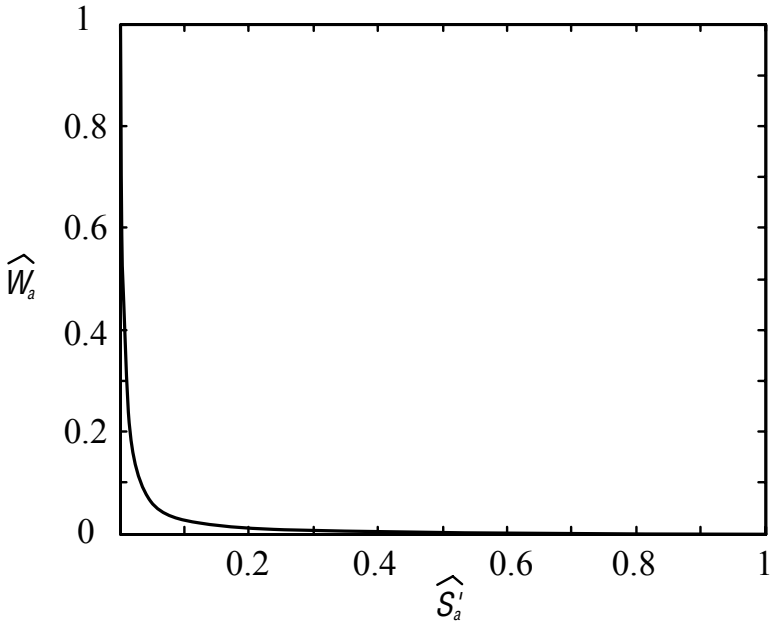

Fig 7.8 Trade-off curve of normalized dome weight $\hat{W}_a$ and normalized enclosed airspace parameter $\hat{S}'_a$ of parabolic domes

Figure 7.8 shows the trade-off curve of normalized dome weight $\hat{W}_a$ and normalized enclosed airspace parameter $\hat{S}'_a$ The contributions these criteria are plotted against each other to give the trade-off between the weightings $\hat{\alpha}$=1 and $\hat{\alpha}$=0.

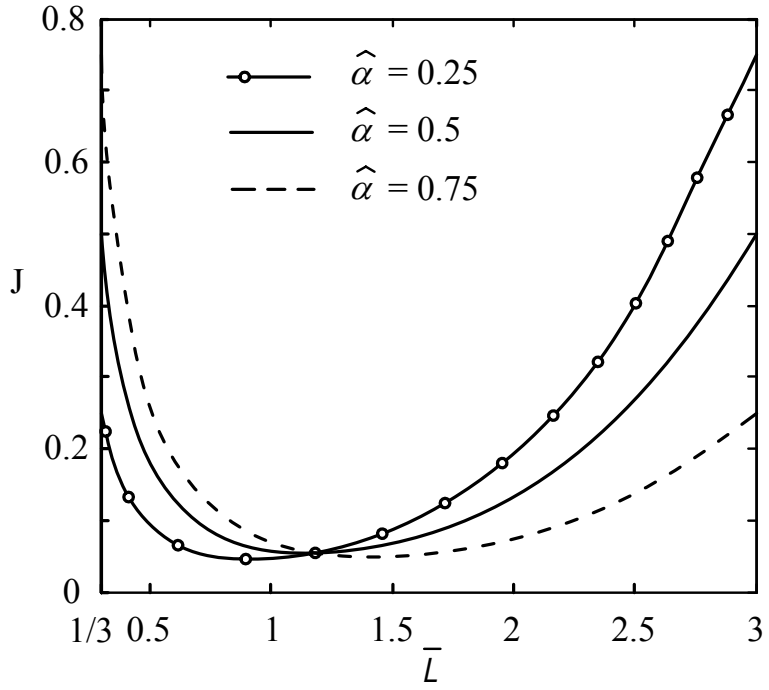

Fig 7.9 Variations of performance index J of parabolic domes with respect to normalized base radius L in case of $\hat{\alpha}$ = 0.25; 0.5 and 0.75

Figure 7.9 shows the variations of performance index J in the case of α =0.25; 0.5 and 0.75. In the case of $\hat{\alpha}$ = 0.25, one obtains the minimum value of the performance index J at $\bar{L}$ =0.8. For $\hat{\alpha}$ =0.5 and 0.75, the performance index reaches the minimum value at $\bar{L}$ =1.1 and $\bar{L}$ = 1.4. It can be seen that the Pareto optimal result is highly dependent on the weight coefficient $\hat{\alpha}$ which the design engineer has to decide in consultation with the client.

7.4 Concluding remarks

This chapter is concerned with the Pareto optimization of a submerged moderately thick dome. The performance index for the optimization problem is formulated as the weighted sum of the dome weight and the enclosed airspace of the dome. It can be seen that the Pareto optimal solutions are highly dependent on the weighting coefficient α which has to be decided by the design engineer in consultation with the client.

CHAPTER 8

CONCLUSIONS AND RECOMMENDATIONS

8.1 Summary and Conclusions

This thesis was concerned with the optimal design of submerged domes where both strength and buckling criteria have been taken into consideration. Membrane analysis was carried out and minimum weight designs of submerged domes of uniform and constant strength were investigated with the view to provide better designs for the construction of submerged domes. The elastic buckling problem of moderately thick domes was also studied. By using the Ritz method, the buckling capacities of moderately thick domes under their own selfweight and hydrostatic pressure were obtained. Moreover, based on a family of spherical and parabolic domes submerged under a given water depth, the optimal dome shapes for maximum enclosed airspace and minimum weight were determined.

The first part of the thesis presented the membrane analysis and minimum weight design of submerged spherical domes. An analytical expression, in the form of power series, for the thickness variation of a submerged spherical dome of uniform strength design as governed by the Tresca yield condition was presented. Numerical examples showed that 9 terms in the power series sufficed for accurate solutions. Further, the optimal subtended angle α_{opt} and the optimal dome height H_{opt} for the minimum weight design of spherical domes were determined. It was found that α_{opt} varies within a narrow range of 1 radian $\leq \alpha_{opt} \leq$ 1.25 radians. The insensitivity of the dome weight over this range, which contains the optimal subtended angle, is a good feature for engineers as it means that there is some flexibility when designing the dome shape without compromising too much on the optimum weight.

Next, we extended the formulation to submerged domes of general shapes. The equations governing the geometry of constant strength domes under combined hydrostatic pressure, selfweight and skin cover load were derived. These equations described the curvature and thickness variation of the dome as well as the Cartesian coordinates of its meridian. The equations were purposely expressed in terms of the arc length *s* as measured from the apex of the dome instead of using the Cartesian coordinate system. This allowed the entire shape of the submerged dome to be determined in a single integration process even in the presence of vertical or infinite slope that may be encountered in the meridian curve. Based on parametric studies of dome shapes under different water depths and selfweight, one may understand better the optimal shape of submerged domes.

In the second part of the thesis, the optimal design of domes against buckling was investigated. Although buckling of shells under compressive loading is of practical

significance in the design of these structures, most studies found in the open literature thus far have focused on spherical domes modelled by classical thin shell theory. In the present study, we developed the model and solution technique to predict the critical buckling pressure of moderately thick rotational shells generated by any meridional shape under external pressure. In order to capture the effect of transverse shear deformation, which is significant for moderately thick shells, Mindlin shell theory was used. Based on Mindlin shell theory, the energy functional was first derived and the Ritz method was used to derive the eigenvalue equation. The Ritz method was automated to handle any boundary conditions. This was made possible by adopting Ritz functions formed by taking the product of mathematically complete polynomial functions and boundary equations raised to appropriate powers; the latter ensured the satisfaction of the geometric boundary conditions at the outset. The desired accuracy of the results can be achieved by taking appropriate degree of polynomials for approximating the displacement functions. The presented buckling results were more accurate than those reported earlier (such as by Uddin 1989, and Muc 1992) since the effect of transverse shear deformation was incorporated. Moreover, the Ritz method developed in the thesis was simple to understand and to code. The Ritz results should be useful benchmark data for analysts developing numerical techniques for shell analysis.

Upon establishing the validity of the Ritz formulation and computer code and its ability to furnish accurate buckling results for dome structures under uniform pressure, we extended the work to submerged domes with allowance for the effect of selfweight. New solutions for the buckling pressure of moderately thick spherical and parabolic shells of various dimensions and boundary conditions were presented. Further, based on a family of spherical and parabolic domes associated with a given

dome height submerged under a water depth, we determined the Pareto optimal dome designs for the maximum enclosed airspace and minimum weight.

The vast optimal dome design data presented in this thesis should serve as a rich reference source for researchers and engineers who are working on analysis and design of shell structures.

8.2 Recommendations for Future Studies

The analysis and design of submerged domes involves the consideration of many factors which expand the scope of this study for future research. Below are some recommendations for future studies.

8.2.1 Domes with very large thickness

In this thesis, we dealt with moderately thick domes. The Mindlin shell theory is adequate for the treatment of such shell structures. However, when the dome has a very large thickness for deep sea deployment, it is necessary to use three-dimensional elasticity theory to account for the thickness effect. Preliminary research along this line has been initiated by Kang and Leissa (2005).

8.2.2 Non-axisymmetric domes

This thesis only dealt with axisymmetric dome structures as axisymmetric domes are one of the most popular dome shapes. However, research should be extended to investigate other non-axisymmetric domes such as a dome with a projected rectangular or square plan area. Least weight designs of such domes approximated by archgrids were investigated by Rozvany *et al.* (1982), Alwis and Wang (1985) and

Thevendran and Wang (1986). However, the buckling capacities of such archgrids have yet to be studied.

8.2.3 Vibration of submerged domes

This thesis focused on identifying the optimal design of submerged spherical and general dome structures. During the analysis of submerged dome structures, we considered the buckling problem which is the most important criterion in designing thin shell structures. However, it is also important to consider the vibration behaviour of such shell structures so as to avoid the resonant frequencies which may be excited by wave induced vibrations. In such problems, the computational method used by Kang and Leissa (2005) on the free vibration of domes can be applied to solve the vibrations of domes under hydrostatic pressure.

8.2.4 Other design loads on submerged domes

In this thesis, we considered selfweight, skin cover and the hydrostatic pressure as the design loads on submerged domes. Although, in deep water, the hydrostatic pressure is the largest load acting on submerged domes, other environmental loads such as wave and current loads as well as incidental loads such as blast loads must be taken into account.

REFERENCES

Abdul Azis, P. K., Al-Tisan, I., Al-Daili, M., Green, T.N., Dalvi, A.G.I. and Javeed, M.A. (2002). "Effects of environment on source water for desalination plants on the eastern coast of Saudi Arabia." *Desalination*, 132(1-3), 29-40.

Alwis, W.A.M. and Wang, C.M. (1985). "On optimal archgrids." *Engineering Optimization*, 8(4), 315-331.

Archer, R.R. (1956). On the post buckling behavior of thin spherical shells, PhD thesis, Massachusetts Institute of Technology.

Aron, H. (1874). "Das Gleichgewicht und die Bewegung einer unendluch dünnen, beliebig gekrümmten, elastischen Shale." *Journ. für reine und ang*. Math, 78.

Baiz, P.M., Aliabadi, M.H. (2007)."Buckling analysis of shear deformable shallow shells by the boundary element method." *Engineering Analysis with Boundary Elements*, 31, 361–372

Barski M, Krużelecki J.(2005). "Optimal design of shells against buckling by means of the simulated annealing method." *Structural and Multidisciplinary Optimization*, 29, 61–72.

Barski, M., Krużelecki J. (2005). "Optimal design of shells against buckling under overall bending and external pressure." *Thin-Walled Structure*s, 43, 1677–1698

Beltramy, E. (1881). “Sull equibrio delle supperficie flessibili ed inestendibili.” *Mem. R. Acad.* Sci di Bologna.

Beltzer, A. I.(1990). “Engineering analysis via symbolic computation-a breakthrough.” *Applied Mechanics Review*. 43, 127.

Bhat, R.B.(1985). “Natural frequencies of rectangular plates using characteristic orthogonal polynomials in the Rayleigh–Ritz method.” *Journal of Sound and Vibration*, 102, 493–499.

Błachut J. (1987). “Combined axial and pressure buckling of shells having optimal positive gaussian curvature.” *Computers and Structures*, 26(3), 513–9.

Błachut J.(1987). “On optimal barrel-shaped shells under buckling constraints.” *AIAA Journal*, 25, 186–8.

Budiansky, B. (1959). “Buckling of clamped shallow spherical shells.” *Proceeding of the Symposium on the Theory of Thin Elastic Shells*, Amsterdam, North Holland.

Bushnell, D. (1976). “BOSOR5-Program for buckling of elastic plastic complex shells of revolutions including large deflections and creep.” *Computers and structures*, 6, 221.

Bushnell, D. (1984). “Computerized analysis of shells-governing equations.” *Computers and Structures*, 18(3), 471-536.

Chai, Y.H. and Wang, C.M. (2005). “Approximate solution for the shape of submerged funicular arches with selfweight.” *Journal of Structural Engineering, ASCE*, 131

Chai, Y.H. and Kunnath, S.K. (2003). “Geometry of submerged funicular arches in Cartesian coordinates.” *Journal of Structural Engineering*, 129(9), 1087-1092.

Chao C.C., Tung T.P., Chern Y.C. (1988). “Buckling of thick orthotropic spherical shells.” *Composites Structures*, 9, 113-137.

Cohen, G.A. (1981). “FASOR- A program for stress, buckling, and vibration of shells of revolutions.” *Advanced Engineering Software*, 3(4), 155-162.

Computers and Structures, Inc. (2007). SAP2000 *Linear and Nonlinear, Static and Dynamics Analysis Design of Three Dimensional Structures*, Berkeley, California, USA.

Cowan, H.J. (1977). "A history of masonry and concrete domes in building construction." *Building and Environment*, 12, 1-24.

Dumir, P.C., Dube, G.P. and Mallick A. (2005). "Axisymmetric buckling of laminated thick annular spherical cap." *Communications in Nonlinear Science and Numerical Simulation*, 10, 191–204

Dumir, P.C., Gandhi, M.L. and Nath, Y. (1984). " Axisymmetric static and dynamic buckling of orthotropic shallow spherical caps with flexible supports." *Acta Mechanica*, 52, 93.

Dym, C. L. (1974). *Introduction to the Theory of Shells*. Pergamon Press, Oxford.

El-Deeb, K.M. and Royles, R. (1993). "Dynamic and static buckling assessment of an echinodome." *Computer and structures*, 46(5), 899-903.

Fu, Y. (1997). "Some asymptotic results concerning the buckling of a spherical shell of arbitrary thickness." *International Journal Of Non-Linear Mechanics*, 33(6), 1111-1122.

Fung, T.C. (2003). "Shapes of submerged funicular arches." *Journal of Engineering Mechanics*, 129(1), 120-125.

Gajewski A, Życzkowski M. (1988). *Optimal Structural Design under Stability Constraints.* Kluwer Academic Publishers. The Netherlands.

Gajewski A. (1990). "Multimodal optimization of uniformly compressed cylindrical shells." *Engineering Optimization in Design Processes*. New York: Springer, 275–82.

Garlerkin, B.G. (1942). "Equilibrium of an elastic spherical shell." *Prikl. Mat. Mekh. Akademiya Nauk.* S.S.S.R., IV, 6.

Gavin, H.P. and Reilly, K.J. (2000). "Submerged funicular arches." *Journal of Structural Engineering*, 126(1), 120-125.

Geannakakes, G.N. (1995). "Natural frequencies of arbitrarily shaped plates using the Rayleigh-Ritz method together with natural co-ordinate regions and normalized characteristic orthogonal polynomials." *Journal of Sound and Vibration*, 182(3), 441-478.

Gol'denweiger, A.L. (1946). "Certain examples of the integration of the equations of the theory of thin shells." *Prikl. Mat. Mekh. Akademiya Nauk*. S.S.S.R, X, 3.

Haftka, R.T. and Gürdal, Z. (1992). Elements of Structural Optimization. Kluwer, Dordrecht.

Hinton, E., Sienz, J. and Ozakca, M. (2003). *Analysis and Optimization of Prismatic and Axisymmetric Shell Structures - Theory , Practice and Software*. Springer, London.

Hou, Y., Wei, G.W., Xiang, Y. (2005). "DSC Ritz method for the free vibration analysis of Mindlin plates." *International Journal for Numerical Methods in Engineering*, 62, 262-288.

Huang, N.C. (1964). "Unsymmetrical buckling of thin shallow spherical." *Journal of Applied Mechanics*, 31, 447.

Hyman B.I. and Lucas Jr A.W. (1971). An optimum design for the instability of cylindrical shells under lateral pressure. *AIAA Journal*, 9, pp. 738–40.

Ichikawa, Y. and Yonezawa, T. (2003). "The outline of the MH21 program and the R&D plan of methane hydrate development system for offshore Japan." *Proceedings of International Symposium on Ocean Space Utilization*, National Maritime Research Institute, 28 Jan – 1 Feb 2003, Tokyo, Japan, 398-404.

Imam, M.H.(1982). "Three dimensional shape optimization." *International Journal of Numerical Methods in Engineering*, 18, 661–73.

Infante Barbosa, J., Mota Soares, C.M. and Mota Soares, C.A. (1991). "Sensitivity analysis and shape optimal design of axisymmetric shell structures." *Computing Systems in Engineering*, 2(5,6), 525-533.

Ioakimidis, N.O. (1992a). "Applications of MATHEMATICA to the direct semi-numerical solution of finite element problems." *Computers and Structures*, Vol. 45 No. 5/6, 833-9.

Ioakimidis, N.O. (1992b). "Applications of MATHEMATICA to the direct solution of torsion problems by the energy method." *Computers and Structures*, Vol. 43, No. 4, 803-7.

Ioakimidis, N.O. (1992c). "Semi-numerical iterative series solution of linear algebraic equations with MATHEMATICA." *Communications Applied Numerical Methods*, Vol. 8, 421-9.

Issler, W. (1964). "Membranschalen gleicher Festigeit." Ing. Arch., 33, 330-345.

Kang, J.H., Leissa, A.W. (2005). "Three-dimensional vibrations of thick spherical shell segments with variable thickness." *International journal of Solids and Structures*, 37 (2000), 4811-4823.

Kawai, T. (1974). *Analysis of Buckling Problems*, Baifukan, Tokyo

Kirchhoff, G. (1876). Vorlesungen über Mathematische Physik, Mechanik, Vol. 1.

Koiter, W.T. (1969). "The nonlinear buckling problem of a complete spherical shell under uniform external pressure." *Proc. Kon. Nederl. Acad. Wet*. Amsterdam B.

Komai, T. (2003). "Replacement and sequestration techniques of CO2 hydrate in the developing gas hygrates." *Proceedings of International Symposium on Ocean Space Utilization,* National Maritime Research Institute, 28 Jan – 1 Feb 2003, Tokyo, Japan, 381-384.

Kraus, H. (1967). *Thin Elastic Shells*, John Wiley & Sons. Inc, New York.

Kreyszig, E. (1993). Advanced Engineering Mathematics, 7th ed., John Wiley & Sons Inc., Canada.

Kreyszig, E. (1993). Advanced Engineering Mathematics, 7th ed., John Wiley & Sons Inc., Canada, 1040-1043.

Krużelecki J. and Trzeciak P. (2000). "Optimal design of axially symmetrical shells under hydrostatic pressure with respect to their stability." *Structural and Multidisciplinary Optimization*, 19(2), 148–54

Krużelecki, J. (1988). "Optimal design of a cylindrical shell under overall bending with axial force." *Bull Pol Acad Sci Tech Sci*, 36(3–4), 141–50.

Krużelecki, J. and Trzeciak, P.(2000). "Optimal design of axially symmetrical shells under hydrostatic pressure with respect to their stability." *Structural and Multidisciplinary Optimization*, 19(2), 148–54.

Krużelecki, J. and Życzkowski, M. (1984). "Optimal design of an elastic cylindrical shell under overall bending with torsion." *Solid Mechanics Archive*, 9, 269–306.

Krużelecki, J. and Życzkowski, M. (1985). "Optimal design of shells—a survey." *Solid Mechanics Archives*, 10, 101–70.

Kukreti, A.R., Farsa, J. and Bert, C.W. (1996). "Differential quadrature and Rayleigh–Ritz methods to determine the fundamental frequencies of simply supported rectangular plates with linearly varying thickness." *Journal of Sound and Vibration*, 189, 103–122.

Ladson, L.S., Waren, A.D., Jain, A., and Ratner, M. (1978). "Design and testing a generalized reduced gradient code for nonlinear programming." *ACM Transaction on Mathematical Software*, 4(1), 34-50.

Lamé, G. and Claperon, B.P.E. (1833). "Mémoire sure l' équilibre interieur des corps solides." *Mém. prés. par div. savants*, 4.

Lecornu, Z. (1938). "Sur l'équilibre des surfaces flexibles et inextendibles." *Journ. de l'école Polytechnique*, c.XLVIII.

Leissa, A.W. (2005). "The historical bases of the Rayleigh and Ritz methods." *Journal of Sound and Vibration*, 287, 961-978.

Levy, R. and Spillers, W.R. (1989). "Optimal design for axisymmetric cylindrical shell buckling." *Journal of Engineering Mechanics*, 115, 1683-1690.

Li, Q.S., Liu, J. and Tang, J. (2003).. "Buckling of shallow spherical shells including the effects of transverse shear deformation." *International Journal of Mechanical Sciences*, 45, 1519-1529.

Liew, K.M. and Lim, C.W. (1995). "A Ritz vibration analysis of doubly-curved rectangular shallow shells using a refined first-order theory." *Computer Methods in Applied Mechanics and Engineering*, 127, 145–162.

Liew, K.M., Lim, M.K., Lim, C.W., Li, D.B. and Zhang, Y.R.(1995). "Effects of initial twist and thickness variations on the vibration behaviour of shallow conical shells." *Journal of Sound and Vibration*, 180 (2), 271–296.

Liew, K.M., Wang, C.M., Xiang, Y. and Kitipornchai, S. (1998). *Vibration of Mindlin Plates*, Elsevier, Amsterdam.

Liew, K.M. (1990). *The Development of 2-D Orthogonal Polynomials for Vibration of Plates*, Ph.D. Thesis, National University of Singapore, Singapore.

Liew, K.M. and Wang, C.M. (1992). "Vibration analysis of plates by pb-2 Rayleigh-Ritz method: mixed boundary conditions, reentrant corners and curved internal supports." *Mechanics of Structures and Machines*, 20(3), 281-292.

Liew, K.M. and Wang, C.M. (1993). "pb-2 Rayleigh-Ritz method for general plate analysis." *Engineering Structures*, 15(1), 55-60.

Liew, K.M., Chen, X.L. and Reddy, J.N. (2004). "Mesh-free radial basis function method for buckling analysis of non-uniformly loaded arbitrarily shaped shear deformable plates." *Computer Methods in Applied Mechanics and Engineering*, 193, 205-224.

Lim, C.W. and Liew, K.M.(1994). "A pb-2 Ritz formulation for flexural vibration of shallow cylindrical shells of rectangular planform." *Journal of Sound and Vibration*, 173 (3), 343–375.

Lim, C.W, Ma, Y.F., Kitipornchai, S., Wang, C.M. and Yuen, R.K.K. (2003). "Buckling of vertical Cylindrical Shells Under Combined End Pressure and Body Force." *Journal of Engineering Mechanics ASCE*, 876-884

Love, A.E. (1888). "The small free vibrations and deformations of a thin elastic shell". *Phil. Trans. Roy. Soc.*, London. Ser. A, 179, 491-546

Magnucki, K., Lewinski, J. and Stasiewicz, P.(2004). "Optimal sizes of a ground-based horizontal cylindrical tank under strength and stability constraints." *International Journal of Pressure Vessels and Piping*, 81(12), 913–917.

Mindlin, R.D. (1951). "Influence of rotatory inertia and shear on flexural motions of isotropic, elastic plates." *Transaction of ASME, Journal of Applied Mechanics*, 18, 31-38.

Mizusawa, T. (1986). "Natural frequencies of rectangular plates with free edges." *Journal of Sound and Vibration*, 105, 451-459.

Muc, A. (1992). "On the buckling of composite shells of revolution under external pressure." *Composite Structures*, 21(2), 107-119.

Mushtari, K. M. (1949). "A qualitative study if the state of stress of an elastic shell subject to small deformations and arbitrary displacements." *Prikl. Mat. Mekh. Akademiya Nauk*. S.S.S.R, XIII, 2.

Nakamura, H., Dow, M. and Rozvany, G.I.N. (1981). "Optimal spherical cupola of uniform strength: allowance for selfweight." *Ing. Arch*, 51, 159-181.

Narita, Y. and Leissa A.W. (1990). "Buckling studies for simply supported symmetrically laminated rectangular plates." *International Journal of Mechanical Sciences*, 32, 909–924.

Neut, A. van der (1932). The elastic stability of thin-walled sphere. Dissertation, Delft.

Novozhilov, V.V. (1970). The Theory of Thin Shells, Wolters-Noordhoff Publishing, The Netherlands, Groningen, 138-147.

Ohga, M., Shigematsu, T. and Kawaguchi, K. (1996). "Buckling analysis of thin-walled members with variable thickness." *Journal of Structural Engineering*, 121, 919-924.

Parlett, B.N., Dhillon, I.S.(2000). "Relatively robust representations of symmetric tridiagonals." *Linear Algebra and its Applications*, 309, 121–151

Pesciullesi, C., Rapallini, M., Tralli, A. and Cianchi, A. (1997). "Optimal spherical masonry domes of uniform strength." *Journal of Structural Engineering*, 123, 203-209.

Prager, W. and Rozvany, G.I.N. (1980). "Optimal spherical cupola of uniform strength." *Ing. Arch*., 49, 287-293.

Rayleigh, J.W. (1977). *Theory of Sound*, Macmillan Vol 1 (reprinted by Dover Publications. 1945).

Rayleigh, L. (1911). "On the calculation of Chladni's figures for a square plate." *Philosophical Magazine Sixth Series*, 22, 225-229.

Reddy, J.N. (2004). *Mechanics of Laminated Composite Plates and Shells: Theory and Analysis*. Second edition. CRC Press, Florida.

Redekop, D. (2005). "Buckling analysis of an orthotropic thin shell of revolution using differential quadrature." *International Journal of Pressure Vessels and Piping*, 82, 618–624

Reiss, E.L. (1958). "Axially buckling of shallow spherical shells under external pressure." *Journal of Applied Mechanics*, Trans. ASME, 25, 556.

Reissner, E. (1945). "The effect of transverse shear deformation on the bending of elastic plates." *Journal of Applied Mechanics*, 12, A69-A77.

Ritz, W. (1909). "Uber eine neue Mehode zur Lösung gewisser Variationprobleme der mathematischen Physik." *Journal fur Reine and Angewandte Mathematik* 135, 1-61.

Ross, C. T. F. (1990). *Pressure Vessels under External Pressure*. Chapman & Hall

Ross, C. T. F. (1996). "Vibration and elastic instability of thin-walled domes under uniform external pressure." *Thin-Walled Structures*, 26(3), 159-177.

Ross, C. T. F., Mackney, M. D. A., (1983). "Deformation and stability studies of thin-walled domes under uniform pressure, *J. Strain Analysis*, 18, 167-172

Ross, C.T.F., Youster, P. and Sadler, R. (2001). "The buckling of plastic oblate hemi-ellipsoidal dome shells under external hydrostatic pressure." *Ocean Engineering*, 28(7), 789-803.

Ross, C.T.F., Huat B.H., Chei T.B., Chong C.M. and Mackney M.D.A.(2003). "The buckling of GRP hemi-ellipsoidal dome shells under external hydrostatic pressure." *Ocean Engineering*, 30, 691–705.

Royles, R. and Llambias, J.M. (1985). "Buckling behavior of an underwater storage vessel." *Experimental Mechanics*, 25, 421-428.

Royles, R., Sofoluwe, A.B., Baig, M.M. and Currie, A.J. (1980). "Behavior of underwater enclosures of optimum design." *Strain*, 16(1), 12-20.

Rozvany, G.I.N., Wang, C.M. and Dow, M. (1982). "Prager-structures: arch-grids and cable networks of optimal layout." *Computer Methods in Applied Mechanics and Engineering*, 31, 91-133.

Rysz, M. and Życzkowski, M. (1989). "Optimal design of a cylindrical shell under overall bending with axial force with respect to creep stability." *Structural Optimization*, 1(1), 29–36.

Sayir, M. and Schumann, W. (1972). "Zu den anissotropen Membranschalen mit gegebenefalls gleicher Festigkeit." *A. Angew. Math. Phys.*, 23, 815-827.

Schumann, W. and Wüthrich, W. (1972). "Über Schalen gleicher Festigkeit." *Acta Mechanica*, 14, 89-197.

Smith, S.T., Boyle, J.M., Garbow, B.S. Ikebe, Y., Klema, V.C. and Moler, C.B. (1974). *Matrix Eigensystem Routines-EISPAC Guide*. Springer-Verlag, New York.

Sofiyev, A.H. and Aksogan, O. (2004). "Buckling of a conical thin shell with variable thickness under a dynamic loading." *Journal of Sound and Vibration*, 270, 903-915.

Sofoluwe, A.B., Royles, R. and Ibidapo-Obe, O. (1981). "An improved numerical approach to the analysis of the echinodome." *Mechanics Research Communications*, 8(4), 237-243.

Sokolovskii, V.V. (1938). "On membrane shells of revolution." *Prikl. Mat. Mekh. Akademiya Nauk*. S.S.S.R., I, 3.

Sun, G. (1989). "A practical approach to optimal design of laminated cylindrical shells for buckling." *Composites Science and Technology*, 36, 243-253.

Sun, G. and Hansen, J. S.(1988). "Optimal design of laminated composite circular-cylindrical shells subjected to combined load." *Journal of Applied Mechanics*. 55, 136-142.

Tennyson, R. C. and Hansen J. S. (1983). "Optimum design for buckling of laminated cylinders." *The buckling of Structures in Theory and Practice* (Edited by J. M. T. Thomnson and G. W. Hunt). Cambridge University Press, Cambridge.

Thevendran, V. and Wang, C.M. (1986). "On the optimality criteria for archgrid." *Journal of Structural Engineering ASCE*, 112(1), 185-189.

Thurston, G.A. (1961). "A numerical solution of the nonlinear equations for axisymmetric bending of shallow spherical shells." *Journal of Applied Mechanics*, 28, 557

Timoshenko, S.P. and Woinowsky-Krieger, W. (1959). *Theory of Plates and Shells*, McGraw-Hill, New York, 2nd Edition, 442-445.

Tsai, S.W. and Pagano, N.J. (1968). "Invariant properties of composite materials." *Composite Materials Workshop*, Technomic Publishing Co., Stamford, Connecticut, 233-253.

Uddin, M. W. and Haque, M.M. (1994). "Instability of semi-ellipsoidal shells." *International Journal of Pressure Vessels and Piping*, 58, 65-74.

Ugural, A.C. (1999). Stresses in Plates and Shells, 2nd Edition, McGraw-Hill, USA.

Uysal, H., Gula, R. and Uzmanb, U. (2007). "Optimum shape design of shell structures." *Engineering Structures*, 29, 80–87

Vermeulen, A. H. and Heppler, G. R.(1998). "Structural analysis of shells by the b-spline field approximation method." *Computers and Structures*, 68 (1-3), 167-179.

Vlasov, V.Z. (1939). "Membrane theory of thin shells, formed by second order surfaces." *Plates and Shells*, Gosstroiizdat.

Walker, M., Reisst, T. and Adalit, S. (1997). "Multiobjective design of laminated cylindrical shells for maximum torsional and axial buckling loads." *Computers and Structures*, 62(2), 231-242.

Wang, C.M. and Kitipornchai, S. (1992). "Shooting-optimization technique for large deflection analysis of structural members." *Engineering Structures*, 14(4), 231-240.

Wang, C.M. and Ler, C.W. (2003). "Optimization of submerged funicular arches." *Mechanics Based Design of Structures and Machines*, 31(2), 181-200.

Wang, C.M. and Wang, C.Y. (2002). "Funicular shapes of submerged arches." *Journal of Structural Engineering*, 128(2), 266-270.

Watanabe, E. and Utsunomiya, T. (2003). "Analysis and design of floating bridges." *Progress in Structural Engineering and Materials*, 5, 127-144.

Wolfram, S. (1999). Mathematica book, 4th Edition. Cambridge University Press, New York.

Yang, M. F., Liang, C. C. and Chen, C. H. (1992). "A rational shape design of externally pressurized torispherical dome ends under buckling constraints." *Computers & Structures* 43(5), pp. 839-851.

Yoshida, K. (2003). "A brief review of recent activities of VLFS in Japan." *Proceedings of International Symposium on Ocean Space Utilization*, National Maritime Research Institute, Tokyo, Japan, 21-28.

Zbigniew, E.M. and Roman, T.N. (1991). *Shells of Revolution*. PWN- Polish Scientific Publishers, Warszawa.

Ziegler, H. (1958). "Kuppelm gleicher festigkeit." Ing. Arch., 26, 378-382.

Zingoni, A. (1997). Shell structures in civil and mechanical engineering - Theory and closed-form analytical solutions, Thomas Telford Publishing, London.

Zoelly, R. (1915). Über ein Kinckungsproblem an der Kugelschale. Dissertation, Zurich.

Życzkowski, M., Krużelecki J. and Trzeciak P. (2001). "Optimal design of rotationally symmetric shells for buckling under thermal loadings." *Journal of Theory Applied Mechanics*, 39(2), 443–55.

Życzkowski, M. and Krużelecki, J. (1973). "Optimal design of shells with respect to their stability." *IUTAM Symposiums on Optimization in Structural Design*. New York, Springer. 229–47.

Życzkowski, M. (1992). "Recent advances in optimal structural design of shells." *European Journal of Mechanics - A/Solid*, 11, 5–24.

APPENDIX

This part details the use of Mathematica (Wolfram 1999) to obtain the buckling strength of rotational shells according to the Ritz method and the formulations presented in Chapter 4.

- Material properties

```
νθs = 3 / 10;
νsθ = 3 / 10;
Eθ = 200 10^4;
Es = 200 10^4;
Gsz = Es / 2 / (1 + νsθ);
```

- Calculation of the material parameters for the stiffness matrix [K] (Eq. 4.24)

$$Q11 = \frac{E\theta}{Eb};$$

$$Q22 = \frac{Es}{Eb};$$

$$Q12 = \frac{\nu\phi\theta\, E\theta}{Eb};$$

$$Q44 = \frac{5}{6}\,\frac{Gsz}{Eb}\,(1 - \nu\theta s\, \nu s\theta);$$

$$A11[z\_] = Q11\,\text{Integrate}\left[\frac{1+\xi\frac{\xi}{r1[z]}}{1+\xi\frac{\xi}{r2[z]}}, \{\xi, -1/2, 1/2\}\right];$$

$$A12[z\_] = Q12\,\text{Integrate}[1, \{\xi, -1/2, 1/2\}];$$

$$A22[z\_] = Q22\,\text{Integrate}\left[\frac{1+\xi\frac{\xi}{r2[z]}}{1+\xi\frac{\xi}{r1[z]}}, \{\xi, -1/2, 1/2\}\right];$$

$$A44[z\_] = Q44\,\text{Integrate}\left[\frac{1+\xi\frac{\xi}{r2[z]}}{1+\xi\frac{\xi}{r1[z]}}, \{\xi, -1/2, 1/2\}\right];$$

$$B12[z\_] = Q12\,\text{Integrate}[\xi, \{\xi, -1/2, 1/2\}];$$

$$D11[z\_] = Q11\,\text{Integrate}\left[\frac{1+\xi\frac{\xi}{r1[z]}}{1+\xi\frac{\xi}{r2[z]}}\xi^2, \{\xi, -1/2, 1/2\}\right];$$

$$D12[z\_] = Q12\,\text{Integrate}\left[\xi^2, \{\xi, -1/2, 1/2\}\right];$$

$$D22[z\_] = Q22\,\text{Integrate}\left[\frac{1+\xi\frac{\xi}{r2[z]}}{1+\xi\frac{\xi}{r1[z]}}\xi^2, \{\xi, -1/2, 1/2\}\right];$$

- Geometrical properties of spherical dome

$$f[z\_] = \sqrt{2\,z\,R - z^2}\;;$$

$$r0[z\_] = f[z];$$

$$r1[z\_] = R;$$

$$r2[z\_] = R;$$

$$\eta[z\_] = \frac{R}{\sqrt{(2\,R - z)\,z}};$$

$$n_{s1}[z\_] = -\frac{R}{2};$$

$$n_{\theta 1}[z\_] = -\frac{R}{2};$$

- Geometrical properties of parabolic domes

$$A = \frac{L^2}{4};$$

$$f[z\_] = 2\sqrt{Az};$$

$$r0[z\_] = f[z];$$

$$r1[z\_] = \frac{2\,(A\,(A+z))^{\frac{3}{2}}}{A^2};$$

$$r2[z\_] = 2\sqrt{A\,(A+z)};$$

$$\eta[z\_] = \sqrt{\frac{A+z}{z}};$$

$$n_{s1}[z\_] = -\sqrt{A\,(A+z)};$$

$$n_{\theta 1}[z\_] = -2\sqrt{A\,(A+z)}\left(\frac{A}{2\,(A+z)}+1\right);$$

- Basic functions need to be defined for different boundary functions

➢ Clamped edge (Eq. 4.42)

$$\eta_u = (z-1)\,z;$$

$$\eta_w = (z-1);$$

$$\eta_\psi = (z-1)\,z;$$

➢ Simply supported edge (Eq. 4.43)

$$\eta_u = (z-1)\,z;$$

$$\eta_w = (z-1);$$

$$\eta_\psi = z;$$

- The mathematically complete polynomial functions are formed as a list. (Eq. 4.28)

$$\text{Table}\left[p_i = \eta_u\, z^{i-1},\ \{i,\ 1,\ N1\}\right];$$
$$\text{Table}\left[p_i = \eta_w\, z^{i-N1-1},\ \{i,\ N1+1,\ N2\}\right];$$
$$\text{Table}\left[p_i = \eta_\psi\, z^{i-N2-1},\ \{i,\ N2+1,\ N3\}\right];$$

- The matrix elements of the [K] matrix (Eqs. (4.31-35)

$$\text{Table}\left[\tilde{q}_i = \frac{\partial_z r0[z]}{\eta[z]\, r0[z]}\ p_i\ ,\ \{i,\ 1,\ N1\}\right];$$
$$\text{Table}\left[\tilde{q}_i = \frac{p_i}{r2[z]},\ \{i,\ N1+1,\ N2\}\right];$$
$$\text{Table}[\tilde{q}_i = 0,\ \{i,\ N2+1,\ N3\}];$$
$$K1[z\_] = \text{Table}[A11[z]\ \tilde{q}_i \tilde{q}_j\, r0[z]\, \eta[z],\ \{i,\ 1,\ N3\},\ \{j,\ 1,\ i\}];$$

$$\text{Table}[\tilde{w}_i = 0,\ \{i,\ 1,\ N1\}];$$
$$\text{Table}[\tilde{w}_i = 0,\ \{i,\ N1+1,\ N2\}];$$
$$\text{Table}\left[\tilde{w}_i = \xi\, \frac{\partial_z r0[z]}{\eta[z]\, r0[z]}\ p_i,\ \{i,\ N2+1,\ N3\}\right];$$
$$K2[z\_] = \text{Table}[D11[z]\ \tilde{w}_i \tilde{w}_j\, r0[z]\, \eta[z],\ \{i,\ 1,\ N3\},\ \{j,\ 1,\ i\}];$$

$$\text{Table}\left[\tilde{e}_i = \frac{\partial_z p_i}{\eta[z]},\ \{i,\ 1,\ N1\}\right];$$
$$\text{Table}\left[\tilde{e}_i = \frac{p_i}{r1[z]},\ \{i,\ N1+1,\ N2\}\right];$$
$$\text{Table}[\tilde{e}_i = 0,\ \{i,\ N2+1,\ N3\}];$$
$$K3[z\_] = \text{Table}[A22[z]\ \tilde{e}_i \tilde{e}_j\, r0[z]\, \eta[z],\ \{i,\ 1,\ N3\},\ \{j,\ 1,\ i\}];$$

```
Table[r̃i = 0, {i, 1, N1}];
Table[r̃i = 0, {i, N1 + 1, N2}];
Table[r̃i = ξ ∂z pi / η[z], {i, N2 + 1, N3}];
K4[z_] = Table[D22[z] r̃i r̃j r0[z] η[z], {i, 1, N3}, {j, 1, i}];

Table[t̃i = - pi / r1[z], {i, 1, N1}];
Table[t̃i = ∂z pi / η[z], {i, N1 + 1, N2}];
Table[t̃i = pi, {i, N2 + 1, N3}];
K5[z_] = Table[A44[z] t̃i t̃j r0[z] η[z], {i, 1, N3}, {j, 1, i}];

K6a[z_] = Table[B12[z] q̃i w̃j r0[z] η[z], {i, 1, N3}, {j, 1, i}];
K6b[z_] = Table[B12[z] q̃j w̃i r0[z] η[z], {i, 1, N3}, {j, 1, i}];

K7a[z_] = Table[B12[z] ẽi r̃j r0[z] η[z], {i, 1, N3}, {j, 1, i}];
K7b[z_] = Table[B12[z] ẽj r̃i r0[z] η[z], {i, 1, N3}, {j, 1, i}];

K8a[z_] = Table[A12[z] q̃i ẽj r0[z] η[z], {i, 1, N3}, {j, 1, i}];
K8b[z_] = Table[A12[z] q̃j ẽi r0[z] η[z], {i, 1, N3}, {j, 1, i}];

K9a[z_] = Table[D12[z] w̃i r̃j r0[z] η[z], {i, 1, N3}, {j, 1, i}];
K9b[z_] = Table[D12[z] w̃j r̃i r0[z] η[z], {i, 1, N3}, {j, 1, i}];

K10a[z_] = Table[B12[z] q̃i r̃j r0[z] η[z], {i, 1, N3}, {j, 1, i}];
K10b[z_] = Table[B12[z] q̃j r̃i r0[z] η[z], {i, 1, N3}, {j, 1, i}];

K11a[z_] = Table[B12[z] w̃i ẽj r0[z] η[z], {i, 1, N3}, {j, 1, i}];
K11b[z_] = Table[B12[z] w̃j ẽi r0[z] η[z], {i, 1, N3}, {j, 1, i}];
```

- The matrix [K] can be obtained as follow (Eq. 4.30)

```
K[z_] = K1[z] + K2[z] + K3[z] + K4[z] + K5[z] + K6a[z] + K6b[z] + K7a[z] + K7b[z] +
        K8a[z] + K8b[z] + K9a[z] + K9b[z] + K10a[z] + K10b[z] + K11a[z] + K11b[z];
```

- The elements of matrix [M] can be obtained as Eq. (4.37-39)

$$\text{Table}\left[\tilde{y}_i = \frac{\partial_z r0[z]}{\eta[z]\, r0[z]}\, p_i,\ \{i, 1, N1\}\right];$$
$$\text{Table}\left[\tilde{y}_i = \frac{p_i}{r2[z]},\ \{i, N1+1, N2\}\right];$$
$$\text{Table}[\tilde{y}_i = 0,\ \{i, N2+1, N3\}];$$
$$M1[z\_] = \text{Table}[n_{\theta 1}[z]\, \tilde{y}_i\, \tilde{y}_j\, r0[z]\, \eta[z],\ \{i, 1, N3\},\ \{j, 1, i\}];$$

$$\text{Table}\left[\tilde{u}_i = \frac{\partial_z p_i}{\eta[z]},\ \{i, 1, N1\}\right];$$
$$\text{Table}\left[\tilde{u}_i = \frac{p_i}{r1[z]},\ \{i, N1+1, N2\}\right];$$
$$\text{Table}[\tilde{u}_i = 0,\ \{i, N2+1, N3\}];$$
$$M21[z\_] = \text{Table}[n_{s1}[z]\, \tilde{u}_i\, \tilde{u}_j\, r0[z]\, \eta[z],\ \{i, 1, N3\},\ \{j, 1, i\}];$$

$$\text{Table}\left[\tilde{g}_i = \frac{p_i}{r1[z]},\ \{i, 1, N1\}\right];$$
$$\text{Table}\left[\tilde{g}_i = -\frac{\partial_z\, p_i}{\eta[z]},\ \{i, N1+1, N2\}\right];$$
$$\text{Table}[\tilde{g}_i = 0,\ \{i, N2+1, N3\}];$$
$$M31[z\_] = \text{Table}[n_{s1}[z]\, \tilde{g}_i\, \tilde{g}_j\, r0[z]\, \eta[z],\ \{i, 1, N3\},\ \{j, 1, i\}];$$

- The matrix [M] can be obtained as follow (Eq. 4.36)

$$M[z\_] = M1[z] + M2[z] + M3[z];$$

For elastic buckling, the aforementioned eigenvalue problems can be expressed in the standard form of a generalized eigenvalue problem and a standard eigenvalue routine, for e.g. EISPAC (Smith *et al*., 1974), can be used to solve the problem. However, it was found that the built-in function "**Eigenvalues**" in Mathematica (Wolfram, 1999) can be used instead of Gaussian elimination. The use of built-in function "**Eigenvalues**" is found to be faster than using the Gaussian elimination in the determination of the eigenvalues for this class of problems. ***Eigenvalues*** function in

Mathematica used the function DSYEVR in LAPACK<www.netlib.org/lapack/> routines to calculate the numerical eigen values and vectors of a real and symmetric matrice.

LAPACK, the Linear Algebra PACKage, is a software library for numerical computing written in Fortran 77. It provides routines for solving systems of simultaneous linear equations, least-squares solutions of linear systems of equations, eigenvalue problems, and singular value problems.

DSYEVR function computes selected eigenvalues and, optionally, eigenvectors of a real symmetric matrix A. Eigenvalues and eigenvectors can be selected by specifying either a range of values or a range of indices for the desired eigenvalues. DSYEVR first reduces the matrix A to tri-diagonal form T with a call to DSYTRD. Then, DSYEVR calls DSTEMR to compute the eigen spectrum using Relatively Robust Representations (Parlett and Dhillon, 2000)

LIST OF AUTHOR'S PUBLICATIONS

Journal Papers

1. **Vo, K.K.**, Wang, C.M. and Chai, Y.H. (2007), "Buckling analysis of moderately thick rotational shells under uniform pressure using Ritz method." *Journal of Structural Engineering*, ASCE, 134(4), 593-607.

2. **Vo, K.K**., Wang, C. M. and Chai, Y. H. (2006), "Membrane analysis and optimization of submerged domes with allowance for selfweight and skin cover load." *Archive of Applied Mechanics*, 75, 235-247.

3. Wang, C.M., **Vo, K.K.** and Chai, Y. H. (2006), "Membrane analysis and minimum weight design of submerged spherical domes." *Journal of Structural Engineering*, ASCE, 132(2), 253-259.

Conference Papers

1. Vo, K.K., Wang, C.M. and Chai, Y.H. (2005) "Membrane analysis and optimization of submerged domes with allowance for selfweight and skin cover load." *Proceedings of the Tenth International on Civil, Structural and Environmental Engineering Computing,* ed. B.H.V. Topping, Civil-Comp Press, 30 Aug - 2 Sep 2005, Rome, Italy, 1-12.

2. Wang, C.M., Aung, T.M. and Vo, K.K. (2005) "Ritz Method for Plastic Buckling Analysis of Thick Plates." *Proceedings of the Tenth International on Civil, Structural and Environmental Engineering Computing* ed. B.H.V. Topping, Civil-Comp Press, 30 Aug - 2 Sep 2005, Rome, Italy, 1-13.

3. Wang, C.M. and Vo, K.K. (2004) "Least weight design of submerged spherical domes." *Computational Mechanics, The Sixth World Congress on Computational Mechanics (WCCM) in conjunction with the Second Asian-Pacific Congress on Computational Mechanics (APCOM),* 5-10 Sep 2004, Beijing, China.